

*An efficient computational approach to guide  
intervention in treatment of stroke*

A Thesis Presented by **Ahmed Mustafa** for the degree of

Doctor of Philosophy

University of Sheffield

The Department of Mechanical Engineering

Insigneo: Institute for *in-silico* Medicine

Supervisor: Dr. Alberto Marzo

CoSupervisor: Dr. Andrew Narracott

Clinical Supervisor: Dr. Ana Paula Narata

September 2021



*"Yesterday is history, tomorrow is a mystery, and today is a gift... that's why they call it the present"*

- Master Oogway 2008



# Acknowledgements

Firstly, and most importantly, I would like to thank the opportunities that God has given me, past and present, and what is yet to come. I thank God for the lessons I have learned and experienced through the successes and struggles I have been through. From this, I have become more aware and deeply grateful for the patience and support of my family.

I would also like to express my sincere gratitude to my supervisors Dr. Alberto Marzo, Dr. Andrew Narracott and Dr. Ana Paula Narata for their motivation, guidance, patience, continuous and invaluable support during the years of the PhD, especially during the troubling times of the coronavirus pandemic. I would also like to thank the guidance of my INSIGNEO colleagues of past and present, specifically Dr. Ivan Benmerito and Dr. Alessandro Melis, their support has been impactful. I would like to also express my thanks to the students I have supervised during the PhD and their contributions to the research: Freya Sewell, Kingsely Hanlon and Rouven Deines.

Outside the PhD, my life during these past few years has been difficult and I would like to sincerely thank those that kept me sane through the process. I would like to thank specifically the moral support of my dearest friend Matthew Drummond, for all the motivation and equally entertaining procrastination.

Last but not the least, my biggest thanks goes out to my furry little friend, my heart and soul and the real reason I love my life, Akiro, my Akita pup.



# Abstract

Ischaemic stroke (IS) occurs when a cerebral vessel becomes obstructed by a blood clot. One of the most effective treatment options consists of capturing the clot with a catheter-guided stent, while reducing haemodynamic forces on the clot through aspiration and a balloon to halt or reverse flow and reduce risk of clot fragmentation. This often relies on the individual skills of the clinicians performing the operation, and it is difficult to predict how treatment options such as balloon location or aspiration rates might influence clinical outcome. The aim of this thesis is to test and develop a computational tool to examine what-if scenarios prior to IS treatment and identify the scenario most likely to deliver favourable haemodynamic conditions such as flow reversal. Building upon an existing 1D arterial blood flow model (openBF), this was further developed to simulate a typical clinical case of IS and its treatment outcomes following intervention with a balloon guided catheter for a variety of typical anatomies, vascular properties and treatment options. Results show that retrograde flow in the L-MCA (incident area) is not possible to induce with aspiration rates up to 5 ml/s, however the retrieval and treatment path demonstrate flow reversal (L-

ICAs and L-ACA distal). The simulations performed provided understanding of flow directions and their magnitudes throughout the thrombectomy procedure which satisfied the aim of developing a computational tool that can assess flow alterations caused by the treatment. Results also demonstrate the importance of certain vessels during treatment and in networks that have missing vessels as they allow collateral flow and assist in maintaining steady distribution of flow to the brain when there is an occlusion. Missing vessel configurations presented reduced flows in the L-MCA, never retrograde. Configurations that had missing parts of the distal CoW (ACoA and proximal ACAs) presented significantly low flows in the L-ACA distal and L-MCA, and forward flow in the distal L-ICA which was retrograde with its proximal counterpart in all other variations during aspiration. Ageing vascular properties demonstrated unfavourable increase to flow in the L-MCA post-retrieval during aspiration. Increased viscosity presented small reductions in flow globally. To further complement the study, an analytical assessment of the catheter importance was carried out. Results showed that certain catheters in typical vessels present significantly large pressure drops and velocities in comparison to no catheter.

# Contents

<b>Acknowledgements</b>	<b>III</b>
<b>Abstract</b>	<b>V</b>
<b>1 Introduction</b>	<b>1</b>
1.1 The Clinical Problem . . . . .	1
1.2 Hypothesis . . . . .	5
1.3 Aim and Objectives . . . . .	5
1.4 Thesis Outline . . . . .	6
<b>2 Review of Literature</b>	<b>9</b>
2.1 The Cerebrovascular System . . . . .	10
2.1.1 Main Functions and Roles . . . . .	10
2.1.2 Cerebrovascular Anatomy and Variations . . . . .	14
2.2 Ischaemic Stroke . . . . .	18
2.2.1 Pathophysiology, Etiology and Risk Factors . . . . .	18
2.2.2 Diagnosis and Treatment . . . . .	20

2.3	Modelling . . . . .	24
2.3.1	Fundamental Biomechanics of Arterial Blood Flow . . . . .	24
2.3.2	Vascular and Thrombectomy Modelling . . . . .	28
2.4	Conclusions . . . . .	31
<b>3</b>	<b>Blood Flow Model and Methodology</b>	<b>33</b>
3.1	Research Method . . . . .	34
3.1.1	Clinical Procedure and Set-Up . . . . .	34
3.1.2	Network Set-up and Haemodynamic Parameters . . . . .	36
3.2	Initial Modelling Framework: openBF . . . . .	40
3.3	Modelling Ischaemic and Thrombectomy Events . . . . .	44
3.3.1	Occlusion . . . . .	44
3.3.2	Aspiration . . . . .	45
3.4	Conclusion . . . . .	46
<b>4</b>	<b>Baseline Simulation</b>	<b>49</b>
4.1	Methodology . . . . .	50
4.2	Results . . . . .	53
4.3	Discussion . . . . .	61
4.4	Conclusions . . . . .	66
<b>5</b>	<b>Anatomical Network Variations</b>	<b>69</b>
5.1	Methodology . . . . .	71
5.2	Results . . . . .	75
5.2.1	Analysis of Configuration Results . . . . .	75

5.2.2	Configurations and the Treatment Path . . . . .	91
5.3	Discussion . . . . .	94
5.4	Conclusions . . . . .	99
<b>6</b>	<b>Aged Network Variations</b>	<b>101</b>
6.1	Methodology . . . . .	102
6.2	Results . . . . .	107
6.2.1	Simulation of Network with Aged Radius, Wall Thick- ness and Elastic Modulus . . . . .	107
6.2.2	Simulation of Network with Aged Viscosity . . . . .	109
6.3	Discussion . . . . .	113
6.4	Conclusions . . . . .	116
<b>7</b>	<b>The Impact of a Catheter on the Haemodynamics</b>	<b>119</b>
7.1	Analytical Investigation . . . . .	120
7.1.1	Methodology . . . . .	120
7.1.2	Results . . . . .	125
7.1.3	Discussion . . . . .	127
7.2	3D Comparison and Validation . . . . .	128
7.2.1	Methodology . . . . .	128
7.2.2	Results . . . . .	131
7.2.3	Discussion . . . . .	132
7.3	Conclusions . . . . .	134
<b>8</b>	<b>Conclusion</b>	<b>137</b>

8.1	Key Findings . . . . .	139
8.2	Limitations . . . . .	140
8.3	Future Works . . . . .	141

<b>References</b>	<b>142</b>
-------------------	------------

<b>Dissemination</b>	<b>167</b>
----------------------	------------

# List of Figures

2.1	Viscosity and shear rate relationship. . . . .	11
2.2	Superimposition of forward and backward waveform example. .	12
2.3	The Windkessel effect . . . . .	13
2.4	Pressure-Flow auto-regulation curve. . . . .	14
2.5	the cardiovascular network. . . . .	17
2.6	BGC with SR treatment procedure. . . . .	25
2.7	Womersley number waveforms. . . . .	27
3.1	Typical example case study. . . . .	35
3.2	Cardiac output boundary condition. . . . .	37
3.3	The cerebrovascular network and the 1D representation. . . . .	39
3.4	Velocity profile of various viscous losses. . . . .	42
3.5	Three-element Windkessel circuit model. . . . .	43
3.6	Simulation of an occlusion. . . . .	46
3.7	Simulation of aspiration with and without occlusion. . . . .	47
4.1	Defined vessel group classifications. . . . .	51

4.2	Averaged pressure per vessel distribution of baseline model. . . . .	55
4.3	Averaged flow per vessel distribution of baseline model. . . . .	56
4.4	Baseline normalized results of pressure for vessel groups. . . . .	59
4.5	Baseline normalized results of flow for vessel groups. . . . .	60
4.6	Predicted flow direction results for baseline simulation. . . . .	63
4.7	L-MCA flow for phases 1 and 5. . . . .	64
4.8	Flow results of balloon re-position and aspiration variation. . . . .	66
5.1	Vessel single vs. multiple channel. . . . .	71
5.2	Configurations of the Circle of Willis. . . . .	74
5.3	Colour map of normalized results for missing ACoA. . . . .	76
5.4	Colour map of normalized pressure results for missing PCoA(s). . . . .	78
5.5	Colour map of normalized flow results for missing PCoA(s). . . . .	79
5.6	Colour map of normalized pressure results for missing ACA. . . . .	82
5.7	Colour map of normalized flow results for missing ACA. . . . .	83
5.8	Colour map of normalized pressure results for missing PCA. . . . .	85
5.9	Colour map of normalized flow results for missing PCA. . . . .	86
5.10	Colour map of normalized pressure results for missing PCoA + PCA. . . . .	88
5.11	Colour map of normalized flow results for missing PCoA + PCA. . . . .	89
5.12	Treatment path flow results for all variations. . . . .	92
5.13	Treatment path pressure results for all variations. . . . .	95
5.14	Flow path of phases 1 and 5 for full CoW and missing ACoA. . . . .	97

6.1	Colour map of normalized results for aged vascular properties. .	108
6.2	Colour map of normalized pressure and flow results for aged viscosity. . . . .	110
6.3	Colour map of normalized pressure drop results for aged viscosity.	112
6.4	Representation of typical healthy, aged and diseased cross-sections.	116
7.1	BGC and micro-catheter deployment areas. . . . .	120
7.2	Analytical catheterized vessel cross-section. . . . .	122
7.3	Analytical results of catheterized vessels. . . . .	126
7.4	Concentric and eccentric catheterized 3D CFD cases. . . . .	130
7.5	Resistance vs. $\kappa$ results. . . . .	132
7.6	Resistance of eccentric catheter cases. . . . .	133



# List of Tables

2.1	CT and MRI advantages and disadvantages. . . . .	21
3.1	Vessel geometrical and mechanical properties of the network. . . . .	38
5.1	Flow results for missing PCoA + PCA configurations. . . . .	91
5.2	Flow in L-MCA during phases 1 and 5. . . . .	94
5.3	Flow direction in treatment path for all configurations. . . . .	98
6.1	Aged network wall thickness comparison. . . . .	105
6.2	Finalised aged network vascular properties and geometry. . . . .	106
6.3	Network averaged pressure results for baseline and aged simulations. . . . .	114
7.1	Vessels that house catheters during treatment process. . . . .	121
7.2	Catheterized 3D CFD vs. analytical results. . . . .	131



# Chapter 1

## Introduction

### 1.1 The Clinical Problem

Our body highly relies on the function of our brain to perform the variety of commands we require daily, both subconsciously like breathing and consciously such as talking. Among the requirements for a functional brain is a continuous supply of nutrients and oxygen provided by a well controlled stream of blood. This is all achieved through the intricate anatomy and biological mechanisms of the cerebrovascular system. Disruption to these through cerebrovascular disease could display tragic outcomes reaching severities such as lifetime disabilities, cognitive impairments or even death. Cerebrovascular disease is reported as one of the leading causes of disability and death in the western hemisphere and is usually caused by atherosclerosis, the accumulation of plaque inside blood vessels leading to the potential of a stroke [1]. A stroke occurs when the blood

supply to a region of the brain is interrupted or reduced, depriving brain tissue of sufficient nutrients and oxygen and within minutes brain cells begin to die. There are two main types of stroke; ischaemic and haemorrhagic, where ischaemic can have two classifications:

- Ischaemic: A stroke caused by clotting (a thrombus or embolus<sup>1</sup>);
- Hemorrhagic: A stroke caused by bleeding in the brain (e.g. from a ruptured aneurysm);

Alongside these classifications, an additional sub-type of ischaemic stroke (IS) is known as a transient ischaemic attack (TIA), sometimes referred to as a 'mini-stroke'. What defines a TIA is an IS that resolves within 24 hours [2]. An IS is the reduction or blockage of cerebral blood flow limiting the supply of oxygen and nutrients to areas of the functional tissue in the brain. IS occurs when a cerebral vessel becomes obstructed by a blood clot that has become dislodged from another site in the cardiac circulation (emboli or thromboemboli<sup>2</sup>) [3]. IS incidence is reported in approximately 87% of all cases of stroke [4]. Drugs are often used as pharmacological treatment to promote intravenous thrombolysis, dissolving the clot and re-establishing normal blood flow conditions (recanalization) [5]. Limitations have been identified with this procedure, especially its

---

<sup>1</sup>A thrombus is solid mass of platelets and/or fibrin conjoined with other components of the blood which forms an occlusion locally in a vessel and occurs when a clotting mechanism is activated, whereas an embolus is a fragment of a thrombus which has parted and been relocated toward the brain by the bloodstream.

<sup>2</sup>As detailed previously, an embolism occurs when a fragment of a blood clot or other bodily/foreign substance becomes lodged in a blood vessel and obstructs the flow of blood whereas thromboembolism refers to a reduction in blood flow specifically caused by an embolism from a blood clot.

lack of effectiveness in re-establishing blood flow in larger arteries such as the middle cerebral artery (MCA), a crucial distributor of blood to larger areas of the brain and a common site for ischaemic stroke [6, 7]. Alternatively, the mechanical retrieval of a clot through an endovascular procedure, called mechanical thrombectomy (MT), has shown higher success rates of blood flow recanalization and post-treatment survival [8–10].

There is a variety of MT devices and techniques available such as catheter-guided stent retrieval, to penetrate and capture the clot, and aspiration, to reduce haemodynamic forces and avoid clot fragmentation. Balloon guided catheters (BGCs) use a combination of stent retrieval and aspiration at the tip of an inflated balloon which temporarily impedes flow. This reduced blood flow discourages fragmentation of the clot during retrieval. This method has shown higher success of recanalization than other MT procedures (89.2% vs. 67.9%) [11]. To prevent clot fragmentation and downstream embolization it is important to control different variables during the treatment (e.g. position of the balloon, aspiration rates, catheter calibers, etc.) to create flow reversal in the area between the aspiration point and the clot whilst withdrawing the stent retrieval system in an attempt to prevent clot fragmentation and downstream embolization [12–14]. This often relies on the experience and individual skills of the clinicians performing the operation, and it is difficult to predict how factors such as patient anatomy or treatment options (e.g. balloon positioning, aspiration rates) might influence clinical outcome.

In an attempt to develop a quantitative predictive tool to investigate the

mutual influence of the variables at play, scientists have adopted *in-vitro* and *in-silico* approaches. *In-vitro* models have been used mostly as a training tool for clinicians [15, 16]. These approaches focus on qualitative assessment of the relationship between treatment options and recanalization, but rarely provide clinically relevant and detailed haemodynamic data or an insight into the underlying cause-effect mechanisms.

3D computational approaches have either focused on patient-specific image-based computational fluid dynamics models to predict blood flow in the Circle of Willis (CoW) and study the influence of its anatomical variations [17, 18], or in reduced regions of interest to study the influence of aspiration rates on haemodynamics [19]. Although state-of-the-art modelling approaches are quickly advancing towards whole-circulation multi-scale Fluid-Structure-Interaction (FSI) models [20], studies focusing on mechanical thrombectomy often lack an adequate representation of the arterial wall mechanics and its influence on pressure and flow distribution, which would require a FSI approach and introduce additional modelling challenges such as model parameterization. In an attempt to address these challenges, 1D modelling approaches have been developed [21,22] and validated [23–25] as a computationally cheaper way to capture the physics of blood flow and arterial wall mechanics in extended arterial networks. Studies adopting 1D-modelling techniques reported in the literature mostly focus on other clinical aspects, such as cerebral vasospasm, brain tissue infarct, or cerebral aneurysm [26–28]. To the best of the comprehension of the literature review (Chapter 2), research proposed is very limited regarding studies attempting to

predict the influence of ischaemic stroke and mechanical thrombectomy on a larger network comprehension of the cerebrovascular haemodynamics. With the aid of the computational time that 1D models pose, the use of such model would potentially serve as a tool to aid clinical decision providing a more efficient approach for predictive quantitative data pre-administration of treatment.

## **1.2 Hypothesis**

The development and validation of a model able to simulate a stroke event and its treatment can be used to provide valuable information to guide patient management.

## **1.3 Aim and Objectives**

Building upon a verified and validated computational platform [29, 30], the aim of this study is to develop and assess an efficient computational tool to predict flow alterations caused by treatment of ischaemic stroke. The work presented in this thesis is aligned to the following objectives used to achieve the described aim:

1. Perform a literature review to confirm the unmet clinical/scientific challenge;
2. Definition of the required modifications to model basic boundary conditions to simulate the ischaemic event and typical mechanical thrombectomy treatment;

3. Simulate a baseline model of the representative cerebrovascular anatomy from the methodology and use this adapted model to simulate the influence of an ischaemic event and its treatment on relevant haemodynamic parameters and assessing the validity and accuracy of the baseline results before proceeding to alternative studies;
4. Test the model on a variation of typical physiological anatomies including network variations of the CoW and vessel mechanical property ranges of typical diseased and/or older patients;
5. Assess the effects of treatment on the haemodynamics with and without catheter implementation;
6. Summarise the implications of the model outcomes on the current clinical approach to management of stroke patients.

## **1.4 Thesis Outline**

- Chapter 2: Review of Literature - This chapter presents all the relevant background knowledge and literature in support of the approaches adopted in this study, and aimed at identifying the scientific and clinical challenge.
- Chapter 3: Blood Flow Model and Methodology - This chapter describes the initial blood flow model and the adaptation of its boundary conditions to simulate its application to stroke. This is accompanied by a description of the model parameterization.

- Chapter 4: Baseline Simulation - In this chapter, the model presented in Chapter 3 is parameterized to simulate treatment in a typical young and healthy patient. These results are used as a benchmark for comparison for other studies in the thesis.
- Chapter 5: Anatomical Network Variations - The anatomy of the CoW significantly varies across the population, thus this chapter presents the haemodynamic influence and clinical relevance of a selected few from the more likely of these variations.
- Chapter 6: Aged Network Variations- Stroke victims are likely to be of older age than the assumptions of the baseline model, thus in this chapter, results are presented to illustrate the influence of age on certain model parameters, and in turn their influence on relevant haemodynamics during different phases of the clinical treatment.
- Chapter 7: The Impact of a Catheter on the Haemodynamics - This chapter quantifies the likely influence of the presence of the thrombectomy catheter on haemodynamics. These effects are estimated using a simplified analytical approach alongside a 3D CFD analysis.
- Chapter 8: Conclusion - The thesis conclusions are reported with discussions of the key findings, limitations, future work and testing of the original hypothesis.



## **Chapter 2**

# **Review of Literature**

### **Summary**

The cerebrovascular system and its functionality is introduced and explained. This is followed by the details of ischaemic disease, physiology, and continuing from the cerebrovascular introduction, symptomatic effects on the cerebrovascular system are reviewed as well as ischaemic stroke treatment and management. The chapter concludes with a review of the modelling approaches used in this or similar applications.

## 2.1 The Cerebrovascular System

### 2.1.1 Main Functions and Roles

The cardiovascular system comprises of three functional elements: the heart, blood vessels and blood. This circulation is subject to demand that fluctuates widely between sleeping and being awake as well as resting and physically active [31]. Brain parenchyma, the functional tissue in the brain is made up of two cell types: neurons and glial cells. Damage or trauma to this tissue causes anything between potential loss of cognitive ability and death. The cerebrovascular system is vital as reduced blood supply to these tissues causes them to die, a concept known as infarct.

The cerebrovascular system is a part of the cardiovascular network focusing on vessels that specifically supply blood to the brain. Although the brain constitutes of approximately 2% of total body mass ( $\sim 1400$  g), it receives a large proportion of the resting cardiac output in an adult ( $\sim 12 - 15\%$ ) [32].

The capacity of blood to transport and exchange gases and other metabolites depends on its composition (blood cells and plasma) and its rheology. The average adult human has around five litres of blood, where red blood cells (erythrocytes) contribute up to 45% of this content, (the haematocrit value is the ratio of erythrocytes to whole blood volume – e.g. 45% erythrocytes corresponds a haematocrit value of 0.45). The haematocrit varies with age, gender, blood pathologies and bodily activity [33]. The erythrocytes are distinctively shaped to support a larger surface-volume ratio than other cell types to maximise diffusion area and minimising intracellular distances for gas exchange [33]. This aids its task with carrying oxygen through the supplying phase of the cardiac cycle. White blood cells (leucocytes) and platelets (thrombocytes) only being 1% of the whole blood volume, also known as the “buffy coat”. Thrombocytes are cell fragments that arise from megakaryocytes in bone marrow and their function is to ini-

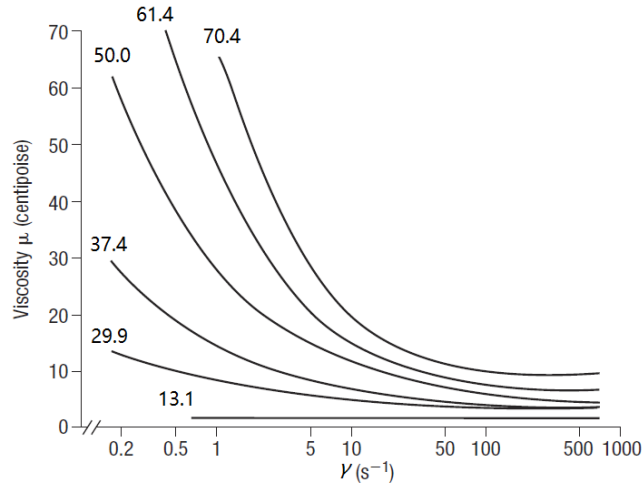


Figure 2.1: Viscosity and shear rate relationship for different haematocrit values. Reproduced from [36] and adapted from [38].

tiate clotting. [34]. The remainder of the blood is plasma, a cell-free watery liquid made up of plasma proteins, electrolytes, carbohydrates and lipids. This composition of the blood has a strong influence to its physiological/mechanical properties. Blood viscosity depends on protein concentration of the blood plasma, the deformability of the blood cells and their tendency to aggregate [35]. Viscosity is the ratio of the substances shear stress against its shear rate ( $\gamma$ ). Blood viscosity is not constant, particularly at lower  $\gamma$  values, therefore the blood is a non-Newtonian fluid [36]. As demonstrated in Figure 2.1, the haematocrit level clearly affects viscosity for  $\gamma < 100/s$  [36, 37].  $\gamma > 100/s$  show asymptotic behaviour, independent from the haematocrit. It is usually understood that blood is considered to be Newtonian in larger arteries as  $\gamma > 100/s$  [38–40]. Furthermore, blood density is accepted to be  $1050 \pm 10 \text{ kg/m}^3$  [41].

The cerebrovascular network within the brain consists of multiple vessel types. Arteries are the largest and thickest of vessels, and carry oxygenated blood at relatively high pressure. Their individual diameter progressively get smaller and bifurcate into

smaller arteries and arterioles that run along the brain surface until they penetrate the brain tissue [42]. These arteries eventually reduce to capillary beds, where the transition of oxygen and other metabolites to brain tissue takes place.

Arteries house the physiological characteristics of well-controlled blood transportation. The source of flow stems from the left ventricle in the heart which supplies the flow in a pulsatile manner. Blood pressure is measured in two readings: systolic and diastolic pressure. Due to certain interference resulting in discontinuity in impedance from such things as wall movement and junctions, waves are partly reflected back which superimpose alongside the forward wave to create the overall pressure and flow waveforms. Figure 2.2 demonstrates this superimposition of the waves. The highest pressure the heart exerts is the systole where the pressure inside arteries in-between beats is the diastole. The supposed normal reading is 120 systolic and 80 diastolic (120/80 mmHg). The systolic and diastolic behaviour shape the fundamental nature of the blood flow which propagates in the system as waves with finite speed, due to the elasticity of the vessel wall.

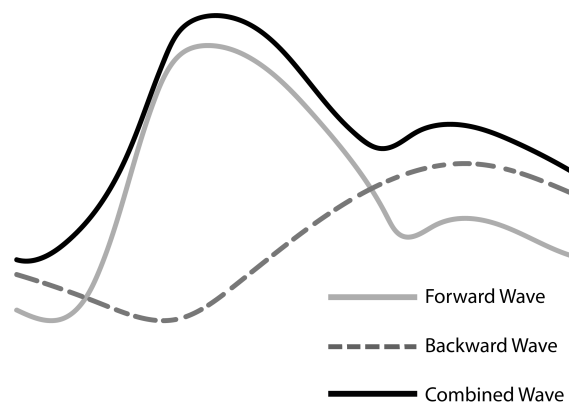


Figure 2.2: Superimposition of forward and backward waveform example.

For nutrients to be absorbed further along in the network requires slow and steady flow at a capillary level. This is achieved through an enlarging overall cross sectional

area as blood flows towards the capillary bed. As the blood flows through the network, the mean arterial pressure progressively drops from 100 mmHg to approximately 2 mmHg. The elasticity of the arteries is responsible for converting the pulsatile flow into a steady flow within the capillaries, this is called the Windkessel effect. Likened to a fire hose, water is driven by a pump (heart), which allows a constant outflow of water to be dispersed out of the nozzle (flow through vessels) due to the air chamber it passes through (arterial elasticity). An illustration of this comparison is presented in Figure 2.3. The viscous properties of the arterial wall dissipate pulsatility to ultimately reach low, steady velocities at capillary level to favour exchanges of gases and metabolites. The elasticity of the arterial wall propagates the pressure and flow waves through the arterial network.

Another important functionality of cerebrovascular system is its ability to maintain a stable level of cerebral blood flow over a wide range of perfusion pressures, this is known as cerebral autoregulation [43]. The concept of autoregulation suggests that in healthy adults, between 50 and 150 mmHg of cerebral perfusion pressure (CPP) or 60 to 160 mmHg of mean arterial pressure (MAP) ( $CPP = MAP - ICP$ , where ICP is intracranial pressure [44]) a homeostatic mechanism takes place. Cerebral blood flow is dependant on CPP and inversely proportional to the vascular resistance. If the CPP increases or

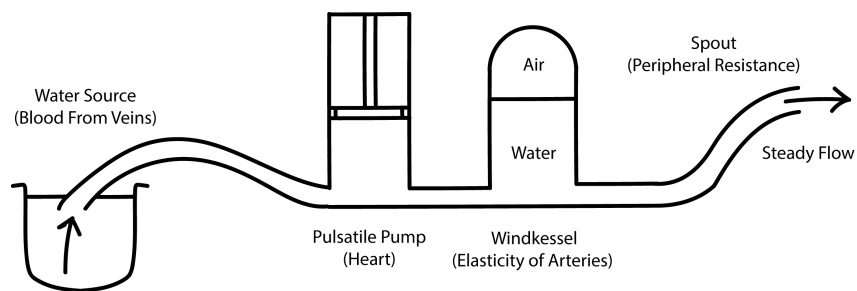


Figure 2.3: The Windkessel effect with the cardiovascular analogy described in brackets. Large artery wall compliance occupies blood volume whilst further down the network, the peripheral resistance assures steady flow.

decreases, the muscular tissue reflex will result in vasoconstriction (narrowing in arterial diameter) or vasodilation (reduction to the vessel diameter to restore physiological values of blood flow physiological values of blood flow), respectively [40, 45, 46]. This relationship can be observed mathematically through the Hagen–Poiseuille equation (Equation 2.2). The graphical representation of autoregulation can be observed in Figure 2.4.

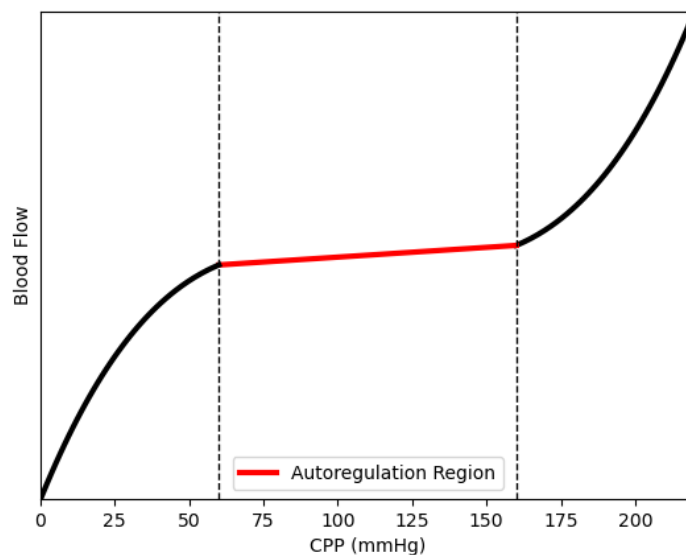


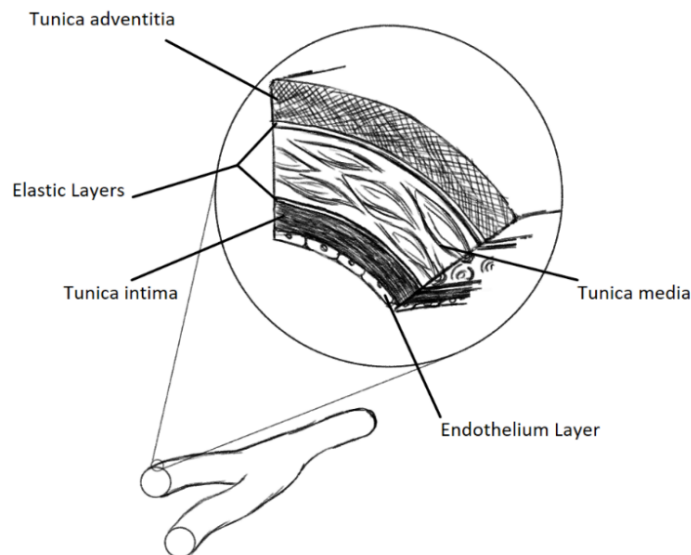
Figure 2.4: The plot represents the extreme low and high boundaries of the CPP (cerebral perfusion pressure) where vascular mechanisms cannot imply vasoconstriction or vasodilation. The red region shows the region where the autoregulation can take place, and where the required modification to resistance is made through altering vessel geometries to still distribute the required blood flow.

### 2.1.2 Cerebrovascular Anatomy and Variations

The cerebral arterial anatomy comprises the network of arteries and the arterial mechanics which respectively has the two main functions; delivering blood to capillaries of bodily organs and tissues according to their need, and to cushion wave pulsations

created by the intermittent contraction of the heart to propagate continuous flow into capillaries [47].

Prior to becoming capillaries, arteries are split into four orders where progressively through the network arterioles reduce in radius; approximately  $30\ \mu\text{m}$  radius for a typical first-order arteriole and  $5\ \mu\text{m}$  for fourth-order arterioles [33]. The general anatomy of the arterial wall consists of three layers of tissue known as tunicae: inner tunica intima, middle tunica media and the outer tunica adventitia, all represented in Figure ???. The lumen area is the blood flow region within a vessel. The barrier between the blood and the inner tunica intima is a single layer of cells known as endothelial cells (endothelium). The endothelium is responsible for material transport from the blood stream, across the vessel wall. Endothelial cells are also responsible for the generation of mechanobiological responses that in turn trigger vasoconstriction and vasodilation. Elastin and collagen are the significant determinants for the mechanical behaviour in larger arteries where the relative amount of elastin compared to collagen varies based on the area of the vascular tree [48], with relatively less elastin in peripheral arteries



where there is a predominance of collagen [49]. Elastin provides reversible extensibility during cycling loading, whereas collagen provides the strength and the ability to withstand high pressure [35, 50, 51]. Vascular wall structure in major arteries differ based on their pathologies which allows the vessel to be more or less susceptible to pressure and flow stresses [52]. These behaviours in arteries is a fundamental attribute for pulse wave propagation.

Arteries similar to other bodily organs and tissues in the population, can differ in their mechanical properties [38]. It is understood that one of the key natural variances to these properties is influenced by age [53]. There are geometrical variances in the population based on age-related size such as younger adults and children although it is recognised that with increasing age, other physiological properties change such as vessel wall thickness [54, 55], wall stiffness [56–58], subsequently outer wall diameter [55], lumen diameter [55] and longitudinal extensibility of the vessel [59]. Other age-related effects from arterial changes stem from the increase in stiffness to the vessels which subsequently cause moderate increase in peripheral resistance and a tendency of increased systolic pulse pressure [53, 58]. On the Contrary, aging effects within the heart are inconsequential and can be referred to the altered load due to change in arterial properties [60].

The arteries connect to build a network of vessels, and in this case of the cerebrovascular network. The network anatomy consists of split pathways that supply blood to the two hemispheres of the brain (left and right). From the aorta, there are four vessels that supply the blood to the brain, the left and right common carotid arteries (CCA) and vertebral arteries (VA). These vessels branch off further downstream and connect into the Circle of Willis (CoW), a central hub and distributor of all cerebral blood flow channelling through six major cerebral arteries and their respective regions (Figure 2.5).

The CoW as demonstrated in Figure 2.5 is a complete CoW. The complete CoW is

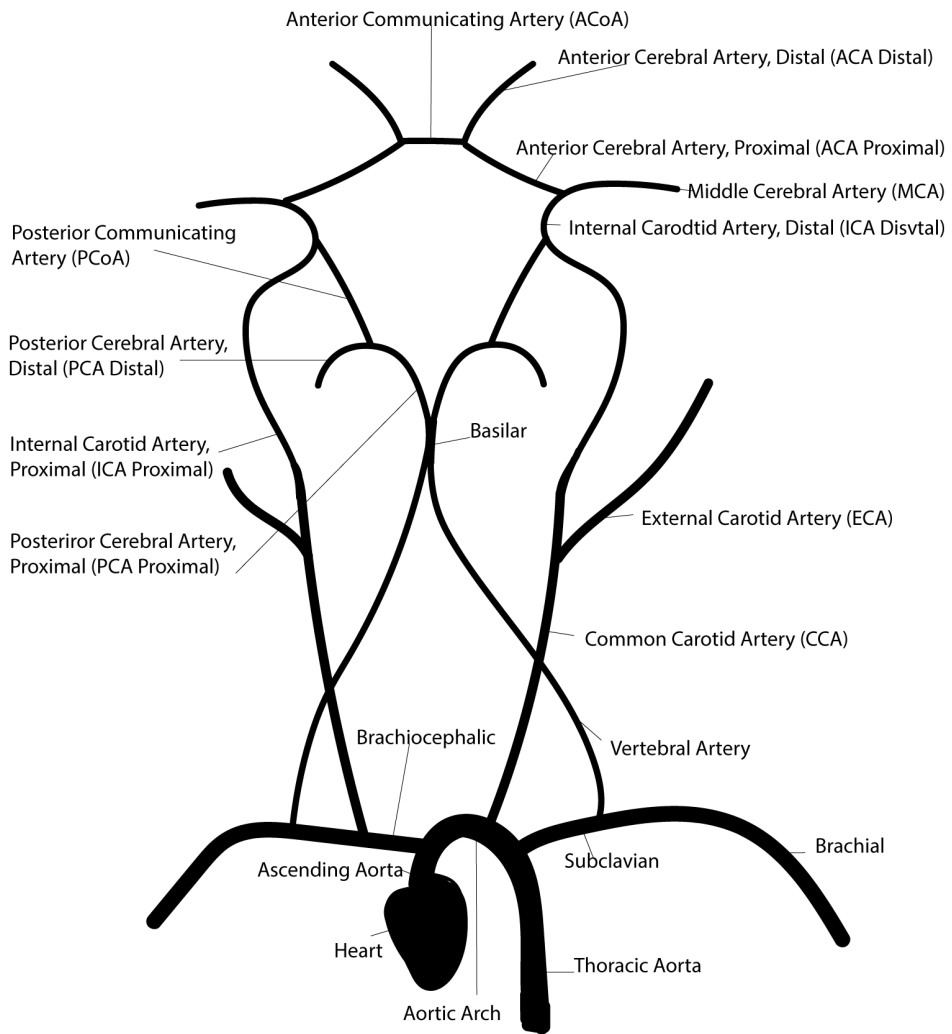


Figure 2.5: Illustration of the CoW and its connection path to the heart.

reported to be present in less than half the population [61]. Non complete variations of the CoW consist of absent vessel(s) effecting the CoW ring-like configuration. With missing or hypoplastic vessels (significantly smaller vessel diameter), there are around 47 different variations of network configurations of the CoW found in large population samples [62]. Amongst the possibility of having a complete CoW or absent vessel(s), other variations can be present. These additional variations consist of hypoplastic vessels, increased channels in a usually single channel path (duplication and triplication) and fenestrations (single vessel dividing into two channels which coalesce back into one, each channel comprises of endothelial and muscular layers and in some cases can share the adventitia [63]) [64, 65].

## **2.2 Ischaemic Stroke**

### **2.2.1 Pathophysiology, Etiology and Risk Factors**

Acute Ischaemia (sudden loss or reduction of perfusion) is caused through several etiologies. The focal cause of the occlusive event is caused by thrombosis (local occlusive event) or embolism (travelled fragment of a thrombus developed elsewhere in the system). Another cause of acute stroke is systemic hypoperfusion which is described as the inadequate delivery of vital oxygen and nutrients to body tissues. Thrombosis is a local occlusion caused by a diseased wall (atherosclerosis) which reduces the flow area. Disruption to the wall causes the atherothrombotic process which initiates clotting through platelets reacting to wall injury and when aggregated form the main composition of an arterial thrombi in the local area [66, 67]. An embolism is non-local and occurs when particles of other thrombi formed elsewhere in the vascular system, are transported and occlude smaller arteries in the cerebrovascular network. It is understood that the majority of ischemic strokes are of an embolic nature [68].

The etiology of acute stroke is classified with reference to the mechanical injury. In 1993, a classification system to categorise the subtypes of ischaemic stroke based on the etiology was developed for the Trial of Org 10172 in Acute Stroke Treatment (TOAST) [69]. Using auxiliary diagnostic study results and clinical features, a set of sub-types were suggested. Decisive opinion of which diagnoses deemed “possible” or “probable” was subjected to two neurologists which did not participate in the creation of the criteria of sub-types. Through using the TOAST classification system for bedside evaluation of 20 patients via clinical features then results of diagnoses tests, the classification identified five sub-types of ischaemic stroke:

- Large-artery atherosclerosis: Significant narrowing, normally more than 50% stenosis or occlusion of a major cerebral artery due to the presumed presence of atherosclerosis. Normally infarcts larger than 1.5cm, (infarcts are a small localized area of dead tissue resulting from failure of blood supply).
- Cardioembolism: Arterial occlusions assumed from an embolus arising in the heart.
- Small-vessel occlusion: infarcts that are smaller than 1.5cm located in cerebral arteries. Also labelled as lacunar infarcts in other classifications.
- Stroke of other determined etiology: Patients that suffer rare cases of stroke; nonatherosclerotic vasculopathies, hypercoagulable states, hematologic disorders.
- Stroke of undetermined etiology: where clinicians can’t provide clear confident diagnosis.

Out of the 20 patients, the neurologists agreed on 19 of the 20, where 11 reached a specific etiologic diagnosis, causality of stroke was not determined in the other nine. Since

the recognition of the TOAST classification, the development of new data, techniques and imaging which led to the updated TOAST classification (SSS-TOAST), the Causative Classification System and the ASCOD phenotyping (A, atherosclerosis; S, small vessel disease; C, cardiac pathology; O, other causes; and D, dissection) classification [70–73].

IS is understood to have several risk factors in association. It is understood that the most significant risk factors that contribute over 90% of risk of ischaemic stroke are preventable [74]. The prominent preventable risk factors are high blood pressure (hypertension) [75–78], smoking [79–81], significant alcohol consumption [82], obesity/lack of physical activity/diet quality [83–91] and psychological conditions [92]. Age and gender on the contrary are considered as significant non-preventable risk factors [93]. Subsequently, there are always new developments on understanding cause of ischaemic stroke with new literature on risk factors, the latest being a study demonstrating COVID-19 as an independent risk factor for ischaemic stroke [94].

### **2.2.2 Diagnosis and Treatment**

In 2008, an update of the 2000 European Stroke Initiative (EUSI) Recommendations for Stroke Management [95, 96] was undertaken by the European Stroke Organisation (ESO) [97]. The guidelines cover both Ischaemic stroke and TIA which are to be considered a single category. It highlights that acute stroke management relies on the integration of emergency medical services, emergency department staff and stroke care specialists. Communication and collaboration between the emergency medical services and department staff, radiologists clinical laboratories and neurologists are crucial for the delivery and decision of treatment [98–100]

Regarding diagnostic tests, all patients will undergo brain imaging; computed tomography (CT) or magnetic resonance imaging (MRI), and electrocardiogram (ECG) and a set of lab tests for: erythrocyte and thrombocyte count, blood glucose, C-reactive

protein and sedimentation rate and hepatic and renal chemical analysis. Other diagnostic tests can be issued, but only if the clinician deems necessary due to certain indications [97]. Although the requirement for patients to undergo one of two imaging procedures, they have their individual advantages and subsequently disadvantages (Table 2.1). The option may sometimes depend on the availability in the stroke centre the patient is being treated at. Although CT poses limited haemodynamic assessment, it is suggested that MRI is capable of assessing cardiovascular haemodynamics non-invasively via volumetric and phase-contrast analysis [101]. In fact current MRI techniques are

	Advantages	Disadvantages
Computed Tomography (CT)	<ul style="list-style-type: none"> <li>· Rapid image acquisition</li> <li>· Excellent spatial resolution (&lt;1 mm)</li> <li>· 3D dataset acquisition for ability for post-processing/reconstruction</li> <li>· Typically well tolerated by patients</li> <li>· Not contraindicated in patients with ferromagnetic/metallic implants</li> </ul>	<ul style="list-style-type: none"> <li>· Radiation exposure</li> <li>· Potential need for iodinated contrast dye</li> <li>· Limited temporal resolution (best temporal resolution with current generation scanners on order of 75 ms)</li> <li>· Limited hemodynamic assessment options currently</li> </ul>
Magnetic Resonance Imaging (MRI)	<ul style="list-style-type: none"> <li>· Tissue characterization</li> <li>· Excellent spatial resolution (1–2 mm)</li> <li>· Temporal resolution better than CT (typically 25–50 ms)</li> <li>· Unlimited imaging plane orientation and ability to acquire 3D datasets</li> <li>· No need for contrast (i.e., can be performed on patients with decreased GFR)</li> <li>· Increased ability to assess cardiovascular hemodynamics noninvasively via volumetric and phase-contrast analysis</li> </ul>	<ul style="list-style-type: none"> <li>· Increased image acquisition time</li> <li>· Potential for patient claustrophobia</li> <li>· Possibility, although rare, for NSF following gadolinium contrast administration</li> <li>· Inability to image patients with absolute contraindications including those with ferromagnetic implants (i.e., pacemakers, ICDs, intracerebral vascular coils, etc.)</li> </ul>

Table 2.1: CT and MRI advantages and disadvantages.

able to assess cerebral blood flow, cerebral blood volume, cerebral metabolic rate of oxygen, and oxygen extraction fraction in the setting of cerebrovascular disease [102]. Even with more advanced MRI procedures the resolution of cerebral blood flow is quantified and presented in milliliters of blood per 100 grams of tissue per minute [102].

Post diagnosis, treatment is initiated. Pharmacological treatment of stroke can be split into two categories, general and specific. General refers to the strategies aimed to stabilize a critically ill patient to control systemic issues that may interfere with stroke recovery. Management aspects of this type of treatment revolves around respiratory and cardiac care, fluid and metabolic management, blood pressure control, prevention and treatment of additional conditions (seizures, venous thromboembolism, dysphagia, aspiration pneumonia etc.) and ICP. Specific treatment infers to the problem directly such as thrombolytic therapy. [97]

General thrombolytic therapy (Thrombolysis) is the use of medication of breaking down clots in vessels. The most typical therapy is with intravenous (medication administered through veins) rtPA (recombinant tissue plasminogen activator), and when given within a three-hour period after onset of stroke, usually results with significantly improved outcomes in patients with ischaemic stroke [103]. Other intravenous thrombolytics are intravenous streptokinase and intravenous desmoteplase. Streptokinase is associated with an unacceptable risk of haemorrhage and death [104]. Intravenous desmoteplase is administered within three to nine hours of onset stroke. Alternatively, intra-arterial (administrated medicine through arteries) are also available such as pro-urokinase (PUK), shown to have better outcome given within six hours on set of stroke [105]. To further reduce the chances of another clot forming, antiplatelets are offered such as aspirin, clopidogrel and dipyridamole, usually taken orally. Anticoagulants reduce the risk of a patient developing further clots. Anticoagulants do this by changing the chemical composition of the blood. There are both long term and short-

term anticoagulants that can be given. Anticoagulants that are required for treatment are issued to patients that suffer from atrial fibrillation (condition that results in an irregular heart beat that can cause blood clots), patients that have a history of blood clots or a patient who suffers from deep vein thrombosis [97].

The aim of the treatment is to remove the occlusion to reestablish blood flow, and mechanical thrombectomy (MT) methods demonstrate an alternative way to achieve this. In terms of treatment, between 1985 and 2002 data that assessed vessel flow restoration (partial or complete), either spontaneous or therapeutically induced in an acute ischemic stroke indicated that mechanical treatment was the most successful with a flow restoration rate of 83.6% (92/110 patients) [11]. In addition to this, 16.4% of patients (18/110) failed to have blood flow restored, potentially causing further disability or even death. Looking deeper into MT techniques, some show more superior outcomes than others. Standard stent retrieval (SR) devices are the base to almost all MT techniques. Balloon guided catheters (BGCs) work in conjunction with SR deployment and provide several advantages in application of treating acute stroke. They provide proximal support for retrieving distal intracranial thrombi and allow direct microcatheter application for SR deployment. Inflation of a balloon creates flow seizure and subsequent aspiration through the BGC which is used to create flow reversal in attempt to prevent downstream embolization (smaller clot fragments lodging and occluding smaller vessels downstream) by the targeted clot [106] (Figure 2.6). BGCs in conjunction with SR are providing improved rates of revascularization in comparison to non-BGC thrombectomies, a rate of 89.2% success compared to 67.9% [107]. A reduced time to revascularization, reduced infarct size, and enhanced results was also presented when compared with standard guide catheters such as the Solitaire device [108]. Although this may suggest superiority over pharmacological routes of treatment, MT is effective with treating only larger arteries as smaller vessels are not safe and in cases, not physically

possible to implement catheters into and deploy a retrieval device. In addition to this, combination of both intravenous thrombolysis and MT treatments have reported better functional outcomes, lower mortality, higher rate of successful recanalization, requiring lower number of device passes in comparison to MT alone [109].

Alongside BGC with SR, another successful meta MT technique; the direct aspiration first pass technique (ADAPT) utilizes aspiration through a bore catheter which is placed directly at the face of the thrombus and through aspiration the occlusion is either broken and aspirated or retracted based on the mechanical properties [110]. For both respective techniques, the aspiration is performed by the clinician manually through a 20, 50 or 60 ml syringe [107, 110]. It is also understood that the success is dependant on the thrombus composition suggesting that BGC might be more effective for fibrin-rich clots and ADAPT might be more effective for red blood cell-rich clots [111]. Use of contact aspiration has shown to be more useful and linked with higher recanalization success when utilized with a BGC [112, 113]. This method is suggested to create the required endovascular haemodynamic environment to reduce the risk of distal embolization [113]. Objectively, the main role of aspiration techniques is to prevent distal embolization, which is understood to be affected by the catheterization technique and clot mechanics [114].

## **2.3 Modelling**

### **2.3.1 Fundamental Biomechanics of Arterial Blood Flow**

Haemodynamics is the branch of physiology dealing with the forces involved in the circulation of the blood. The laminar or turbulent behaviour of arterial blood flow is dependant on the Reynolds number:

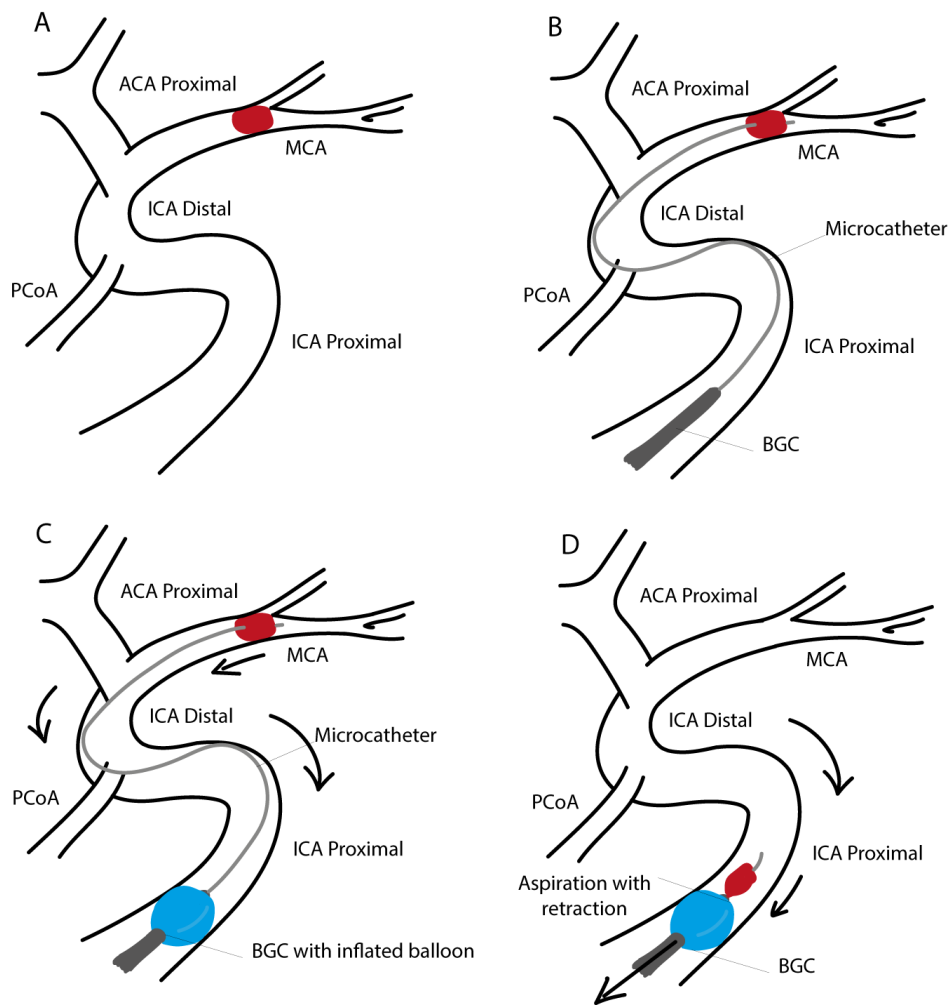


Figure 2.6: Illustration of the BGC with SR treatment. A) A clot is lodged in the network occluding blood flow (middle cerebral artery in this case, MCA). B) the BGC is positioned in the proximal part of the internal carotid artery (ICA) or in the common carotid artery (CCA), a microcatheter of the SR device is deployed and pierces the clot, capturing it. C) The balloon at the tip of the BGC is inflated halting flow upwards of the BGC position. D) Aspiration is applied whilst simultaneously retrieving the SR with the clot.

$$Re = \frac{\rho V D}{\mu} \quad (2.1)$$

where  $\rho$  is blood density, mean flow velocity is  $V$ , vessel diameter is  $D$  and the dynamic viscosity is  $\mu$ . Typical Reynolds numbers readings can range from 1 in small arterioles to approximately 4000 in the largest artery (the aorta) [115]. The Hagen-Poiseuille equation (Equation 2.2 where  $Q$  is the volumetric blood flow,  $R$  is the radius,  $\Delta P$  is the change in pressure ( $P_1 - P_2$ ),  $\mu$  is the dynamic viscosity of the fluid and  $L$  is the length of the pipe), which can be derived from the Navier-Stokes equations, is a solution that describes the pressure drop of a fully developed fluid flowing through a long cylindrical pipe of constant cross section where the fluid is laminar, incompressible and Newtonian.

$$Q = \frac{\pi R^4 \Delta P}{8\mu L} \quad (2.2)$$

Due to the nature of blood vessels, modelling of arterial blood flow has been closely likened to the modelling of pipe flow. Even though blood flow does not satisfy the assumptions underlying the Hagen-Poiseuille's equation, this relationship is often used in Cardiovascular Biomechanics to describe the relationship between volumetric flow rate ( $Q$ ), pressure drop along a vessel ( $\Delta P$ ) and resistance to flow ( $R = 8\mu L/\pi R^4$ ).

An important feature of arterial blood flow is its pulsatility. The pulsatile behaviour of blood flow, and the resulting velocity profiles, can be represented through the Womersley number, a dimensionless number that represents the ratio between inertial forces (pulsatile flow frequency and density) and viscous forces (viscosity). The definition of  $\alpha$  is:

$$\alpha = R \sqrt{\frac{\omega \rho}{\mu}} \quad (2.3)$$

Also interpreted as the lumen radius multiplied by the square root of the transient in-

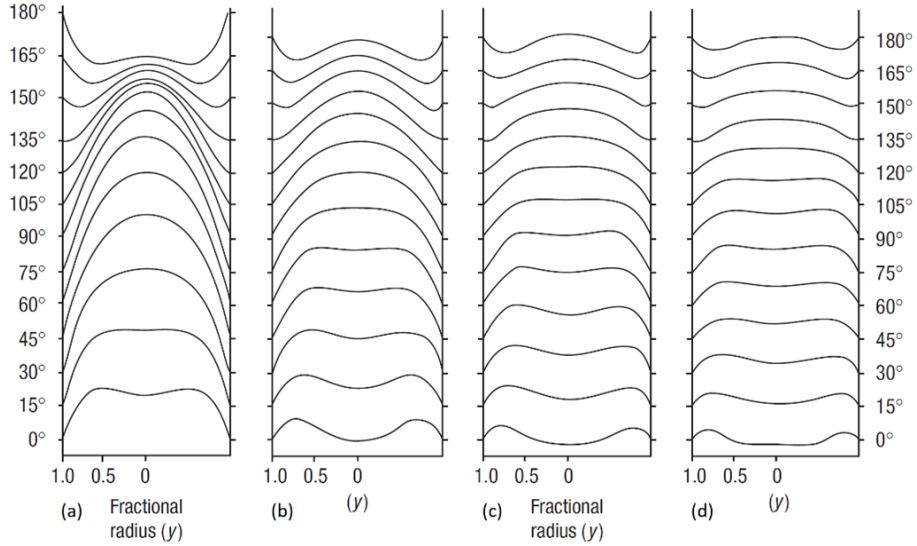


Figure 2.7: Pulsatile wave forms represented by the Womersley number with a sinusoidal pressure gradient of  $\cos(\omega t)$ . Profiles plotted in steps of  $\Delta\omega t = 15^\circ$ . (a)  $\alpha = 3.34$ , (b)  $\alpha = 4.72$ , (c)  $\alpha = 5.78$  and (d)  $\alpha = 6.67$  [38].

ertial force over the viscous force where  $\omega$  is the angular frequency. If the Womersley parameter  $\alpha$  is low (such as in small vessels), viscous forces are significantly larger than the unsteady/transient forces thus the typical velocity profiles are parabolic and oscillates symmetrically to the vessel axis, in phase with the driving pressure gradient [116]. For larger  $\alpha$  at approximately 10 and above, transient forces are more dominant causing a flatter velocity profile. Figure 2.7 demonstrates the progression of the transient pulsatile flow for four values of  $\alpha$ . Typically, flow in the ascending aorta has a Womersley number of around 16.1 to 13.3 in humans before descending, whereas further down in the carotid arteries  $\alpha$  is approximated at 4.4 in canines, presumed similar in humans [40, 117].

Larger arteries have elastic properties which allow expansion as described by with the Windkessel effect. Assuming rigid walls in an arterial model could be limiting, especially when assessing the larger arteries such as the aorta, carotid artery and others of

similar diameter size as they expand to reduce the pulsatile waves propagating through the network. Transmural pressure is a major haemodynamic arterial force, and due to this, the material properties of the vessel resist the expansion force with a hoop stress in the circumferential direction which can be estimated by Laplace's Law:

$$\sigma = \frac{Pr}{h} \quad (2.4)$$

Where  $h$  is the cylinder or vessel wall thickness,  $r$  is radius,  $P$  is the internal pressure. A description of vessel wall displacement would require a more advanced description of wall mechanics, for example Hooke's Law and its material properties such as Young's Modulus  $E$ , Poisson's ratio  $\nu$ . Considering a pulsatile flow inlet and the vessel is fixed, then the compliance and distensibility can be estimated as a change in lumen dimension (radius, diameter or cross-sectional area) or flow rate with the given change in flow pressure [38]. The arterial wall stiffness and thickness are the parameters that impact the pulse wave velocity or wave speed  $c$  and is presented by the Moens-Korteweg equation:

$$c = \sqrt{\frac{hE}{2r\rho}} \quad (2.5)$$

Where  $h$  is wall thickness,  $E$  is elastic modulus,  $r$  is lumen radius and  $\rho$  is blood density. This equation is defined as the so-called phase velocity (wave speed in a tube without reflections) and is derived for non-viscous fluid but is a good approximation for conduit arteries filled with blood [118].

### 2.3.2 Vascular and Thrombectomy Modelling

Vascular modelling approaches through means of analytical calculations, computational simulations, *in-vivo* and *in-vitro* has extensive publications in the literature. When

it comes to simulation of thrombectomy and ischaemic event, the literature poses a growing library of research with various computational models of vasculature and the CoW specifically developed to non-invasively predict the haemodynamics and respective parameters in intracranial arteries for the assessment of ischaemia and other clinical risks [119].

Experimental studies of vascular replicas of patient specific anatomy based on imaging studies yielded new insights to arterial fluid mechanics, and with the advancement of computational fluid dynamics (CFD) a similar benefit was attained [120]. CFD analyses for haemodynamics in the cerebrovascular network are widely studied in the literature from reduced anatomical network models such as bifurcations to full CoW models. The haemodynamics in the CoW is not completely understood which results in medical misjudgement and complications during surgical intervention [121]. It is also understood that subtle changes in vascular geometry are believed to affect blood flow fields significantly [122, 123]. Example scenarios can be plaque build-up in the arterial walls or even vessel wall expansion due to elastic compliance. Although most CFD simulations assume rigid walls, the inclusion of compliant walls concur a more complete comprehension of the haemodynamic behaviour. Simultaneous coupling of wall mechanics through finite element analysis (FEA) on the wall alongside the CFD analysis of the blood flow acknowledge a more comprehensive but computer demanding technique known in the literature as fluid structure interaction (FSI) [120].

Reduced-order modelling, such as those proposed in this thesis, offer a valid alternative to the computationally more demanding higher-dimensionality models, and are capable to describe and capture many of the clinically-relevant blood flow features. On a computational basis, 0D CoW models use electrical analogy and 1D CoW models use reduced/simplified Navier-Stokes equations, both configured using *in-vivo* physiological measurements, compared to the full Navier-Stokes equations used in 3D computa-

tional simulations with the advantage of 3D physiological in-vivo measurements [124]. With the loss of dimensionality and the addition of multiple assumptions required for reduced order models, they are still capable of acquiring a feasible range of information with the advantage of reducing simulation time and increasing network complexity in comparison to 3D.

Features of an acute ischaemic stroke simulation would include an occlusion in the network, emulating the thrombus alongside the respective treatment option also simulated. With a need to understand the haemodynamic interaction between treatment and occlusion(s), the addition of understanding the catheterization and response in variations of the CoW is of interest to the literature [124]. As mentioned, the literature provides an extensive library of vascular models in the form of experimental and computational. Understanding the interaction of thrombectomy devices is an area of research that is only recently becoming of interest.

Recent *in-vitro* studies have used phantoms to assess the efficiency of recanalization through certain MT techniques and understanding embolization behaviours [13,15]. There have been analytical attempts to further understand clot mechanics during aspiration where certain studies developed a mathematical model that presents the clots dynamics using a mass-spring setup, results were validated using computational Finite Element Methods (FEM) and showed good agreement [125]. Other works have used coupling of 1D and 3D models to further assess the interactions of the CoW during aspiration of the clot from different positions where the 3D model was applied in the region between the clot and the catheter tip [126]. Modelling of the clot in that study was presented as a highly viscous fluid. More recent of the studies presents an *in-silico* trial presented by the INSIST research group where a real stroke case was modelled [127]. Vasculature was created from CT and histologic analysis to determine clot composition. The thrombectomy (SR) procedure from deployment to retrieval of the clot was broken

down into four phases. Results showed that clot fragmentation did not occur.

These studies all present their limitations, where the most common of them is the use of rigid vessel walls. Other limitations of these studies is the neglect of wave propagation and reflections, no vessel resistances, no auto-regulation and rigid catheter placement. The literature presents many 1D models that can represent these characteristics but said models have not been applied to simulate stroke and its treatment.

## 2.4 Conclusions

The literature presents several modelling approaches to assess haemodynamics in various applications such as the influence of network variations in the CoW. However, modelling the influence of ischaemic stroke and its treatment on the haemodynamics of the cerebral network is very limited. Existing modelling approaches compromise on several modelling features such as: significant computational time due to the adaptation of higher-dimensionality and complex models, representation of arterial wall mechanics, an appropriate understanding of the influence of wave velocity and propagation on blood flow, simulation of the presence of a clot, and its removal using a balloon-catheter and aspiration. The literature also indicates that thrombectomies which utilise BGCs present higher recanalization rates yet the available computational thrombectomy studies lean more towards distal-aspiration-only catheters or SR analyses. This presents a gap in the literature in terms of a BGC and thrombectomy model that can describe additional, important mechanisms such as wall compliance and a more comprehensive description of the effects of wave propagations and waveforms on blood flow.



## **Chapter 3**

# **Blood Flow Model and Methodology**

### **Summary**

Simulation of arterial blood flow with a 1D model is well covered in the literature. However, the use of 1D models to study mechanical thrombectomy treatment is a novel application of this approach. For it to be possible, modifications to a verified and validated in-house 1D software (openBF) are necessary to simulate the effects of a basic BGC deployment, aspiration, presence of a catheter and blood flow occlusion due to the presence of a blood clot. In this chapter, the method of research is explained followed by an introduction to the initial framework (openBF). In the last part of the chapter, the modifications to the model are described and discussed.

## 3.1 Research Method

Using an already validated 1D model (Section 3.2), a method to allow the simulation of stroke treatment and occlusion (Section 3.3) within the model was required. As proposed in the objectives, a baseline model was required to test a benchmark set of results (Chapter 4) for comparison with other studies. For following studies (Chapters 5 and 6), a single parameter variation was proposed where parameters include network branches, blood or vascular properties in attempt to partly mimic realistic and typical case scenarios. Comparing the benchmark through the single parameter change studies provides a quantitative way of assessing the changes without significant alterations from different studies.

### 3.1.1 Clinical Procedure and Set-Up

The setup of the ischaemic event and the treatment was based on a typical common case presented in the following example performed at the University Hospital of Tours, France. In this example, a BGC was used to mechanically remove a clot occluding the distal part of the left MCA (Figure 3.1). A balloon catheter was placed in the proximal region of the left proximal internal carotid artery (L-ICA). Aspiration was performed manually through a 60 ml syringe.

To implement the treatment procedure, the process was divided into five phases that signify key stages of the procedure and event to observe the present haemodynamic behaviours:

- Phase 1 - blood flow through the described network before the ischaemic event;
- Phase 2 - the ischaemic occlusion is now present in the system, halting complete flow thorough the terminating branch of the L-MCA;
- Phase 3 - through administration of the device, the balloon is inflated in the prox-

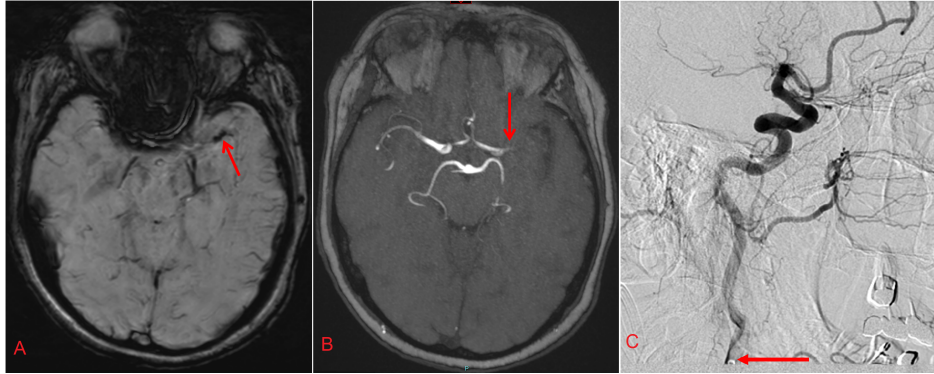


Figure 3.1: Medical images indicating the location of the blood clot in L-MCA. A) Image sequence identified a 7mm clot at M1 segment of L-MCA. B) AngioMRI confirmed left MCA occlusion (M1 segment). C) Images showing the 8F balloon catheter when it was placed in proximal region of the proximal L-ICA.

imal region of the left proximal ICA, at this stage there are two locations within the described network that are halting flow, the ischaemic event and the devices inflated balloon;

- Phase 4 - with the balloon in place, assuming the penetration of the clot via the stent retrieval device, aspiration is now performed (as aspiration would be performed simultaneously with physical retrieval, this phase simulates the small time instance prior to retrieval). The clot is still occluding the L-MCA during this phase;
- Phase 5 - assuming successful retrieval of the clot through the tip of the BGC therefore no longer occluding the L-MCA, aspiration and balloon are still present for a small period of time to consider the role of aspiration in preventing distal embolization.

Phases 1-4 represent the pre-retrieval phase. Phase 5 is the post-retrieval phase. These five phases are to be simulated as independent events to provide details of the haemodynamic behaviours at key intervals. Understandably, this methodology does not

record any transient data between these five stages as the study described is minimised and simplified to instantaneous points during the timeline. Minimising the complexity of the model was intentional to observe the prospect and understand the limitations of a simplified set-up to then comment on the areas of future work for improving the model and the accuracy.

Due to the nature of the 1D model and the five phases taken at instantaneous intervals of the procedure, parameter changes to the network that would take place in the transient representation of the procedure are ignored such as auto-regulation. The thrombectomy procedure induces multiple varied parameters throughout the five defined phases making it difficult to introduce auto-regulation effects. Details of parameters on how auto-regulation would impact the vasculature haemodynamics is already limited in the literature without the induction of a thrombectomy device during stroke treatment that takes place over short time period. This exclusion to the set-up and model does not mean that the mechanistic effects of auto-regulation don't have an effect on outcome but should be considered when observing the simulation results. Overall, this is a limitation of the static five-phased set-up of the model and is discussed further in Chapter 8.

### **3.1.2 Network Set-up and Haemodynamic Parameters**

The basic parameters for the baseline model are as follows: blood was assumed to be incompressible (density of  $1060 \text{ kg/m}^3$ ) and Newtonian ( $\mu$  of  $0.004 \text{ Pa}\cdot\text{s}$ ). Heart rate imposed at the inlet was set to 60 bpm (period  $T = 1 \text{ s}$ ) and is provided with the flow wave presented in Figure 3.2.

For the application of the the aspiration, the rate was set as  $5 \text{ ml/s}$  which is induced by a 60 ml syringe. This value was calculated from a visual observation of a clinician demonstrating the procedure though using the time taken and the volume of contents in

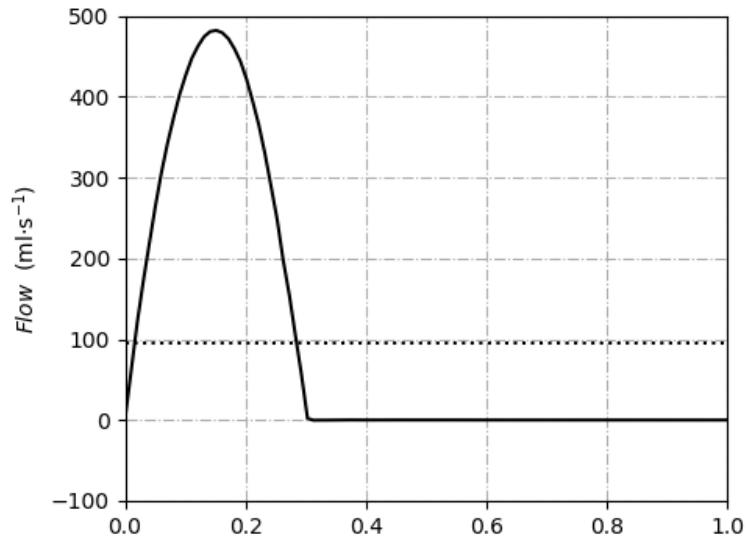


Figure 3.2: Volumetric flow rate waveform applied at the base of the ascending aorta as inlet boundary condition. Dotted lines represent arithmetic average value over the period. Period ( $T$ ) is 1 second.

the syringe to calculate the flow rate. Additionally similar flow rates of typical aspiration catheters are demonstrated in the literature [128].

Creating the network required physiological data taken from the literature. Anatomical data of a typical healthy patient reported in [61], collected from studies [18,129,130], and presented in Table 3.1 was used to develop and parameterize a complete CoW network and the supplying vessels that join it to the heart. Figure 3.3 demonstrates this baseline network set-up.

This network excludes the representation of significantly smaller bifurcating arteries that don't contribute to enabling collateral flow of the CoW unlike the communicating arteries, or are small enough to assume their contributing affects are insignificant. These vessels would be:

- Pontine arteries, anterior inferior cerebellar artery and superior cerebellar artery that branch out from the basilar artery;

Vessel	ID	$L$ (mm)	$R_0$ (mm)	$E$ (MPa)	$h_0$ (mm)
Ascending Aorta	1	40	12	0.4	1.63
Aortic Arch Proximal	2	20	11.2	0.4	1.26
Brachiocephalic	3	34	6.2	0.4	0.8
Aortic Arch Distal	4	39	10.7	0.4	1.15
L-CCA	5	208	2.5	0.4	0.63
R-CCA	6	177	2.5	0.4	0.63
R Subclavian	7	34	4.23	0.4	0.67
Thoracicaorta	8	156	9.99	0.4	1.1
L Subclavian	9	34	4.23	0.4	0.67
L-ECA	10	177	1.5	0.8	0.38
L-ICA Proximal	11	177	2	0.8	0.5
R-ICA Proximal	12	177	2	0.8	0.5
R-ECA	13	177	1.5	0.8	0.38
R Vertebral	14	148	1.36	0.8	0.34
R Brachial	15	422	4.03	0.4	0.67
L Brachial	16	422	4.03	0.4	0.67
L Vertebral	17	148	1.36	0.8	0.34
L-ICA Distal	18	5	2	1.6	0.5
L-PCoA	19	15	0.73	1.6	0.18
R-PCoA	20	15	0.73	1.6	0.18
R-ICA Distal	21	5	2	1.6	0.5
Basilar	22	29	1.62	1.6	0.4
L-MCA	23	119	1.43	1.6	0.36
R-MCA	24	119	1.43	1.6	0.36
L-ACA Proximal	25	12	1.17	1.6	0.29
R-ACA Proximal	26	12	1.17	1.6	0.29
L-PCA Proximal	27	5	1.07	1.6	0.27
R-PCA Proximal	28	5	1.07	1.6	0.27
L-ACA Distal	29	103	1.2	1.6	0.3
R-ACA Distal	30	103	1.2	1.6	0.3
ACoA	31	3	0.74	1.6	0.19
L-PCA Distal	32	86	1.05	1.6	0.26
R-PCA Distal	33	86	1.05	1.6	0.26

Table 3.1: Vessel geometrical and mechanical properties.  $L$  is length,  $R_0$  is characteristic radius under zero loading conditions,  $E$  is Young's modulus and  $h_0$  is the vessel wall thickness. [18, 61, 129, 130]

- Ophthalmic artery which bifurcates from the ICA;
- Posterior inferior cerebellar artery and anterior spinal artery that bifurcate from the vertebral artery;
- Anterior choroidal artery which bifurcates from the MCA.

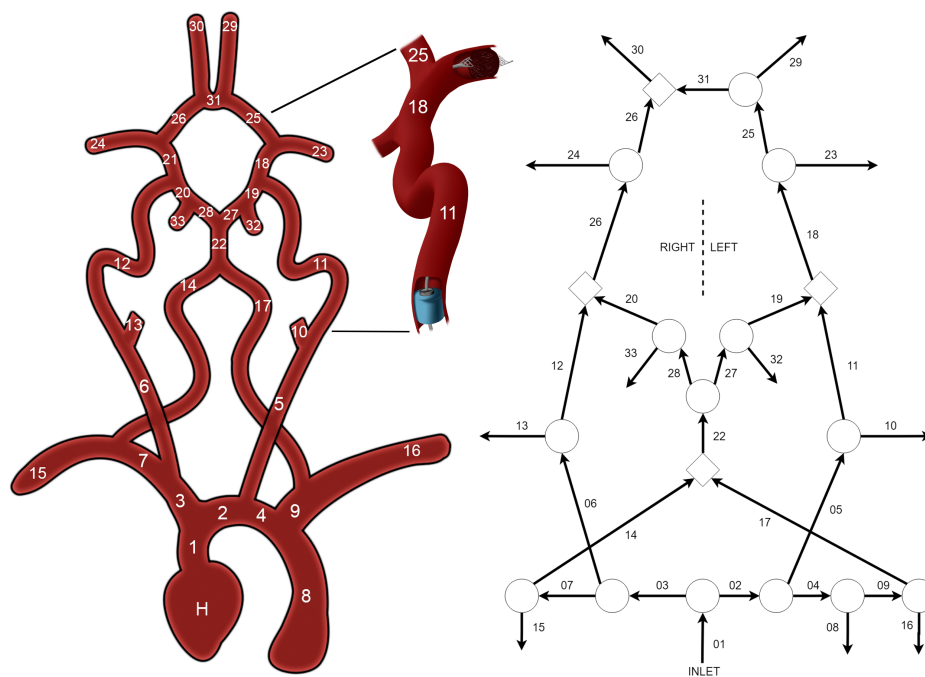


Figure 3.3: Schematic representation of the arterial network. (Left) Illustration of vessels, their IDs as represented in Table 3.1, blood clot and BGC locations. (Right) 1D representation of vessels, arrows indicating assumed direction of flow within each vessel, and junction types (circles signify bifurcation nodes, diamonds signify anastomoses).

### 3.2 Initial Modelling Framework: openBF

openBF is a verified and validated open-source arterial 1D blood flow model [29, 30], where blood vessels are assumed to be circular, straight, long with a narrow geometry (lumen radius  $\ll$  vessel length) with no angulation or curvature, and elastic with zero strain in the axial direction (displacement in radial direction only). Angular separation is not considered at vessel junctions due to the nature of the 1D model. Two 1D governing equations are derived from the 3D equations ensuring conservation of mass (continuity) and momentum (Navier-Stokes). This is achieved through assuming axisymmetric vessels integrated along the  $r$  polar coordinate. The system is closed by an elastic constitutive equation linking transmural pressure to vessel cross sectional area [29]. The following is the complete representation of the three governing equations (continuity, momentum and wall compliance equations respectively):

$$\left\{ \begin{array}{l} \frac{\partial A}{\partial t} + \frac{\partial Q}{\partial z} = 0 \\ \frac{\partial Q}{\partial t} + \frac{\partial}{\partial z} \left( \alpha \frac{Q^2}{A} \right) + \frac{A}{\rho} \frac{\partial P}{\partial z} = -2 \frac{\mu}{\rho} (\gamma_v + 2) \frac{Q}{A} \\ P(A) = P_{ext} + \beta \left( \sqrt{\frac{A}{A_0}} - 1 \right), \quad \beta = \sqrt{\frac{\pi}{A_0}} \frac{E h_0}{1 - \nu^2} \end{array} \right. \quad (3.1)$$

where  $t$  is time,  $z$  represents the longitudinal direction coordinate,  $A(z, t)$  is the vessel cross-sectional area,  $Q(z, t)$  is the volumetric flow rate of the blood,  $\alpha$  is the Coriolis' coefficient,  $\rho$  is the blood density,  $P(z, t)$  is the blood pressure,  $\mu$  is the blood dynamic viscosity,  $\gamma_v$  is a parameter defining the shape of the axial velocity profile,  $P_{ext}$  is the vessel external pressure,  $E(z)$  is the vessel elastic modulus,  $\nu$  is the Poisson's ratio of the vessel material,  $A_0(z)$  is the characteristic reference cross-sectional area and  $h_0(z)$  is the arterial wall thickness reference. Full derivation is found in [29].

The mathematical model is discretized using a finite-volume explicit scheme to compute the numerical solution using the (MUSCL: monotonic upstream-centred scheme for conservation laws) [131]. The model operates with flow or pressure inlet conditions and 0D lumped parameter three-element Windkessel models at the terminal branches of the network. Interface conditions are defined at bifurcations, junctions and anastomoses in which the flow quantities are computed by means of the Newton-Raphson method, and where continuity of mass and static pressure are preserved [29, 30]. The model assumes a flat velocity profile to compute the convective term and calculates viscous losses by assuming a parabolic profile.

The Coriolis' coefficient accounts for the fact that the momentum flux computed with averaged quantities is different from the actual momentum flux. The shape of the velocity profile in openBF is defined through a non-dimensional parameter  $\gamma_v$ . In addition to this,  $\alpha$  satisfies  $\alpha \geq 1$  and is dependent on the velocity profile as:

$$\alpha = \frac{\gamma_v + 2}{\gamma_v + 1} \quad (3.2)$$

As mentioned, the velocity profile is considered parabolic only for the viscous term, whereas otherwise considered as a flat profile (1D). The axial velocity profile  $v_z$  which is described through approximation as:

$$v_z = \frac{\gamma_v + 2}{\gamma_v} u \left[ 1 - \left( \frac{r}{R} \right)^{\gamma_v} \right] \quad (3.3)$$

where  $u$  is axial velocity. A plot representing the variation of  $\gamma_v$  values to profile shape is represented in Figure 3.4. In particular,  $\alpha = 4/3$  for a Poiseuille flow, alternatively, flow with a transient velocity profile would be plausible through the Womersley pulsatile theory as previously discussed in Chapter 2.

Regarding the constitutive equation, it assumes that the only force induced on the

vessel wall is exerted by the fluid in the radial direction and hence shear stress is ignored. The derivation of this equation stems from Laplace's (Equation 2.4) in the  $\theta$  coordinate and the primary terms altered to match the consistency of the other two equations,  $P$ ,  $Q$ ,  $A$ .

openBF and its performance is validated through comparing its simulation results with previous literature of both 1D and 3D simulations as well as experimental results, both *in-vitro* and *in-silico*. Results of comparison for openBF shows significant alignment and reliability in comparison with other 1D and 3D simulations [29]. More specifically the validation for the CoW network was compared through the work of [61], where another 1D model was validated alongside *in-vivo* results, the results of this models for velocity in the subclavian, brachiocephalic, and carotid arteries was used to compare openBFs results in aim of its validation.

Although openBF is a validated model, unlike the model presented by [132], it lacks

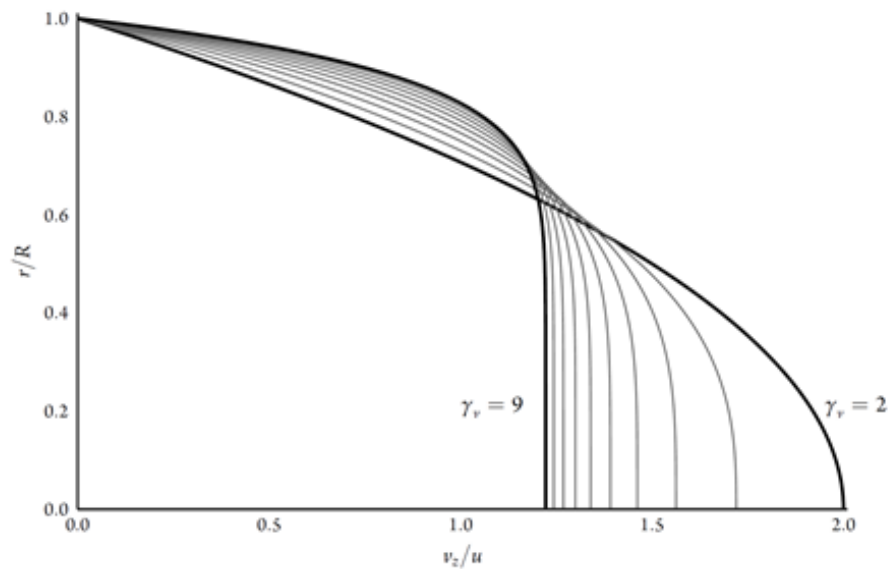


Figure 3.4: Radial velocity profile for different values of  $\gamma_v$ , on show  $2 \leq \gamma_v \leq 9$  [29]

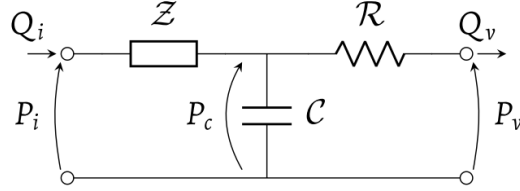


Figure 3.5: Three-element Windkessel circuit. Quantities with subscript  $i$  refer to capillaries entrance; quantities with subscript  $v$  refer to the capillaries-veins interface.  $P_c$  is the pressure across the compliance  $C_s$ . The relative pressure at the end of the capillaries,  $P_v$  is set equal to zero.  $\mathcal{R}$  and  $\mathcal{C}$  are the peripheral viscous resistance and peripheral compliance respectively. Inertial forces within the capillaries are negligible [29]

the description of the convective acceleration terms in the governing momentum equation for radial and angular coordinates. The convective term quantifies the variation of velocity in space. The convective term of the solved Navier-Stokes equations is:

$$v_r \frac{\partial v_z}{\partial r} + \frac{v_\theta}{r} \frac{\partial v_z}{\partial \theta} + v_z \frac{\partial v_z}{\partial z} \quad (3.4)$$

The third term remains in the final openBF momentum equation, whereas the rest are omitted. The first term describes the component of radial velocity and changes in longitudinal velocity with respect to the radial direction whereas the second, the component of angular velocity and changes in longitudinal velocity with respect to angular displacement. Under the conditions of a tapered vessel, the flow experiences a Bernoulli effect where flow enters through a vessel which has different inlet and outlet flow areas. The increase or decrease in velocity is due to the convective acceleration and affects the longitudinal direction which is considered in the present convective term in the momentum equation. Although, for the study at present, the network in use will not include any tapering vessels.

Outlet boundary conditions were set by coupling each 1D model outlet with a three-element Windkessel model (Figure 3.5), representing the peripheral vasculature and

parameterised as described in [26], with the aim of reducing unrealistic reflections at the 0D/1D interface, and satisfy the validation requirements on the predicted waveforms [29]. The same inlet boundary condition and Windkessel model parameterisation was used for all phases of each simulation.

### 3.3 Modelling Ischaemic and Thrombectomy Events

#### 3.3.1 Occlusion

Simulation of the occlusion caused by a clot or balloon is represented through an outlet boundary condition in the model. Figure 3.7 illustrates both the real representation of a clot occlusion and its description in the 1D model. The method proposed was to apply a condition at the point of the vessel that would reflect all incident waves at the desired location of the occlusion.

In order to explain the mathematical context behind the assignment of the reflection coefficients in openBF, one has to refer to the methods of characteristics. Assigning a volumetric flow rate time-function, for example at the inlet of a vessel, is equivalent to assigning the value of the cross-sectional area multiplied by velocity at that node ( $Q = Au$ ). This can be open to multiple interpretation of the mutual values of  $u$  and  $A$  and lead to mathematical and numerical inaccuracies in the model's solution. Therefore, to unambiguously set these values a compatibility relations technique called extrapolation of characteristics is used for the inlet and outlet [133]. The extrapolation of characteristics uses the 1D models hyperbolic system and the Riemann invariants  $W$  which are constant quantities along the characteristic curves traveling at characteristic speed of the eigenvalues  $\lambda_1$  and  $\lambda_2$ , forward and backwards respectively. Considering a single vessel of length  $L$  along axis  $x$ , the new extrapolated inlet invariants can be presented as:

$$\begin{cases} W_{1_0}(t) = Q_{in}(t) \\ W_{2_0}^{n+1} = W_{2_0}^n (L - \lambda_2(L)\Delta t) \end{cases} \quad (3.5)$$

for which  $W_1$  represents the invariant at node 1 (inlet in this case),  $W_2$  represents the invariant at node 2 (outlet in this case), the subscript of the node number ( $x$  in  $W_{1_x}$ ) represents the position,  $n$  is the current time-step and  $Q_{in}(t)$  indicates that at the inlet, the flow value at each time step is assigned by a user-defined time function (Figure 3.2). The same extrapolation of characteristics can yield the following invariants for the outlet:

$$\begin{cases} W_{2_L}^{n+1} = W_{2_L}^n + \frac{W_{2_{L-1}}^n - W_{2_L}^n}{\Delta x} (u_L^n + c_L^n) \Delta t \\ W_{1_L}^{n+1} = W_{1_L}^0 - R_t (W_{1_L}^{n+1} - W_{2_L}^0) \end{cases} \quad (3.6)$$

where  $c$  is the wave speed,  $u$  is the fluid/blood velocity,  $R_t$  is a reflection coefficient that exists between 0 and 1. Therefore, in order to represent total occlusion, applying a reflection coefficient as 1 will reflect the whole (or entire) incident wave at this point. Both the presence of the thrombus and the balloon were simulated by applying an outlet BC with a reflection coefficient of 1.

### 3.3.2 Aspiration

In order to simulate aspiration, an additional inlet was applied at the desired location within the network. A negative inlet flow rate equivalent to the aspiration rate was then applied, simulating the effects of aspiration. Figure 3.7 illustrates the real and modelled representation of aspiration at the catheter tip for two cases, one without a balloon inflated, the other with the balloon inflated, occluding the vessel. In the first case in

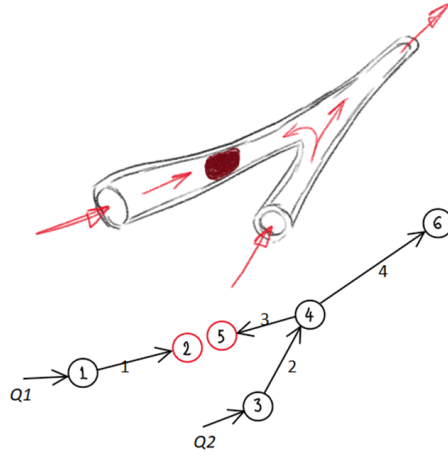


Figure 3.6: Illustration presenting real physical case where a vessel is completely obstructed by a clot (top) and the 1D representation of the physical case in the 1D system (bottom). Red nodes demonstrate where  $R_t$  value of 1 is imposed to emulate an occlusion.

the figure (A), a node is placed where the additional inlet boundary of flow is applied for aspiration. In the latter case (B), the previous aspiration node is split into two, the earlier node has a reflection term applied to emulate the balloon, whereas the latter node is has an inlet boundary condition applied with the aspiration rate of flow.

### 3.4 Conclusion

The research methodology was explained alongside the initial network parameters, blood rheological properties and a description of the clinical phases of a typical mechanical thrombectomy procedure. Alongside this, the definition of the boundary conditions for aspiration and occlusion was presented. In following chapters, the methodology presented here will be used to produce a benchmark study in Chapter 4 and adjusted slightly for the clinical parameter variation studies of the network in Chapter 5 and age related effects in Chapter 6.

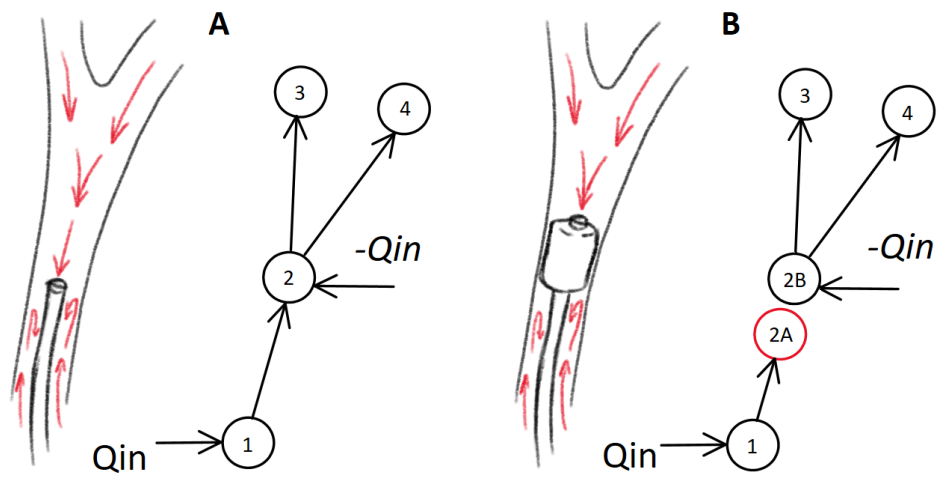


Figure 3.7: A) Illustration presenting real physical case where blood is being aspirated within a vessel (left) and the 1D representation of the physical case in the 1D system (right). B) Illustration presenting real physical case where blood is being aspirated within a vessel at the tip of a BGC with the balloon inflated and obstructing flow (left) and the 1D representation of the physical case in the 1D system (right). Red nodes demonstrate where  $R_t$  value of 1 is imposed to emulate an occlusion.



## **Chapter 4**

# **Baseline Simulation**

### **Summary**

This chapter illustrates the methodology and results predicted by the model for the clinical phases described in Chapter 3, which are representative of a typical BGC procedure. The results described in this chapter will also serve as a reference for the studies included in the chapters that follow, where the influence of some specific model parameters and additional features will be investigated.

## 4.1 Methodology

The methodology proposed and presented in Chapter 3.1 describing the parameters (balloon location, ischaemic event location, network geometry, parameter set-up of each phase) is applied to the study of this baseline simulation. In addition to this described methodology, for the clear comprehension and flexible use of the data collected from the Baseline simulation, the following categorization is proposed to characterize blood flow within each of these vessel groups (These vessel groups can be observed on the CoW in Figure 4.1):

- Supply vessels (L-CCA, R-CCA, L-PCA proximal, R-PCA proximal (following the L/R vertebral's conjoining into the basilar before becoming the PCA's));
- Left-sided CoW circulation vessels (L-ICA proximal, L-ICA distal and L-ACA proximal);
- Right-sided CoW circulation vessels (R-ICA proximal, R-ICA distal and R-ACA proximal);
- Communicating vessels (L-PCoA, R-PCoA and ACoA);
- Distribution vessels (L-MCA, R-MCA, L-ACA distal, R-ACA distal, L-PCA distal and R-PCA distal).

To reiterate, the network used in the baseline model will be a full CoW as illustrated in Figure 3.3 and Table 3.1. The proposed parameters for the baseline simulation are as follows:

- Density:  $\rho = 1060 \text{ Kg/m}^3$ ;
- Viscosity:  $\mu = 0.004 \text{ Pa}\cdot\text{s}$ ;

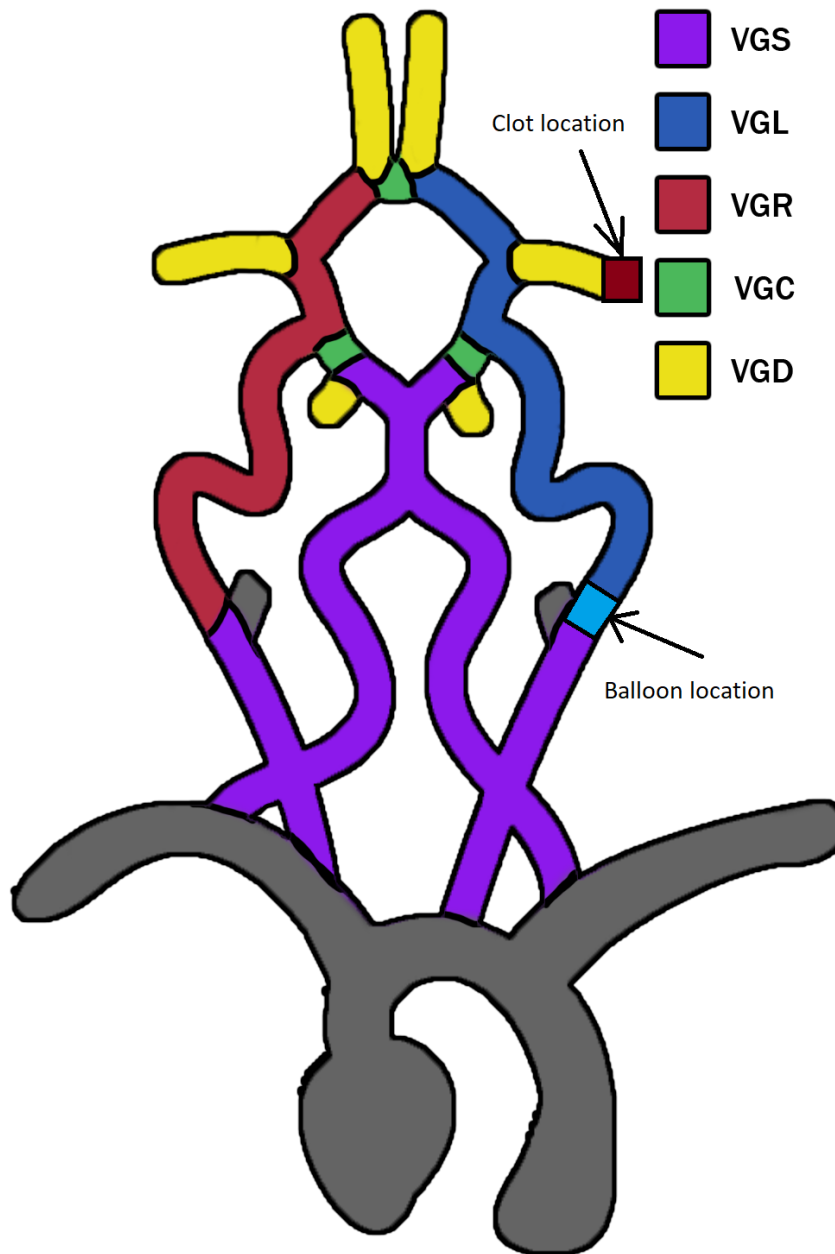


Figure 4.1: Vessel groups (VG) categorized in the groups described and colour coded. VGS (purple) = supply vessels, VGL (blue) = left-sided CoW circulation vessels, VGR (red) = right-sided CoW circulation vessels, VGC (green) = CoW communication vessels, VGD (yellow) = distribution vessels.

- Cardiac cycle:  $T = 1s$  from flow inlet using 100 time-steps presented in Figure 3.2;
- Aspiration rate:  $Q_A = 5 \text{ ml/s}$ .

For the data collection, openBF provides results for each vessel over its characteristic length at five equally spaced discretization points including the start and end nodes. The results computed from the simulation are: volumetric flow rate ( $Q$ ), pressure ( $P$ ), velocity ( $u$ ), pulse wave velocity ( $c$ ) and area of the lumen area ( $A$ ). For the data representation, comprehension of the full network in a quantitative manner can be represented through the computed outputs at each mesh point for any vessel. The clinical interest, and capability and limitation of the model was the main interest when reviewing the results. In addition, the baseline model provides a reference for the further studies presented later in the thesis, thus a method of normalizing the results was carried out to identify significant changes from clinical phases within a study, and the baseline results versus other studies. Equation 4.1 shows the expression used to normalise the data:

$$\frac{X_{PN}}{X_{P1}} = X_{PN}^* \quad (4.1)$$

where  $PN$  signifies clinical phase  $N$  and  $X^*$  is the new normalized dimensionless value  $X$  (where  $X$  is  $Q$ ,  $P$ ,  $A$ ,  $c$  or  $u$ ). Presenting these normalized results per vessel group (VG) as categorized previously was performed for clear representation of the results. Results presented were calculated by averaging over the last simulated iteration of the cardiac cycle from the middle mesh point for each vessel.

## 4.2 Results

The simulations of the five phases presented readings over 100 time-steps (0.01 seconds per time-step) of the cardiac cycle for  $P$ ,  $Q$ ,  $A$ ,  $u$ , and  $c$  for five equally spaced points for each of the 33 vessels featured in the network. This totals 412,500 points of numerical data for this study ( $33 \times 100 \times 5 \times 5 \times 5 = 412,500$ ). To present the results, the central node of each vessel (the centre of the vessel) is considered the marker point. Data over the 100 time-steps on the central node was averaged for each calculated quantity. Vessels that aren't included in a VG were not included (24 remaining vessels out of 33). To assess basic haemodynamics and circulation pathways, the fundamental quantities that provide this information is pressure and flow magnitude. This leaves a single averaged value over the cardiac cycle for  $P$  and  $Q$  for each phase, reducing the number of data points to 240 (120 for all five phases for each  $P$  and  $Q$ ).

Figure 4.2 presents the results for pressure for each individual vessel from supply vessels up to the cerebral network for all five clinical phases.

Prior to the ischemic event (Phase 1), as expected, the distribution of arithmetic-averaged pressure readings are at 97 mmHg in larger arteries such as the CCA's and reduce as flow reaches smaller intracranial vessels providing readings of  $84 \pm 2$  mmHg. During Phase 2, providing a reduced number of outlets to the network, there is a common increase in pressure throughout the system by approximately 2 mmHg for every vessel. The following phase (Phase 3) now occludes a supplying vessel with a balloon (L-ICA proximal), one of the four distributors of flow to the MCA in this network. A reduction of pressure can be observed in most vessels at various magnitudes but mostly relieving the increase effects of the occluded vessels from the previous phase. However, the L-CCA and consequentially the L-ECA experience larger pressures from the previous phase at 0.95 mmHg and 1.26 mmHg respectively. During the final pre-retrieval phase (Phase 4), it is clearly observed that 5 ml/s aspiration impacted the system and

each vessel drastically. Comparing the phases 2 through 4 to Phase 1, the percentage change for the average of the 24 vessels considered are as follows: Phase 2 showed an increase of 3.3%, Phase 3 showed a decrease of 0.1% and Phase 4 presented a significant decrease of 14.9%.

During the final phase (post-retrieval), the removal of the occlusion in the L-MCA demonstrates a reduction in pressure of every vessel from Phase 4, which consequently represents the lowest value of pressure of all the phases. Vessels that connect the path of the aspiration upstream suffer the largest of the pressure drops during the post-retrieval phase with L-ICA proximal dropping 46.2%/10.7%, L-ICA distal dropping 38.6%/9.7%, L-MCA (original location of the occlusion) falling 38.5%/14.6% and L-ACA distal 34.9%/8.5% drop (Phase 5 vs Phase 1/Phase 5 vs Phase 4). The average pressure of the system equates to 73.4 mmHg, a drop of 4.2% from Phase 4. In comparison to the other changes from each phase, Phase 4 has the largest drop in the overall system (14.8%) with the post-retrieval stage being the next biggest change.

Figure 4.3 presents the average flow over the cardiac cycle with the direction arrow presenting the assumed positive direction. From Phase 1, the communicating vessels show signs of little to no flow present. Post ischaemic event, the four supplying vessels experience a drop in average flow supplied to the brain. The vertebral's and CCA's total 12 ml/s of blood supplied per cardiac cycle for Phase 1, compared to Phase 2, a drop to 10.5 ml/s. Due to the occlusion in the L-MCA, all the outlet vessels (terminating vessels of the network: ECA's, R-MCA, distal ACA's) experience a minor increase in flow (0.06 ml/s). During Phase 3, the occlusion via balloon causes the L-CCA to drop significantly due flow only requiring to pass through to the L-ECA. The remaining of the supplying vessels face an increase, potentially compensating for the loss of the supply from the L-CCA. The vertebrals's (subsequently the basilar) and R-CCA increased by 0.2 and 0.7 ml/s respectively from Phase 1. The other increases in flow in Phase 3 are of right-sided

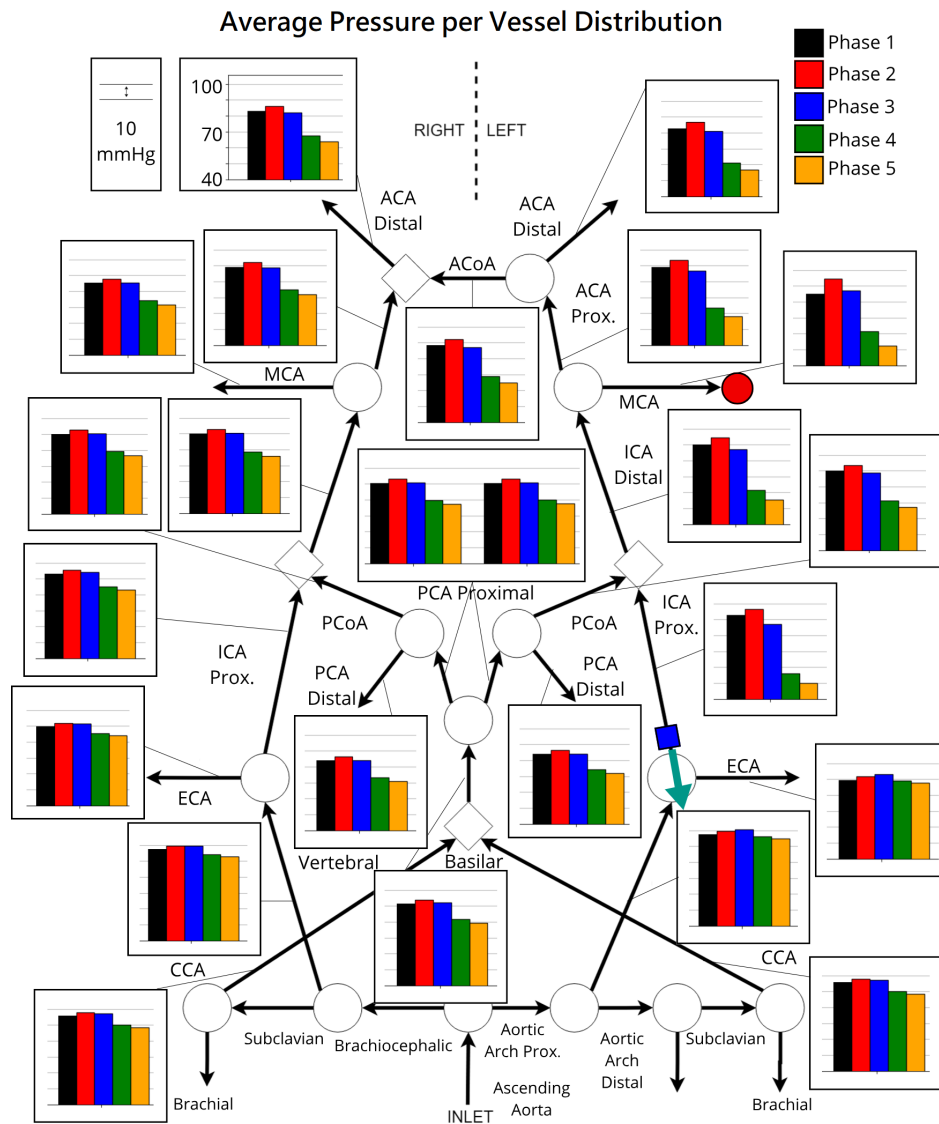


Figure 4.2: Arithmetic-averaged pressure results over the cardiac cycle for each vessel. Thrombus is illustrated as red point at the end of the L-MCA. The balloon location is indicated as a blue square at the proximal part of the proximal L-ICA. Aspiration is indicated as a green arrow on the balloon location with its direction. Positive flow directions of each vessel presented by the arrow direction. Clinical phases: 1 (black) normal network, 2 (red) thrombus present in L-MCA, 3 (blue) the balloon is positioned in the proximal region of the L-ICA proximal, 4 (green) aspiration of 5 ml/s is applied at the balloon, 5 (yellow) the clot in the L-MCA is removed and balloon and aspiration continue in attempt to prevent distal embolization.

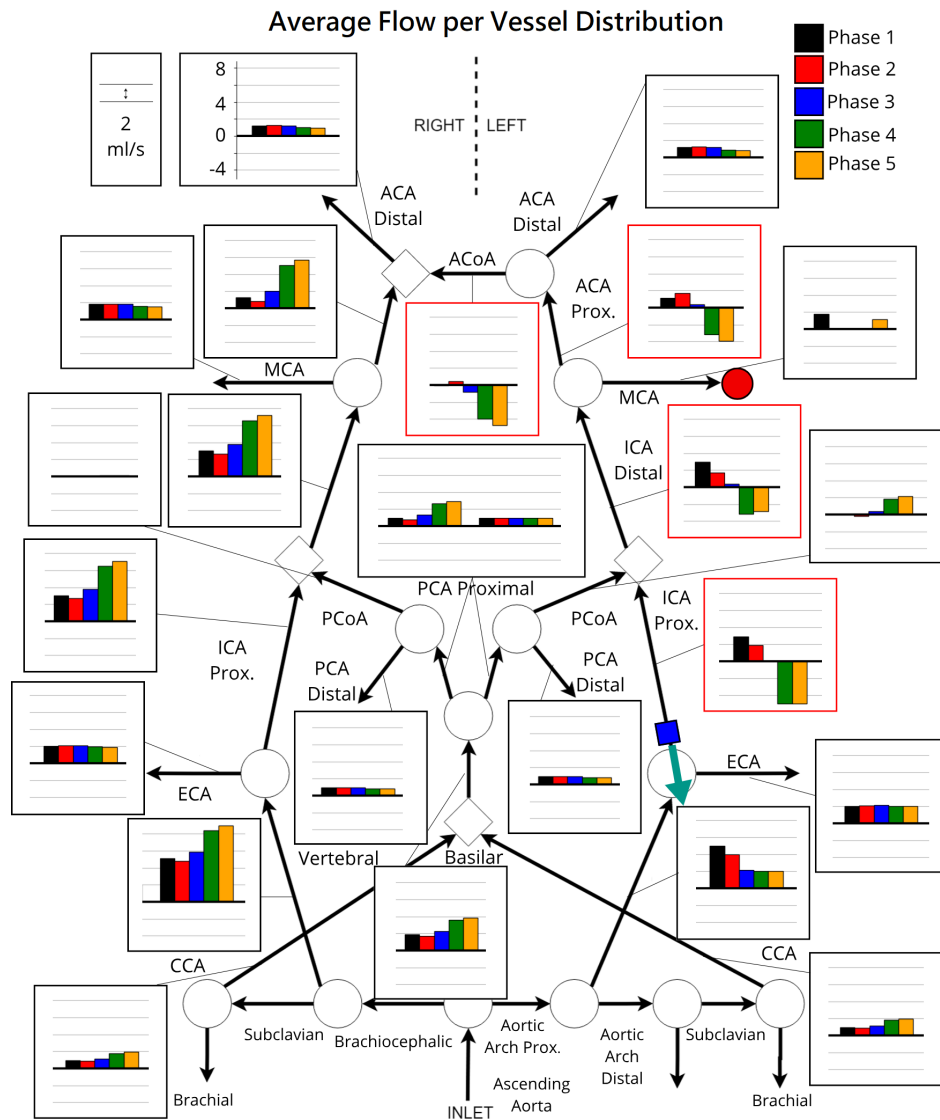


Figure 4.3: Arithmetic-averaged flow results over the cardiac cycle for each vessel. Thrombus is illustrated as red point at the end of the L-MCA. The balloon location is indicated as a blue square at the proximal part of the proximal L-ICA. Aspiration is indicated as a green arrow on the balloon location with its direction. Positive flow directions of each vessel presented by the arrow direction. Red bordered results indicate vessels that demonstrate flow reversal during aspiration phases (Phases 4 and 5). Clinical phases: 1 (black) normal network, 2 (red) thrombus present in L-MCA, 3 (blue) the balloon is positioned in the proximal region of the L-ICA proximal, 4 (green) aspiration of 5 ml/s is applied at the balloon, 5 (yellow) the clot in the L-MCA is removed and balloon and aspiration continue in attempt to prevent distal embolization.

CoW vessels (VGR: R-ICA's and proximal R-ACA). This also imposes the amplified flow through the ACoA, redirecting the flow back towards the left side of the network, significantly reducing the forward flow of the L-ACA proximal (1.2 to 0.4 ml/s from Phase 1 to Phase 3). The flow within the L-MCA up to this point has been significantly small (close to zero), similarly for the L-ICA proximal for the third phase. For the final pre-retrieval phase (Phase 4), the same behaviours are observed from the previous phase but with an increase of amplitude. Non-terminating right sided vessels experience drastic increase in flow within the CoW with 43.4%, 70.9%, 73% and 149.7% increases in the right sided CCA, ICA proximal, distal, and ACA proximal respectively. Two of the three communicating vessels also experience notable changes. The R-PCoA has little to no influence on the collateral flow within the system, whereas the L-PCoA and ACoA are major influencers on redistributing flow with a flow direction change from Phase 1 to 2. This contribution to collateral flow increases in amplitude from Phase 2 through to 4. When it comes to retrograde flow of significance, it is located, as expected, through the pathway from the balloon location to the junction that includes the MCA, ICA distal and the ACA proximal on the left side. The 5 ml/s aspiration causes the proximal L-ICA, directly affected by the aspiration to reverse the flow near to the magnitude of 5 ml/s during Phase 4. The distal CoW vessels (distal ICA, ACA proximal and ACoA) also endure retrograde flow but in small quantity compared to the source value (-3.2, -3.2 and -4 ml/s respectively).

The flow results for the post-retrieval (Phase 5) follow similar patterns discussed for Phase 3 and 4, where terminal vessels experience small change, whereas vessels that aid collateral flow experience large changes with respect to the Phase 1 and a smaller incline to the predecessor phase (Phase 4). Flow within the right-sided CoW vessels contain an average increase of 9.5% increase from Phase 4 (R-CCA, R-ICA's and R-ACA proximal). The vessel path up to the L-MCA still serves as a route for retrograde flow, although

a reduction in flow reversal was present in the L-ICA distal. With the MCA no longer occluded, the results show that there is no retrograde flow in this vessel (+1.1 ml/s), although this is a reduction in comparison to Phase 1 (1.8 ml/s).

Utilising the method discussed and presented in Equation 4.1, the normalized results for pressure and volumetric blood flow can be observed for all five phases separated into their respected VG's in Figures 4.4 and 4.5 respectively. At initial observation, the pressure normalized data follows a very uniform pattern regardless of the vessel group, increasing in percentage slightly in Phase 2 and declining in the proceeding stages (Figure 4.4).

From Figure 4.5 the collateral flow clearly presents two of the communicating vessels as key influences of adjusting flow distribution within the CoW (L-PCoA and ACoA). The R-PCoA has very little change during the process of the phases, which is expected to be countered in the R-PCA distal but also does not deviate much from the initial phase. As can also be seen in this graph, the gradual change in flow as phases change. This suggests the large impact the balloon and aspiration has on altering haemodynamic direction. This is also clear in pressure as during phases 3, 4 and 5 pressure relief within the system was present and decreasing as balloon, then aspiration was applied. This also continued once the occlusion was removed in the L-MCA. Due to the occlusion, the total amount of flow entering the brain circulation was reduced from 12.0 ml/s (11.95602) to 10.5 ml/s. After positioning the balloon (Phase 3), a further drop to 10 ml/s was entering brain. Due to the supply from the L-CCA being blocked, the remaining vessels supplying blood to the brain remain the vertebrales and the R-CCA. With aspiration active, the new supply rate becomes  $\sim 12.0$  ml/s (11.99382), similar to the average of Phase 1. Then, with the occlusion removed, the aspiration and balloon alone cause the system to drive more inflow from the supplying vessels, to produce an average of 12.8 ml/s supplied. This alteration in supply within the phases do not largely affect the

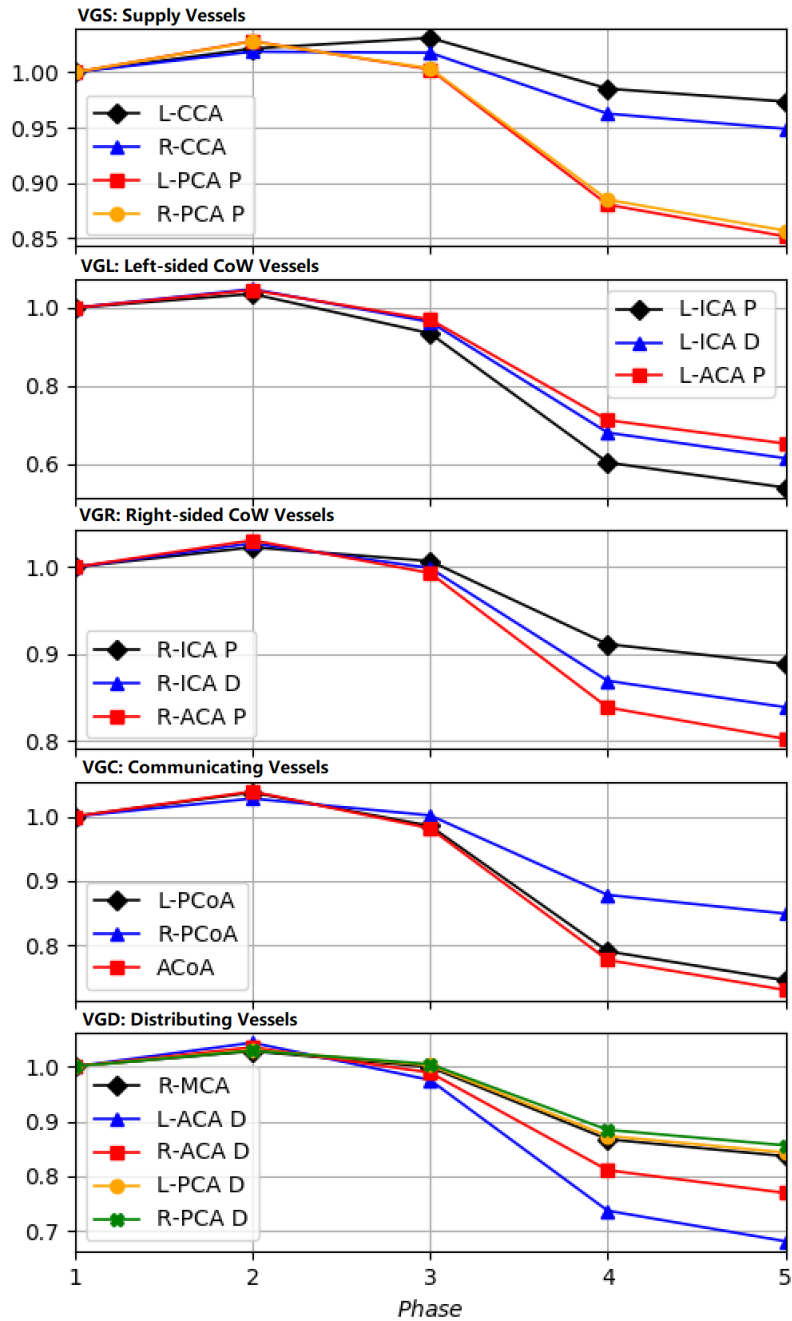


Figure 4.4: The results for pressure following normalization of the results for all phases to Phase 1 presented in the categories VGS, VGL, VGR, VGC, VGD exclusively in that order.

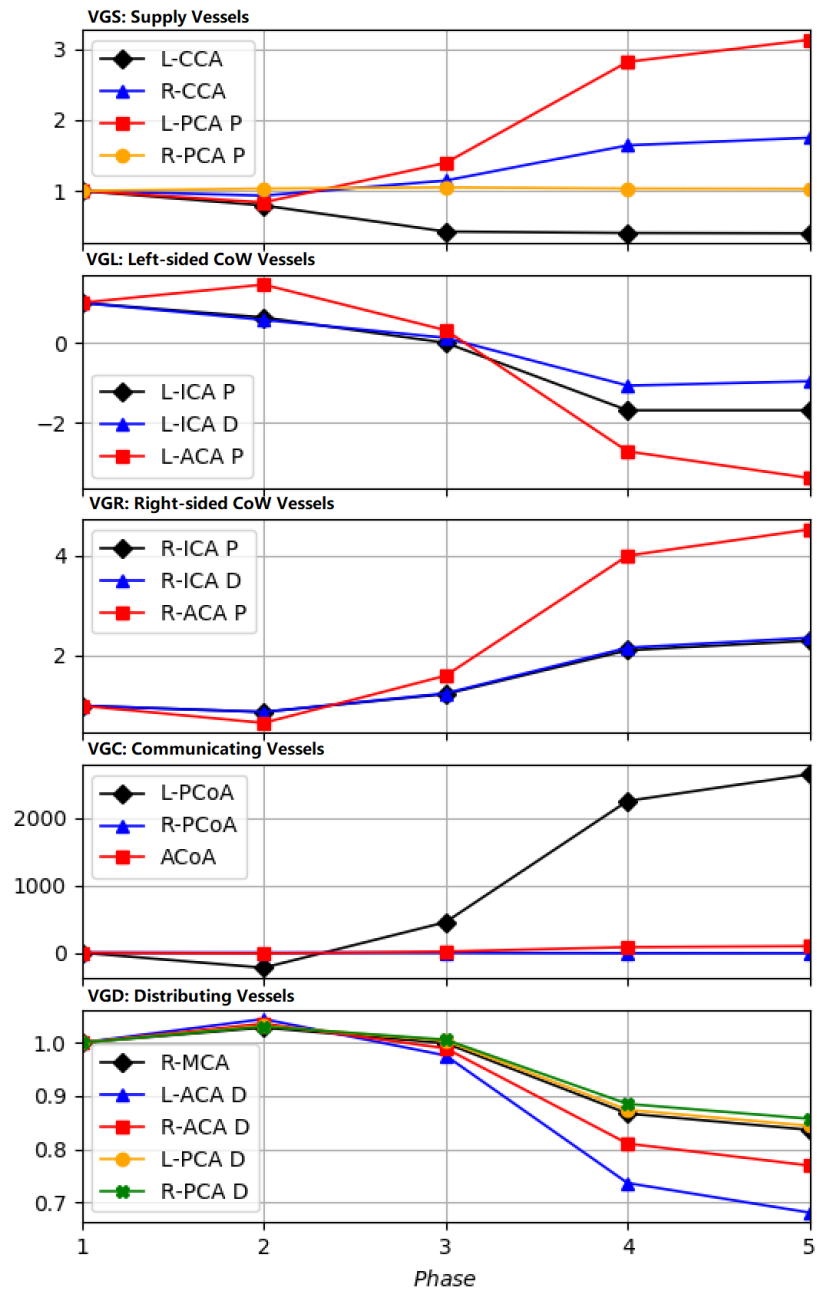


Figure 4.5: The results for flow following normalization of the results for all phases to Phase 1 presented in the categories VGS, VGL, VGR, VGC, VGD exclusively in that order.

overall distribution of terminating vessels. The terminating vessels saw minute changes from phase-to-phase following the typical pattern of slightly increasing in flow after ischaemic event, then reducing gradually from phases 3 to 5.

The distributing vessels (VGD) show a uniformity as the phases change, suggesting that the system utilizes the re-circulation to still try and maintain optimal and uniform outlet to the original Phase 1 performance rather than prioritizing the more convenient outlets.

Overall, the results suggest that the behaviour of the system utilises the non-incident side to drive flow countering the effects of the occluded flow from both the clot and the balloon. This paired with the collateral flow redirecting through communicating vessels allows the distribution of flow to the rest of the brain through the terminating vessels of the system to maintain a fairly consistent flow outlet with respect to each other, but an overall reduction in brain supply as phases progress.

### **4.3 Discussion**

The simulation on the baseline model provides a reference set of data to evaluate the haemodynamic behaviour of the described treatment method and quantitative data to assess against literature to conclude accuracy and clinical benefits surrounding the simulation performance.

From the results, key changes to the haemodynamics occur throughout the phases of treatment. Observing the normalized results, aspiration-present phases (Phase 4 and 5) experience the most changes to pressure and flow. In terms of the progressive changes, the largest influence to the flow and pressure occurs during the initial aspiration phase (Phase 4). General flow direction changes also only begin to occur when the aspiration is applied. Figure 4.6 shows the flow direction as predicted by the model

under intervention through the treatment. Use of the communicating vessels is crucial under the aspiration according to the results. Initially there is minimal or no movement through these (VGC) vessels. Initiation of the treatment mechanisms impose sudden changes to the collateral flow leading to the use of an alternate pathway. With the aspiration active, use of the ACoA to redirect flow around to the left side of the CoW from the right paired with the use of the L-PCoA to allow flow back up to the source of aspiration. Interestingly, the R-PCoA remained at stationary flow through all phases, this is possibly due to the most conventional path supporting left side of the CoW being distributed by the ACoA.

The treatment region is the most influenced with flow direction changes to the L-ICA's and L-ACA proximal but the area of incidence (L-MCA), there is only ever reduced flow, never retrograde. When referring to the literature, there is a wide reporting of different outcomes regarding retrograde flow in the MCA under BGC-SR treatment. In-vitro studies that present identical treatment set-ups as the one presented in this methodology shows that retrograde flow is not present in the MCA, rather a reduction in flow from the baseline flow value (2.5 ml/s to 0.67 ml/s) [134]. Referring to the results from phase 1 and 5 in the L-MCA, the average flow reading was 1.79 ml/s and 1.1 ml/s respectively. Differences in results may be due to the aspiration technique differences as the in-vitro study state use of a 60 ml syringe until full (volume is known, aspiration rate is not), but no time duration stated as well as the cardiac input set to 72 bpm ( $T = 0.83s$ ) compared to the 60 bpm in the present methodology [135]. Following this, the results presented in this Chapter are averaged over the cardiac cycle, limiting the representation of the diastolic and systolic regions. When observing the full wave of the L-MCA flow for the post-retrieval phase in comparison to the first phase (Figure 4.7), there are still no parts of the full wave that enter retrograde territory.

The aspiration rate used in this methodology was 5 ml/s, which is within normal

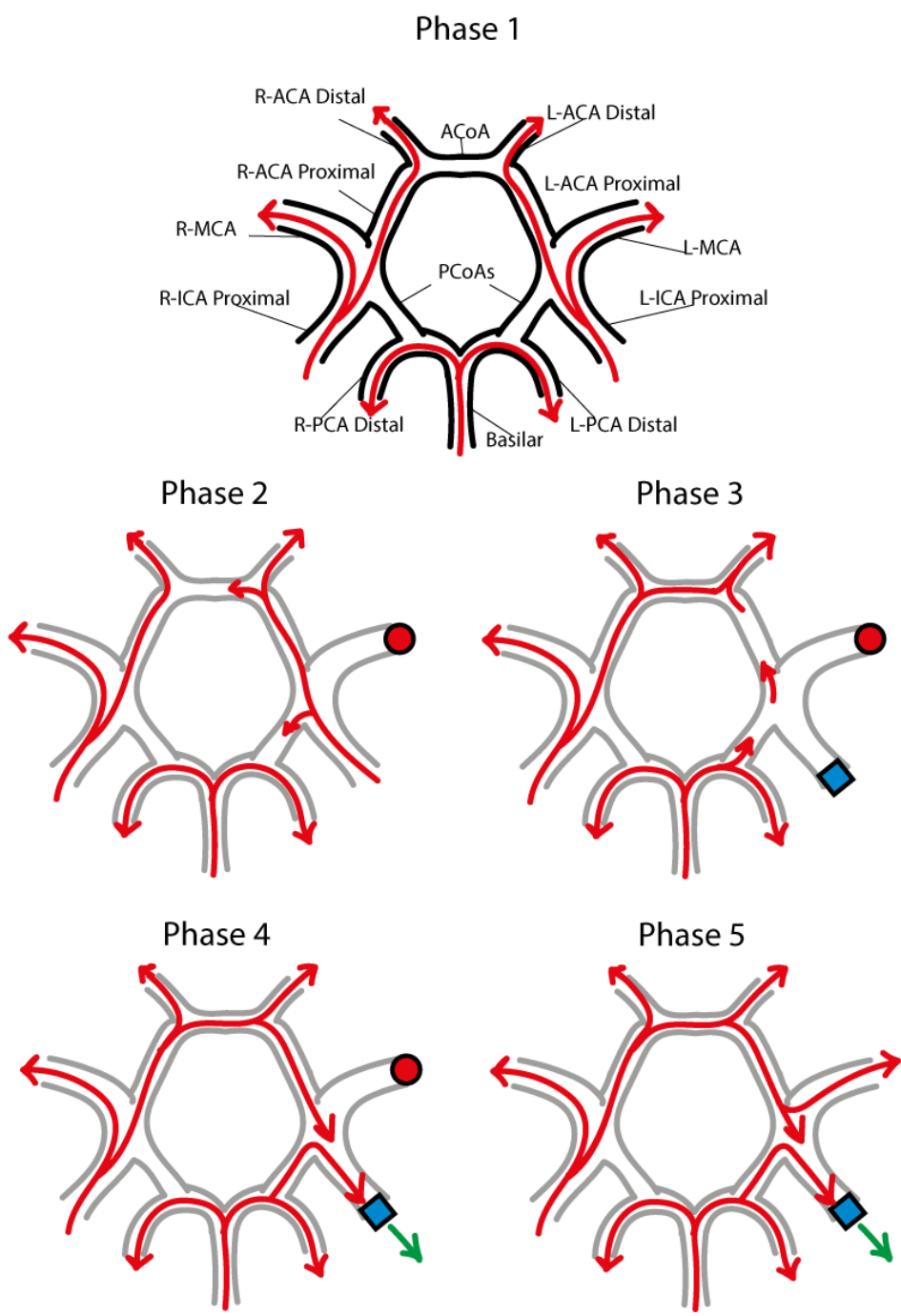


Figure 4.6: Flow directions presented for each phase of the baseline simulation in the CoW. Clot illustrated as a red point, balloon placement illustrated as a blue square and aspiration direction illustrated by a green arrow. Red arrow directions are representative of flow directions and not magnitudes.

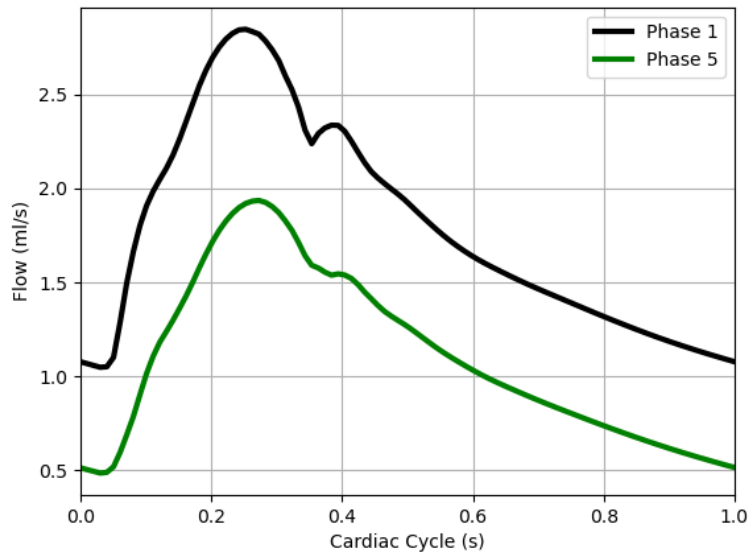


Figure 4.7: Flow waves in the L-MCA over the cardiac cycle for clinical phases 1 and 5 (pre-clot in L-MCA and post-retrieval of clot in L-MCA).

expected parameters [136]. For the purpose of outcome evaluation, the balloon was re-positioned into three other locations and evaluated for the post-retrieval phase for three aspiration rates of 1, 3 and 5 ml/s. The locations were central positions of the L-CCA, L-ICA proximal and distal (although the latter being physiologically not medically safe as this enters intracranial regions). The purpose for this post result analysis was to review the effects of flow in the MCA in attempt to understand the effects of the positioning as well as the aspiration impact. Figure 4.8 presents the results. It is clear that the aspiration changes imply partial effects on the overall average outflow within the MCA and the overall effects on positioning are minimal in comparison to the L-CCA placement and the L-ICA proximal. There is a larger reduction when positioned in the distal L-ICA, but this set-up is not adopted in medical practice. With the BGC positioned in the L-CCA, the L-ICA proximal experiences more flow reversal of 2, 4 and 6 ml/s for

aspiration magnitudes of 1, 3 and 5 ml/s respectively from the BGC. This characteristic behaviour is also experienced in the ACA distal when the BGC is positioned in the L-ICA distal, where retrograde flow is approximately 1 ml/s more than the applied aspiration. This similarity in these two occurrences happen when there is a supply vessel along the reverse path. With the BGC in the L-CCA, the difference in flow driven from the L-ICA proximal and the aspiration magnitude (1 ml/s approximately) has access to the L-ECA, and subsequently in the second occurrence, with the BGC in the L-ICA distal, the difference in flow driven from the L-ACA proximal and the aspiration magnitude (also 1 ml/s approximately) has access to the L-MCA. The re-circulation of the CoW is emphasised through the ACoA and the L-ACA distal where placement of the BGC shows the lowest utilisation of these vessels when positioned in the L-ICA proximal. The overall placement doesn't alter the outcome in the MCA significantly, however there are clear variances in flow behaviours based on how the BGC intercepts certain flow pathways. One would presume that positioning the aspiration and balloon point closer to the clot would have a larger impact on flow reversal. However, these results can be explained by concomitant alterations affecting the communicating vessels which is only evident when a comprehensive model of the vessels in the CoW is simulated. From a more clinical point of view, the significant influence of aspiration rates also highlights the importance of controlling such rates, e.g. through the use of a pump, in a clinical procedure that is commonly performed manually.

Alternatively, there are studies that present retrograde flow in the MCA. An *in-vitro* study [13] performed on a reduced network involving only the ICA, PCoA and MCA, reported reverse flow in the MCA ranging from between 2.5 and 0.31 ml/s ( $1.4 \pm 1.1$  ml/s). Similarly, in another *in-vitro* study [136] where flow was simulated through the entire CoW, retrograde flow was observed in the distal ICA (3.8 ml/s) as well as in the MCA (1.7 ml/s) when using simultaneously balloon and aspiration (6 ml/s). Interestingly, the

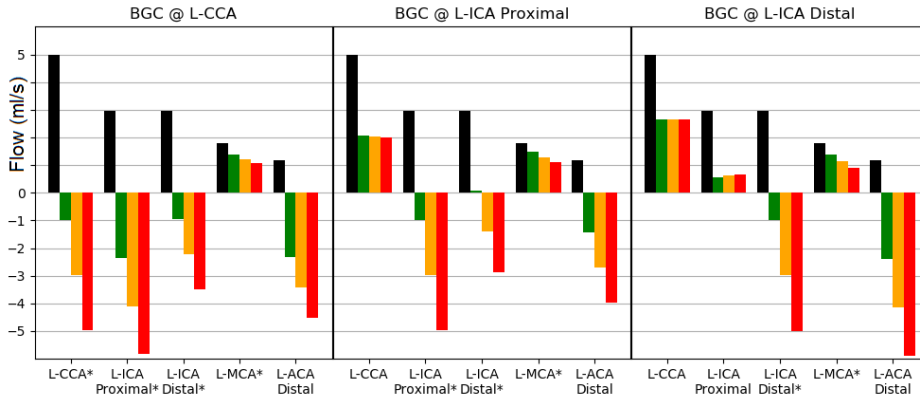


Figure 4.8: Effects of BGC positioning and aspiration rates on average flow for post-retrieval phase (Phase 5) in L-CCA, proximal and distal L-ICA, L-MCA, and distal L-ACA. Aspiration range is 1 ml/s (green bars), 3 ml/s (yellow bars) and 5 ml/s (red bars). Phase 1 results (black bars) are presented as a reference. (\* signifies vessels that are in the pathway between BGC location and MCA, original clot location.)

results of the simulations in this chapter produces approximately 3 ml/s of retrograde flow in the distal ICA when applying an aspiration rate of 5 ml/s in the ICA proximal. However, none of the phases and configurations investigated in this study predicted reverse flow in the L-MCA, where the clot caused blood flow blockage. This discrepancy might be caused by a different approach used in these *in-vitro* studies, whereby only a reduced cerebral network is used such as the one presented in [13] where the network consisted of ICA, MCA and ACA only. Comparatively, the study in this chapter adopted a much more comprehensive model of the network, where blood through the MCA is quickly re-established through the action of the communicating vessels in the CoW.

## 4.4 Conclusions

The five clinical phases were simulated on the proposed network to create a benchmark set of results for later simulations. Results showed that communicating vessels were more influential on the haemodynamics during treatment phases. Results also

demonstrated the flow path of the CoW during the phases and indicated where flow reversal was present. Retrograde flow was successful in all treatment path vessel during aspiration phases except the L-MCA where flow was only reduced.



## **Chapter 5**

# **Anatomical Network**

## **Variations**

### **Summary**

The CoW experiences collateral flow due to its ring-like nature. If the nine vessels in the CoW are present in an individual's anatomy, they possess a full CoW. The case of a complete CoW is true in a minority of the human population (believed to be around 12.2% [137] to 45% [138]) against people with structural alterations [139]. In this chapter, the variations of network configurations are narrowed down to a range of likely networks in the general population. These configurations will be simulated under the same ischaemic events described in Chapter 3 and subsequently the simulations of Chapter 4 with the five treatment phases. The aim of this chapter was to highlight any influence these variations might have on the results of the baseline model, together with its

clinical relevance and implications. The results will be analysed individually and comparatively to the baseline to demonstrate the capabilities and limitations of the 1D model whilst presenting any key findings that would prove useful on a clinical perspective.

## 5.1 Methodology

There are many structural variations of the vasculature regarding the CoW. These structural alterations of the network can be in the form or combination of absent vessel(s), hypoplastic vessels (vessels that are significantly narrow and stiff), multiple branching vessels within a usually singular vessel channel (fenestration, duplication or triplication of vessels) and conjoining of vessels for example Azygos ACA where the two distal ACA's join together to form a single ACA. There are many variations of the CoW but for this study, a select few that were clinically more present in the population were assessed using the 1D model.

When considering a CoW network that features a vessel that is a fenestration, duplication or triplication, perfusion through this segment of the CoW is still present but through multiple channels rather than one as presented in Figure 5.1. Flow within these multi-channel vessels do not affect the completeness or the collateral capacity of the CoW but will present different flow resistances.

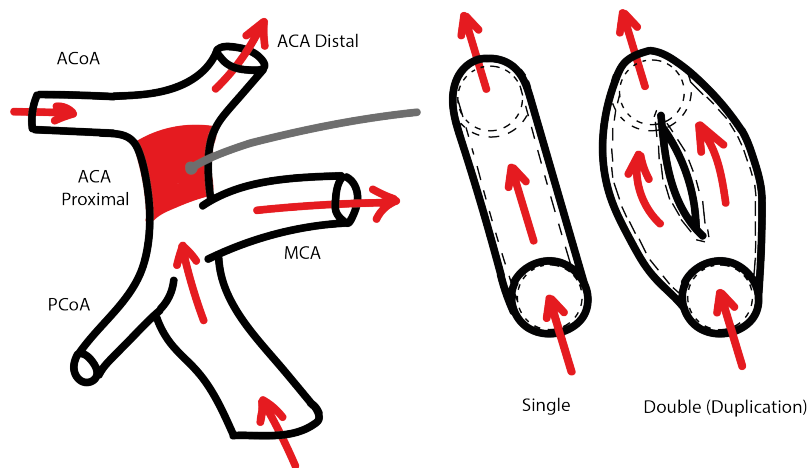


Figure 5.1: This example demonstrates that if the ACA proximal was a single vessel or duplicated vessel (selected two examples), flow of some form is still allowed to circulate through the beginning and end points of this channel but resistance to flow will be different.

Alternatively, when segments of the CoW are missing or hypoplastic, this renders the CoW as incomplete (if missing) or contains high flow resistance pathways (if hypoplastic), thus decreasing the collateral capacity of the CoW and increasing the brain's vulnerability to changes in the blood flow [137, 140, 141]. With hypoplastic vessels, flow area is significantly reduced with very little elastic potential. Comparatively, missing vessels demonstrate the most extreme case of altering flow behaviours in the CoW from the complete system as no flow can be present. These cases demonstrate the most clinically relevant cases as incomplete CoW variants are associated with an increased risk of stroke [142, 143].

When performing the MT procedure, the proximal part of the proximal L-ICA is occluded by the balloon, as is the L-MCA by the clot (in reference to the described methodology in Chapter 3) and subsequently aspiration is applied in Phases 4 and 5. With multi-channel flow vessels, the completeness of the CoW is still present thus the procedure likely to perform similarly to the baseline network of the complete CoW. In comparison, the missing vessel network variations have increased impact on the collateral flow and subsequently may pose potential advantageous or disadvantageous interactions with the clinical procedure.

From this, the methodology carried in this study considered the most likely network variations which had absent vessel(s). With certain study's demonstrating around 47 variants of missing/hypoplastic networks found in a large population samples [62], a selection of the most common networks that included absent vessels was used for the simulations in this study. Through a compromise of two studies [62, 144], the most common missing vessel variations were narrowed down to the following:

- Missing ACoA;
- Missing Left/Right/both PCoA(s);

- Missing Left/Right ACA;
- Missing Left/Right PCA;
- Missing Left/Right PCoA and the collateral Right/Left PCA.

These configurations total ten individual cases when including the left and right components and in some, the symmetrical case (eleven when considering the complete CoW case). These configurations can be observed in Figure 5.2. The benefits of also observing the left, right and symmetric alternate possibilities of each configuration is necessary in alignment with the treatment location. An example of this would be; an ischaemic occlusion in the L-MCA may have completely different haemodynamic results with a configuration that features an absent L-ACA proximal compared to missing a R-ACA proximal. This is due to the nature of the circulation and physical locations of the treatment and vessels.

The simulation methodology proposed and presented in Chapter 3.1 describing the parameters (balloon location, ischaemic event location, network geometry, parameter set-up of each phase) was also applied to these network variations for all five phases of the simulation.

The specifications of all the configurations used in these simulations are taken from Table 3.1 (with the omission of any description for missing vessel(s) for the respective case simulated). From clinician advice, certain configurations cause altered development to the surrounding vessels. For example, if there is an absent or hypoplastic L-PCoA, the surrounding vessels (L-PCA proximal and L-ICA's) could potentially have different geometrical characteristics to compensate for the altered haemodynamics. In this study, it is assumed that these potential variations to the surrounding vessels are omitted and the vessel parameters such as lumen wall thickness and diameter remain the same as the baseline model. The only variation will be the omission of the vessel

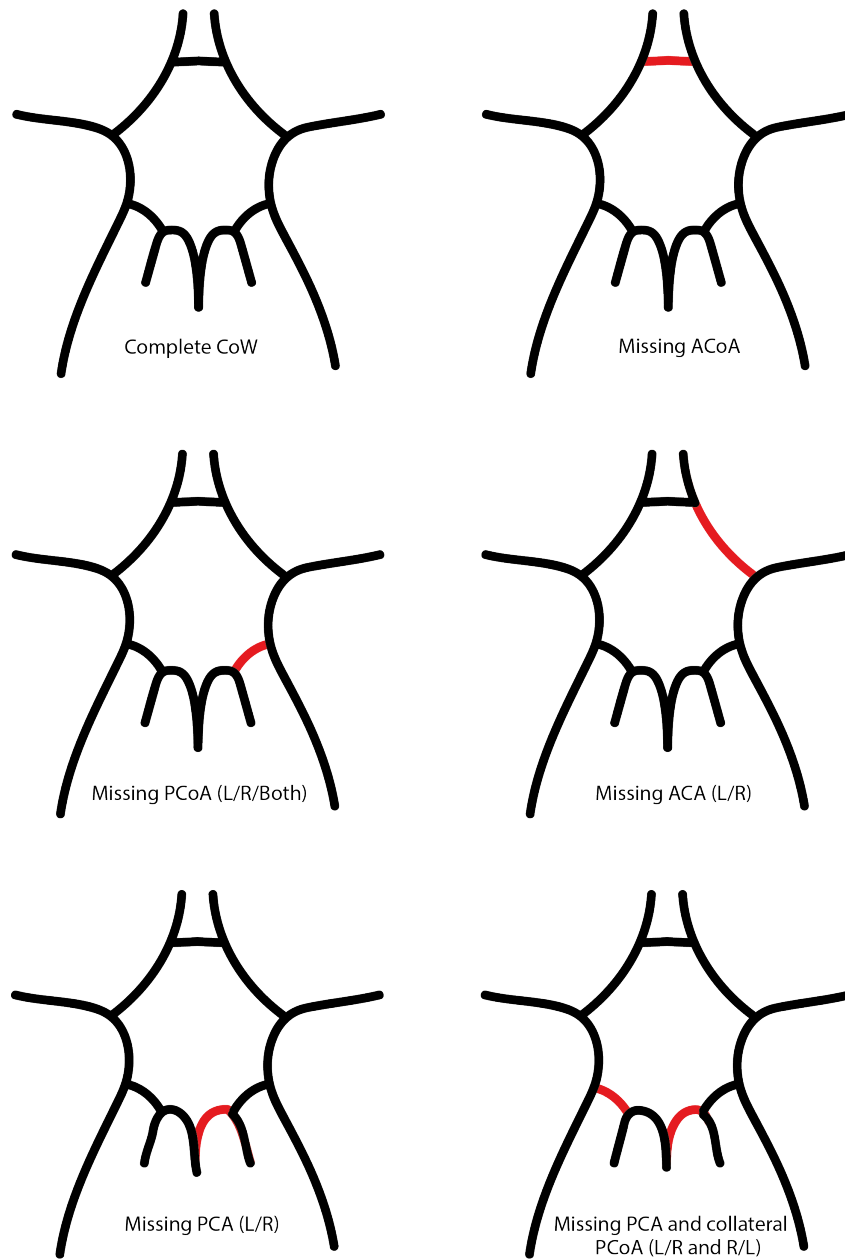


Figure 5.2: The configurations for missing vessels for CoW anatomies. Each variation has the potential of existing in the left, right or both of the respective vessels as labelled in the illustration.

for its respective configuration.

As proposed in Chapter 4, the results calculated by the model will be in the form of  $P$  and  $Q$  provided for each vessel over its characteristic length at five equally spaced meshed points including the start and end nodes where  $P$  and  $Q$  are prioritised to assess basic haemodynamic circulation. Alongside this, Chapter 4 was used as the comparative datum for normalizing the results. In Chapter 4, Equation 4.1, results of Phases 2 through to 5 are normalized to the results of Phase 1. The normalization of the results presented in this chapter were instead normalized to their respective phase to the baseline model such that:

$$\frac{PN_X}{PN_{Baseline}} = PN_X^* \quad (5.1)$$

Where  $PN$  is Phase N of configuration  $X$  and  $PN^*$  is the normalized result. The reason for this is to demonstrate the proportional changes within each variation with respect to the complete CoW, rather than to compare all the phases of each variation to the baseline Phase 1.

## 5.2 Results

### 5.2.1 Analysis of Configuration Results

#### No ACoA Configuration

Figure 5.3 presents a colour map of the pressure and flow results for all five phases averaged over the cardiac cycle and normalized to the baseline results presented in Chapter 4 for the CoW configuration of no ACoA.

From the colour map, it is clear that there is not much change in pressure from Baseline for Phase 1 and Phase 2 throughout the system. With the ACoA not present,

	Variation:	No ACoA (P)					No ACoA (Q)				
VG	Phase:	1	2	3	4	5	1	2	3	4	5
S	L-CCA	1.00	1.00	1.00	1.01	1.02	1.01	0.92	1.00	1.01	1.02
S	R-CCA	1.00	1.00	1.00	1.01	1.03	0.99	1.06	0.92	0.73	0.69
D	L-ECA	1.00	1.00	1.00	1.01	1.02	1.00	1.00	1.00	1.01	1.02
L	L-ICA P	1.00	1.01	0.90	0.18	0.13	1.01	0.83	0.86	1.00	1.00
R	R-ICA P	1.00	1.00	1.01	1.05	1.08	0.99	1.12	0.87	0.64	0.59
D	R-ECA	1.00	1.00	1.00	1.02	1.04	1.00	1.00	1.00	1.02	1.04
S	R Vert.	1.00	1.00	0.99	0.97	0.98	1.00	1.00	1.16	1.50	1.42
S	L Vert.	1.00	1.00	0.99	0.97	0.98	1.00	1.00	1.16	1.50	1.42
L	L-ICA D	1.00	1.01	0.90	0.25	0.22	1.01	0.76	2.86	-0.07	-0.14
C	L-PCoA	1.00	1.00	0.95	0.65	0.66	9.58	1.48	2.87	2.85	2.52
C	R-PCoA	1.00	1.00	1.00	0.99	1.01	1.56	-3.55	-12.6	-10.9	-9.52
R	R-ICA D	1.00	0.99	1.01	1.09	1.12	0.98	1.15	0.80	0.43	0.39
S	Basilar	1.00	1.00	0.98	0.91	0.93	1.00	0.99	1.16	1.50	1.42
D	L-MCA	1.00	1.01	0.90	0.25	0.22	1.00	0.62	1.35	1.25	0.22
D	R-MCA	1.00	0.99	1.01	1.09	1.13	1.00	0.99	1.01	1.09	1.13
L	L-ACA P	1.00	1.01	0.89	0.24	0.21	1.04	0.76	2.86	-0.07	-0.04
R	R-ACA P	1.00	0.99	1.02	1.13	1.17	0.96	1.49	0.61	0.23	0.20
L	L-PCA P	1.00	1.00	0.98	0.89	0.91	1.00	0.89	1.51	2.24	2.08
R	R-PCA P	1.00	1.00	0.98	0.91	0.93	0.99	1.08	0.68	-0.57	-0.63
D	L-ACA D	1.00	1.01	0.89	0.23	0.20	1.00	1.01	0.89	0.23	0.20
D	R-ACA D	1.00	0.98	1.02	1.17	1.22	1.00	0.98	1.02	1.17	1.23
C	ACoA	-	-	-	-	-	-	-	-	-	-
D	L-PCA D	1.00	1.00	0.98	0.87	0.89	1.00	1.00	0.98	0.87	0.89
D	R-PCA D	1.00	1.00	0.98	0.91	0.93	1.00	1.00	0.98	0.91	0.93

Figure 5.3: Colour map of normalized results for the configuration of the CoW without ACoA. Left side column indicates the vessel group of each vessel illustrated in Figure 4.1 (S = supply vessel, L or R = left or right sided CoW vessel, C = communicating vessel, D = distributing vessel). The ECAs are assumed to be in VGD (Distributing Vessel). The treatment path (L-ICAs and L-MCA) are highlighted as well as the L-ACA distal. Colour map key: Red < 1, White = 1, Blue > 1.

the two sides of the CoW are isolated as flow interference was not possible except from the proximal PCA's in which flow remained positive to their respective sides. From this, it can be observed that the small increases in pressure are independent for the side of incidence (left), whereas the right side of the CoW experiences a reduction in few vessels (1-2% drop and left side max increase of 1%). This isolation of the sides becomes more apparent in phases 3 through 5 with the left sided vessel experiencing more of a pressure drop in comparison to the baseline model with drops of up to 87% in the proximal L-ICA in phase 5.

The isolation of sides also impacts the channels of flow within the CoW, restricting flow to cross over through the ACoA causes a large increase in use of the L-PCoA. The comparison between the baseline and the present configuration shows a 958% increase on use of the L-PCoA. Due to the additional conditions to the network as phases develop, more reliability of transferring flow from the right side to the left is induced with the R-PCA proximal and R-PCoA altering the direction of flow towards the left.

The configurations flow behaviour partially assists the area of treatment. During phase 5, the aspiration in the baseline model still presents a positive flow though the L-MCA of 1.1 ml/s, whereas the missing ACoA configuration reduces the positive flow into the L-MCA to 0.24 ml/s. Although it is not retrograde or stationary there is a 78% reduction in flow from the full CoW configuration.

### **No PCoA Configurations**

Figures 5.4 and 5.5 demonstrate colour maps of the results for pressure and flow respectively for the three variations of the missing PCoA configurations. The colour maps use the same normalization technique presented in Equation 5.1.

With the L-PCoA absent, clear pressure changes are present in phases 4 and 5 with the administration of the aspiration. Pressure drops are experienced mainly in left sided

VG	Variation:	No L-PCoA (P)					No R-PCoA (P)					No PCoAs (P)					
		Phase:	1	2	3	4	5	1	2	3	4	5	1	2	3	4	5
S	L-CCA	1.00	1.00	1.00	1.00	1.00	1.00	1.00	1.00	1.00	1.00	1.00	1.00	1.00	1.00	1.00	1.01
S	R-CCA	1.00	1.00	1.00	1.00	1.00	1.00	1.00	1.00	1.00	1.00	1.00	1.00	1.00	1.00	0.99	1.00
D	L-ECA	1.00	1.00	1.00	1.00	1.01	1.00	1.00	1.00	1.00	1.00	1.00	1.00	1.00	1.00	1.00	1.01
L	L-ICA P	1.00	1.00	0.98	0.81	0.79	1.00	1.00	1.00	1.00	1.00	1.00	1.00	0.97	0.78	0.75	
R	R-ICA P	1.00	1.00	1.00	0.98	0.99	1.00	1.00	1.00	1.00	1.00	1.00	1.00	1.00	0.97	0.97	
D	R-ECA	1.00	1.00	1.00	0.99	1.00	1.00	1.00	1.00	1.00	1.00	1.00	1.00	1.00	0.99	0.99	
S	R Vert.	1.00	1.00	1.00	1.02	1.03	1.00	1.00	1.00	1.00	1.00	1.00	1.00	1.01	1.04	1.05	
S	L Vert.	1.00	1.00	1.00	1.02	1.03	1.00	1.00	1.00	1.00	1.00	1.00	1.00	1.01	1.04	1.05	
L	L-ICA D	1.00	1.00	0.98	0.83	0.81	1.00	1.00	1.00	1.00	1.00	1.00	1.00	0.97	0.80	0.77	
C	L-PCoA	-	-	-	-	-	1.00	1.00	1.00	1.00	1.00	-	-	-	-	-	
C	R-PCoA	1.00	1.00	1.00	1.02	1.03	-	-	-	-	-	-	-	-	-	-	
R	R-ICA D	1.00	1.00	0.99	0.97	0.97	1.00	1.00	1.00	1.00	1.00	1.00	1.00	0.99	0.94	0.94	
S	Basilar	1.00	0.99	1.01	1.05	1.07	1.00	1.00	1.00	1.00	1.00	1.00	0.99	1.02	1.09	1.12	
D	L-MCA	1.00	1.00	0.98	0.83	0.81	1.00	1.00	1.00	1.00	1.00	1.00	1.00	0.97	0.80	0.77	
D	R-MCA	1.00	1.00	0.99	0.97	0.97	1.00	1.00	1.00	1.00	1.00	1.00	1.00	0.99	0.94	0.94	
L	L-ACA P	1.00	1.00	0.98	0.86	0.84	1.00	1.00	1.00	1.00	1.00	1.00	1.00	0.98	0.83	0.81	
R	R-ACA P	1.00	1.00	0.99	0.95	0.95	1.00	1.00	1.00	1.00	1.00	1.00	1.00	0.99	0.92	0.92	
L	L-PCA P	1.00	0.99	1.01	1.06	1.09	1.00	1.00	1.00	1.00	1.01	1.00	0.99	1.02	1.11	1.14	
R	R-PCA P	1.00	0.99	1.01	1.06	1.08	1.00	1.00	1.00	1.00	1.01	1.00	0.99	1.02	1.10	1.13	
D	L-ACA D	1.00	1.00	0.98	0.88	0.87	1.00	1.00	1.00	1.00	1.00	1.00	1.00	0.98	0.85	0.84	
D	R-ACA D	1.00	1.00	0.99	0.93	0.93	1.00	1.00	1.00	1.00	1.00	1.00	1.00	0.99	0.91	0.90	
C	ACoA	1.00	1.00	0.99	0.91	0.91	1.00	1.00	1.00	1.00	1.00	1.00	1.00	0.98	0.89	0.88	
D	L-PCA D	1.00	0.99	1.01	1.07	1.10	1.00	1.00	1.00	1.00	1.01	1.00	0.99	1.02	1.12	1.15	
D	R-PCA D	1.00	0.99	1.01	1.05	1.07	1.00	1.00	1.00	1.00	1.01	1.00	0.99	1.02	1.10	1.13	

Figure 5.4: Colour map of normalized results of pressure for the configurations of the CoW without PCoA(s). Left side column indicates the vessel group of each vessel illustrated in Figure 4.1 (S = supply vessel, L or R = left or right sided CoW vessel, C = communicating vessel, D = distributing vessel). The ECAs are assumed to be in VGD (Distributing Vessel). The treatment path (L-ICAs and L-MCA) are highlighted as well as the L-ACA distal. Colour map key: Red < 1, White = 1, Blue > 1.

VG	Variation:	No L-PCoA (Q)					No R-PCoA (Q)					No PCoAs (Q)				
		Phase:	1	2	3	4	5	1	2	3	4	5	1	2	3	4
S	L-CCA	1.00	0.97	1.00	1.00	1.00	1.00	1.00	1.00	1.00	1.00	1.00	0.97	1.00	1.00	1.01
S	R-CCA	1.00	1.00	1.03	1.11	1.10	1.00	1.00	1.00	1.01	1.01	1.00	0.99	1.06	1.19	1.19
D	L-ECA	1.00	1.00	1.00	1.00	1.00	1.00	1.00	1.00	1.00	1.00	1.00	1.00	1.00	1.00	1.01
L	L-ICA P	1.00	0.94	0.82	1.00	1.00	1.00	1.00	0.91	1.00	1.00	1.00	0.93	0.92	1.00	1.00
R	R-ICA P	1.00	1.00	1.05	1.14	1.13	0.99	0.99	1.00	1.01	1.01	0.99	0.98	1.09	1.25	1.24
D	R-ECA	1.00	1.00	1.00	0.99	1.00	1.00	1.00	1.00	1.00	1.00	1.00	1.00	1.00	0.99	0.99
S	R Vert.	1.00	1.07	0.91	0.72	0.69	1.00	1.01	0.99	0.98	0.98	1.01	1.10	0.84	0.51	0.47
S	L Vert.	1.00	1.07	0.91	0.72	0.69	1.00	1.01	0.99	0.98	0.98	1.01	1.10	0.84	0.51	0.47
L	L-ICA D	1.00	1.04	0.00	1.57	1.75	1.00	1.00	1.02	0.99	0.98	0.99	1.03	0.00	1.57	1.75
C	L-PCoA	-	-	-	-	-	-4.96	1.02	1.02	1.02	1.02	-	-	-	-	-
C	R-PCoA	0.96	4.06	7.72	6.87	6.62	-	-	-	-	-	-	-	-	-	-
R	R-ICA D	1.00	0.98	1.09	1.24	1.24	1.00	1.00	1.00	0.99	0.99	1.00	0.98	1.08	1.23	1.22
S	Basilar	1.00	1.07	0.91	0.72	0.69	1.00	1.00	0.99	0.98	0.98	1.01	1.10	0.84	0.51	0.47
D	L-MCA	1.00	1.04	3.10	1.30	0.81	1.00	0.76	1.00	0.31	1.00	1.00	1.31	3.86	1.31	0.77
D	R-MCA	1.00	1.00	0.99	0.97	0.97	1.00	1.00	1.00	1.00	1.00	1.00	1.00	0.99	0.94	0.94
L	L-ACA P	1.00	1.04	0.00	1.58	1.49	0.99	1.00	1.02	0.99	0.99	0.99	1.03	0.00	1.58	1.48
R	R-ACA P	1.00	0.92	1.17	1.33	1.31	1.00	1.00	1.00	0.99	0.99	1.00	0.95	1.16	1.32	1.29
L	L-PCA P	1.00	1.22	0.73	0.33	0.29	0.99	0.99	1.01	1.02	1.02	1.00	1.22	0.73	0.35	0.31
R	R-PCA P	1.00	0.94	1.16	1.79	1.91	1.02	1.02	0.98	0.88	0.85	1.02	1.01	1.00	0.96	0.96
D	L-ACA D	1.00	1.00	0.98	0.88	0.87	1.00	1.00	1.00	1.00	1.00	1.00	1.00	0.98	0.85	0.84
D	R-ACA D	1.00	1.00	0.99	0.93	0.93	1.00	1.00	1.00	1.00	1.00	1.00	1.00	0.99	0.91	0.90
C	ACoA	1.07	1.15	1.42	1.42	1.38	1.08	0.99	0.99	0.99	0.99	1.12	1.11	1.42	1.42	1.37
D	L-PCA D	1.00	0.99	1.01	1.07	1.10	1.00	1.00	1.00	1.00	1.01	1.00	0.99	1.02	1.12	1.15
D	R-PCA D	1.00	0.99	1.01	1.05	1.07	1.00	1.00	1.00	1.00	1.01	1.00	0.99	1.02	1.10	1.13

Figure 5.5: Colour map of normalized results of flow for the configurations of the CoW without PCoA(s). Left side column indicates the vessel group of each vessel illustrated in Figure 4.1 (S = supply vessel, L or R = left or right sided CoW vessel, C = communicating vessel, D = distributing vessel). The ECAs are assumed to be in VGD (Distributing Vessel). The treatment path (L-ICAs and L-MCA) are highlighted as well as the L-ACA distal. Colour map key: Red < 1, White = 1, Blue > 1.

vessels that are directly inline with the treatment path line (L-ICA's and L-ACA proximal). With the R-PCoA absent the pressure results present little to no difference from the baseline model with normalized values between 1 and 1.01. The results for flow demonstrate similarity with the baseline, although the L-PCoA shows a 496% flow difference in the first phase only from this configuration and the baseline. This is due to the size of flow present in both simulations being significantly small as demonstrated in 5.2.

$$\left( \frac{P1_{R-PCoA}}{P1_{Baseline}} \right)_{@L-PCoA} = \frac{-4.009 \times 10^{-9} \text{ ml/s}}{0.8075 \times 10^{-9} \text{ ml/s}} = -4.96 \quad (5.2)$$

Similarly, results reported in Figure 5.5 for alteration to flow in the L-MCA for the model without the R-PCoA during Phase 4 show a 69% difference, also attributable to a nearly zero flow in the baseline full CoW value in the same vessel. The baseline flow results little flow within the R-PCoA throughout the phases (Figure 4.4), the R-PCA proximal experiences less flow (0.12 ml/s and 0.14 ml/s) in phases 4 and 5 respectively, 12% and 15% drop relative to the baseline.

The final variation with both left and right PCoA missing demonstrates a combination of the previous two variations for both pressure and flow. Similar to the missing L-PCoA variation, the vertebrae provide less flow into the CoW during phase 3 onward. The flow results in the R-PCA proximal is increased by 0.74 ml/s and 0.85 ml/s from the baseline result during phase 4 and phase 5 respectively when only the L-PCoA is absent. This isn't seen in the symmetric case where there is a reduction. With both PCoAs removed, the outcome presents an almost baseline like flow in the R-PCA proximal at 96% of the baseline flow.

Most of the effects of this configuration become clearer after the start of aspiration, completely altering the haemodynamics and requiring flow to utilise the communicating vessels. For the treatment path (L-ICAs and L-MCA) during post-retrieval, the

L-MCA reduces in flow to 0.89 ml/s and 0.85 ml/s for no L-PCoA and No PCoAs respectively, the R-PCoA sees a negligible change from the baseline.

### **No ACA Proximal Configurations**

Figures 5.6 and 5.7 demonstrate colour maps of the results for pressure and flow respectively for the two variations of the missing proximal ACA configurations. The colour maps use the same normalization technique presented in Equation 5.1.

The pressure results show that there are significant pressure drops during phase 4 and 5 with the left side missing ACA proximal causing the L-PCoA to average 48.5 mmHg for both aspiration active phases. The areas directly linked to the aspiration (L-ICA proximal) experiences considerable drops with 14 and 9.4 mmHg present during phases 4 and 5 respectively for no L-ACA proximal. The same impact occurs in the missing R-ACA proximal configuration with an averaged pressure reading of 9.7 and 6.9 mmHg for the last two phases respectively. This impact continues into the distal L-ICA but with a reduced pressure drop. As before, the normalized data has little deviation with the pressure results of both variations until the aspiration phases.

The flow results demonstrate significant changes from the baseline model in multiple vessels across all five phases. The first two phases demonstrate reduced flow in the CCA on the side and variant that has the missing ACA proximal vessel. The communicating vessels show the most significant changes in both variants of the configuration with extreme deviation from the baseline throughout the five phases.

Observing closer to the area of the absent vessel, the L-ICA distal is no longer able to supply up to the distal ACA as the L-ACA proximal is no longer present, thus the only route is the occluded MCA causing the missing L-ACA variant to stabilize flow in the distal L-ICA. Prior to the distal L-ICA, the proximal does incur flow but noticeably less in comparison to the baseline for the first two phases. With one of the two pos-

Variation:		No L-ACA Proximal (P)					No R-ACA Proximal (P)				
VG	Phase:	1	2	3	4	5	1	2	3	4	5
S	L-CCA	1.00	1.01	1.00	1.00	1.01	1.00	1.00	1.01	1.02	1.03
S	R-CCA	1.00	1.00	1.00	1.00	1.01	1.00	1.00	1.01	1.03	1.04
D	L-ECA	1.01	1.01	1.00	1.00	1.01	0.99	0.99	1.01	1.02	1.03
L	L-ICA P	1.02	1.02	1.05	0.25	0.19	0.99	0.99	0.80	0.17	0.14
R	R-ICA P	0.99	0.98	1.00	1.03	1.05	1.02	1.01	1.03	1.08	1.10
D	R-ECA	1.00	0.99	1.00	1.01	1.02	1.01	1.00	1.01	1.04	1.06
S	R Vert.	1.00	1.00	1.00	0.96	0.97	1.00	1.00	0.99	0.98	0.99
S	L Vert.	1.00	1.00	1.00	0.96	0.97	1.00	1.00	0.99	0.98	0.99
L	L-ICA D	1.03	1.04	1.05	0.32	0.27	0.98	0.98	0.80	0.25	0.23
C	L-PCoA	1.01	1.02	1.03	0.68	0.68	0.99	0.99	0.89	0.66	0.68
C	R-PCoA	0.99	0.99	1.00	0.97	0.99	1.01	1.01	1.00	1.01	1.04
R	R-ICA D	0.98	0.97	0.99	1.05	1.08	1.03	1.02	1.04	1.13	1.17
S	Basilar	1.00	1.00	1.01	0.91	0.92	1.00	1.00	0.97	0.93	0.95
D	L-MCA	1.02	1.04	1.05	0.32	0.27	0.98	0.98	0.80	0.25	0.23
D	R-MCA	0.98	0.97	0.99	1.05	1.09	1.03	1.01	1.04	1.13	1.17
L	L-ACA P	-	-	-	-	-	0.97	0.98	0.79	0.24	0.21
R	R-ACA P	0.97	0.96	0.99	1.08	1.12	-	-	-	-	-
L	L-PCA P	1.00	1.00	1.01	0.89	0.90	1.00	1.00	0.97	0.91	0.93
R	R-PCA P	1.00	1.00	1.01	0.90	0.91	1.00	1.00	0.97	0.92	0.94
D	L-ACA D	0.96	0.94	1.00	1.22	1.31	0.96	0.97	0.78	0.23	0.20
D	R-ACA D	0.96	0.95	0.99	1.11	1.16	0.96	0.98	0.76	0.20	0.17
C	ACoA	0.95	0.93	0.99	1.15	1.21	0.95	0.96	0.76	0.21	0.18
D	L-PCA D	1.00	1.00	1.01	0.87	0.89	1.00	1.00	0.96	0.89	0.91
D	R-PCA D	1.00	1.00	1.01	0.91	0.92	1.00	1.00	0.97	0.93	0.95

Figure 5.6: Colour map of normalized results of pressure for the configurations of the CoW without ACA. Left side column indicates the vessel group of each vessel illustrated in Figure 4.1 (S = supply vessel, L or R = left or right sided CoW vessel, C = communicating vessel, D = distributing vessel). The ECAs are assumed to be in VGD (Distributing Vessel). The treatment path (L-ICAs and L-MCA) are highlighted as well as the L-ACA distal. Colour map key: Red < 1, White = 1, Blue > 1.

Variation:		No L-ACA Proximal (Q)					No R-ACA Proximal (Q)				
VG	Phase:	1	2	3	4	5	1	2	3	4	5
S	L-CCA	0.82	0.67	1.00	1.00	1.01	1.18	1.15	1.01	1.02	1.03
S	R-CCA	1.16	1.24	1.03	0.82	0.77	0.81	0.87	0.79	0.63	0.59
D	L-ECA	1.01	1.01	1.00	1.00	1.01	0.99	0.99	1.01	1.02	1.03
L	L-ICA P	0.70	0.28	1.09	1.00	1.00	1.30	1.32	0.84	1.00	1.00
R	R-ICA P	1.27	1.44	1.05	0.76	0.70	0.68	0.76	0.66	0.50	0.47
D	R-ECA	1.00	0.99	1.00	1.01	1.02	1.01	1.00	1.01	1.04	1.06
S	R Vert.	0.99	0.99	0.91	1.50	1.44	1.00	1.00	1.33	1.50	1.42
S	L Vert.	1.00	0.99	0.91	1.50	1.44	1.00	1.00	1.33	1.50	1.42
L	L-ICA D	0.62	0.00	0.00	0.00	-0.10	1.38	1.45	4.97	-0.13	-0.20
C	L-PCoA	-272.52	2.90	-0.01	2.73	2.46	284.33	0.11	4.99	2.96	2.59
C	R-PCoA	-9.76	-17.10	7.93	-9.09	-8.20	13.15	10.21	-30.08	-12.64	-10.96
R	R-ICA D	1.34	1.56	1.09	0.58	0.53	0.60	0.70	0.49	0.27	0.24
S	Basilar	1.00	0.99	0.91	1.50	1.44	1.00	1.00	1.33	1.50	1.42
D	L-MCA	1.03	0.51	1.27	1.66	0.27	0.98	0.04	0.98	1.33	0.22
D	R-MCA	0.98	0.97	0.99	1.06	1.09	1.03	1.01	1.04	1.13	1.17
L	L-ACA P	-	-	-	-	-	1.99	1.45	4.97	-0.13	-0.08
R	R-ACA P	1.85	2.87	1.18	0.43	0.38	-	-	-	-	-
L	L-PCA P	0.77	0.57	0.73	2.17	2.05	1.25	1.20	2.09	2.32	2.15
R	R-PCA P	1.23	1.34	1.16	-0.35	-0.45	0.75	0.83	0.29	-0.78	-0.84
D	L-ACA D	0.96	0.94	1.00	1.22	1.31	0.96	0.97	0.77	0.23	0.20
D	R-ACA D	0.96	0.95	0.99	1.11	1.17	0.95	0.98	0.76	0.20	0.17
C	ACoA	23.90	2.77	1.45	0.27	0.23	-23.78	2.87	-1.11	-0.05	-0.03
D	L-PCA D	1.00	1.00	1.01	0.87	0.89	1.00	1.00	0.96	0.89	0.91
D	R-PCA D	1.00	1.00	1.01	0.91	0.92	1.00	1.00	0.97	0.93	0.95

Figure 5.7: Colour map of normalized results of flow for the configurations of the CoW without ACA. Left side column indicates the vessel group of each vessel illustrated in Figure 4.1 (S = supply vessel, L or R = left or right sided CoW vessel, C = communicating vessel, D = distributing vessel). The ECAs are assumed to be in VGD (Distributing Vessel). The treatment path (L-ICAs and L-MCA) are highlighted as well as the L-ACA distal. Colour map key: Red < 1, White = 1, Blue > 1.

sible channels for the flow to pass through being stationary (L-ICA distal) the flow is forced down through the L-PCoA with flows of -0.22 and -0.52 ml/s in phase 1 and 2 respectively.

The treatment path post-retrieval show similar outcomes for both configurations. Neither of the configurations reverse flow in the L-MCA but do reduce the magnitude of flow to less than 0.3 ml/s (73% and 78% drop in flow magnitude respectively for L-ACA and R-ACA proximal absent).

### **No PCA Proximal Configurations**

Figures 5.8 and 5.9 show colour maps of the results for pressure and flow respectively for the two variations of the missing proximal PCA configurations. The colour maps use the same normalization technique presented in Equation 5.1.

The placement of the PCA directly links to one of the key sources of inflow to the CoW, the basilar artery. With a missing PCA, flow from the basilar must be forced to proceed through the alternate PCA. Results demonstrate an increase in flow and pressure in the existing proximal PCA when the opposing one is missing across the five phases. With the L-PCA proximal missing the largest pressure drops in comparison to the baseline appear in the last 2 phases but in a particular region of vessels. The L-PCA distal demonstrates significant loss of pressure with values dropping to 36.5 mmHg in phase 5. With the L-PCA proximal missing, the pressure present in the L-PCoA also reduces through the phases with the lowest being 41.5 mmHg in phase 5. With the R-PCA proximal missing, the overall effect on pressure for the system is minimal. The largest affects are imposed on small overall pressure reductions from the baseline mode of up to 7% in the R-PCoA and up to 12% in the R-PCA distal.

The results for flow demonstrate the systems inability of the system to supply flow through the basilar artery when a PCA proximal is occluded, regardless the side, with

Variation:		No L-PCA Proximal (P)					No R-PCA Proximal (P)				
VG	Phase:	1	2	3	4	5	1	2	3	4	5
S	L-CCA	1.00	1.00	1.00	1.01	1.01	1.00	1.00	1.00	1.00	1.00
S	R-CCA	1.00	1.00	1.00	1.00	1.01	1.00	1.00	1.00	1.00	1.00
D	L-ECA	1.00	1.00	1.00	1.01	1.01	1.00	1.00	1.00	1.00	1.00
L	L-ICA P	0.99	0.99	0.94	0.78	0.75	1.00	1.00	1.00	0.99	0.99
R	R-ICA P	1.00	1.00	0.99	0.99	0.99	0.99	0.99	0.99	0.99	0.99
D	R-ECA	1.00	1.00	1.00	1.00	1.00	1.00	1.00	1.00	1.00	1.00
S	R Vert.	1.01	1.01	1.02	1.04	1.05	1.01	1.01	1.01	1.02	1.02
S	L Vert.	1.01	1.01	1.02	1.04	1.05	1.01	1.01	1.01	1.02	1.02
L	L-ICA D	0.99	0.99	0.94	0.80	0.78	1.00	1.00	1.00	0.99	0.99
C	L-PCoA	0.95	0.96	0.88	0.66	0.62	1.02	1.02	1.01	1.01	1.01
C	R-PCoA	1.02	1.01	1.01	1.04	1.05	0.95	0.95	0.95	0.93	0.93
R	R-ICA D	1.00	1.00	0.99	0.97	0.98	0.99	0.99	0.99	0.98	0.98
S	Basilar	1.03	1.02	1.04	1.09	1.11	1.03	1.03	1.03	1.04	1.04
D	L-MCA	0.99	0.99	0.94	0.80	0.78	1.00	1.00	1.00	0.99	0.99
D	R-MCA	1.00	1.00	0.99	0.97	0.97	0.99	0.99	0.99	0.98	0.98
L	L-ACA P	0.99	0.99	0.94	0.83	0.82	1.00	1.00	1.00	0.99	0.99
R	R-ACA P	1.00	1.00	0.98	0.95	0.95	0.99	0.99	0.99	0.98	0.98
L	L-PCA P	-	-	-	-	-	1.03	1.03	1.03	1.02	1.02
R	R-PCA P	1.03	1.02	1.04	1.09	1.11	-	-	-	-	-
D	L-ACA D	0.99	0.99	0.95	0.86	0.85	1.00	1.00	0.99	0.99	0.99
D	R-ACA D	1.00	1.00	0.97	0.93	0.93	0.99	0.99	0.99	0.98	0.98
C	ACoA	0.99	0.99	0.96	0.90	0.90	0.99	0.99	0.99	0.98	0.98
D	L-PCA D	0.90	0.92	0.83	0.57	0.52	1.03	1.03	1.03	1.02	1.02
D	R-PCA D	1.03	1.02	1.03	1.08	1.10	0.91	0.91	0.90	0.89	0.88

Figure 5.8: Colour map of normalized results of pressure for the configurations of the CoW without PCA. Left side column indicates the vessel group of each vessel illustrated in Figure 4.1 (S = supply vessel, L or R = left or right sided CoW vessel, C = communicating vessel, D = distributing vessel). The ECAs are assumed to be in VGD (Distributing Vessel). The treatment path (L-ICAs and L-MCA) are highlighted as well as the L-ACA distal. Colour map key: Red < 1, White = 1, Blue > 1.

Variation:		No L-PCA Proximal (Q)					No R-PCA Proximal (Q)				
VG	Phase:	1	2	3	4	5	1	2	3	4	5
S	L-CCA	1.10	1.11	1.00	1.01	1.01	1.01	1.01	1.00	1.00	1.00
S	R-CCA	1.01	1.01	1.10	1.13	1.12	1.10	1.11	1.09	1.07	1.07
D	L-ECA	1.00	1.00	1.00	1.01	1.01	1.00	1.00	1.00	1.00	1.00
L	L-ICA P	1.17	1.23	0.98	1.00	1.00	1.01	1.02	1.02	1.00	1.00
R	R-ICA P	1.01	1.01	1.15	1.17	1.15	1.16	1.19	1.15	1.09	1.09
D	R-ECA	1.00	1.00	1.00	1.00	1.00	1.00	1.00	1.00	1.00	1.00
S	R Vert.	0.65	0.68	0.64	0.54	0.53	0.66	0.62	0.70	0.80	0.81
S	L Vert.	0.65	0.69	0.64	0.55	0.53	0.66	0.63	0.71	0.80	0.81
L	L-ICA D	0.89	0.84	-2.10	1.72	1.89	1.10	1.18	1.73	0.94	0.94
C	L-PCoA	-1044.49	4.92	-2.11	-0.25	-0.19	316.99	-0.49	1.73	1.11	1.08
C	R-PCoA	-12.59	-11.60	22.94	8.85	8.16	43.88	50.07	-40.12	-6.12	-4.98
R	R-ICA D	1.10	1.10	1.27	1.31	1.29	0.89	0.87	0.92	0.96	0.97
S	Basilar	0.65	0.69	0.64	0.54	0.53	0.66	0.62	0.71	0.80	0.81
D	L-MCA	0.99	0.53	3.19	2.70	0.78	1.00	0.86	0.90	-0.17	0.99
D	R-MCA	1.00	1.00	0.99	0.97	0.97	0.99	0.99	0.99	0.98	0.98
L	L-ACA P	0.73	0.84	-2.10	1.72	1.59	1.24	1.18	1.73	0.94	0.95
R	R-ACA P	1.23	1.31	1.52	1.41	1.37	0.76	0.62	0.86	0.95	0.96
L	L-PCA P	-	-	-	-	-	1.30	1.38	1.23	1.08	1.07
R	R-PCA P	1.32	1.25	1.52	2.07	2.16	-	-	-	-	-
D	L-ACA D	0.99	0.99	0.95	0.86	0.85	1.00	1.00	0.99	0.99	0.99
D	R-ACA D	1.00	1.00	0.97	0.93	0.93	0.99	0.99	0.99	0.98	0.98
C	ACoA	7.18	0.39	2.33	1.53	1.46	-4.90	1.71	0.66	0.95	0.96
D	L-PCA D	0.90	0.92	0.83	0.56	0.51	1.03	1.03	1.03	1.02	1.02
D	R-PCA D	1.03	1.02	1.04	1.08	1.10	0.91	0.91	0.90	0.88	0.88

Figure 5.9: Colour map of normalized results of flow for the configurations of the CoW without PCA. Left side column indicates the vessel group of each vessel illustrated in Figure 4.1 (S = supply vessel, L or R = left or right sided CoW vessel, C = communicating vessel, D = distributing vessel). The ECAs are assumed to be in VGD (Distributing Vessel). The treatment path (L-ICAs and L-MCA) are highlighted as well as the L-ACA distal. Colour map key: Red < 1, White = 1, Blue > 1.

drops reaching low values of 1 ml/s, almost half of the baseline. With the L-PCA missing, the flow on the right side demonstrates flow reversal to supply a higher than usual amount to the distal R-PCA, an increase of 3-10% throughout the phases. With the missing R-PCA, there is still significant activity regarding flow in the R-PCoA with flow moving towards the R-PCA distal at 0.85 to 0.71 ml/s as phases progress.

Observing the treatment path post-retrieval, the missing R-PCA proximal variant shows little to no change from the baseline results for flow, whereas the missing L-PCA proximal helps reduce the overall flow outlet of the baseline value by 12% for both flow and pressure.

### **No PCoA and Collateral PCA Configurations**

Figures 5.10 and 5.11 demonstrate colour maps of the results for pressure and flow respectively for the two variations of the missing proximal PCA configurations. The colour maps present the same normalization technique presented in Equation 5.1.

The pressure results for the collateral variants of missing PCoA and PCA appear to have similarities with the results for missing PCA and missing PCoA results individually. As assessed individually, when the network configuration doesn't include a R-PCA or R-PCoA, the overall impact on the haemodynamics are very small. This is also reflected in the present variations where they (R-PCA and R-PCoA) also don't exist alongside their collateral counterparts (L-PCoA and L-PCA respectively). The results show a similarity to the individual results of the missing L-PCoA and L-PCA configurations.

Observing the results of the variant with missing L-PCoA and R-PCA, there is a significant increase in pressure within the basilar and the L-PCA's, a 7%, 9% and 10% increase from the baseline model for missing L-PCoA alone and 17%, 19% and 20% increase from the baseline for the missing L-PCoA and R-PCA for the basilar, L-PCA proximal

Variation:		No L-PCoA + R-PCA P. (P)					No R-PCoA + L-PCA P. (P)				
VG	Phase:	1	2	3	4	5	1	2	3	4	5
S	L-CCA	1.00	1.00	1.00	1.00	1.01	1.00	1.00	1.00	1.01	1.01
S	R-CCA	1.00	1.00	1.00	1.00	1.00	1.00	1.00	1.00	1.00	1.01
D	L-ECA	1.00	1.00	1.00	1.00	1.01	1.00	1.00	1.00	1.01	1.01
L	L-ICA P	1.00	1.00	0.96	0.76	0.73	0.99	0.99	0.92	0.73	0.71
R	R-ICA P	0.99	0.99	0.98	0.96	0.96	1.00	1.00	0.99	0.97	0.97
D	R-ECA	1.00	1.00	1.00	0.99	0.99	1.00	1.00	1.00	0.99	1.00
S	R Vert.	1.02	1.01	1.03	1.06	1.07	1.02	1.01	1.03	1.06	1.08
S	L Vert.	1.02	1.01	1.03	1.06	1.07	1.02	1.01	1.03	1.06	1.08
L	L-ICA D	1.00	1.00	0.96	0.78	0.76	0.98	0.99	0.92	0.76	0.74
C	L-PCoA	-	-	-	-	-	0.95	0.96	0.87	0.63	0.58
C	R-PCoA	0.95	0.95	0.93	0.88	0.88	-	-	-	-	-
R	R-ICA D	0.99	0.99	0.97	0.93	0.93	1.00	1.00	0.97	0.94	0.94
S	Basilar	1.04	1.03	1.06	1.14	1.17	1.04	1.03	1.06	1.14	1.17
D	L-MCA	1.00	1.00	0.96	0.78	0.76	0.98	0.99	0.93	0.76	0.74
D	R-MCA	0.99	0.99	0.97	0.93	0.93	1.00	1.00	0.97	0.94	0.94
L	L-ACA P	0.99	1.00	0.96	0.81	0.79	0.99	0.99	0.93	0.80	0.78
R	R-ACA P	0.99	0.99	0.97	0.91	0.91	0.99	0.99	0.97	0.91	0.92
L	L-PCA P	1.04	1.03	1.06	1.16	1.19	-	-	-	-	-
R	R-PCA P	-	-	-	-	-	1.04	1.03	1.06	1.15	1.19
D	L-ACA D	0.99	0.99	0.96	0.83	0.82	0.99	0.99	0.94	0.82	0.82
D	R-ACA D	0.99	0.99	0.97	0.89	0.89	0.99	0.99	0.96	0.89	0.89
C	ACoA	0.99	0.99	0.97	0.87	0.86	0.99	0.99	0.95	0.87	0.87
D	L-PCA D	1.04	1.03	1.07	1.17	1.20	0.90	0.92	0.82	0.54	0.49
D	R-PCA D	0.91	0.91	0.89	0.84	0.84	1.04	1.03	1.06	1.16	1.19

Figure 5.10: Colour map of normalized results of pressure for the configurations of the CoW without PCoA and the collateral PCA. Left side column indicates the vessel group of each vessel illustrated in Figure 4.1 (S = supply vessel, L or R = left or right sided CoW vessel, C = communicating vessel, D = distributing vessel). The ECAs are assumed to be in VGD (Distributing Vessel). The treatment path (L-ICAs and L-MCA) are highlighted as well as the L-ACA distal. Colour map key: Red < 1, White = 1, Blue > 1.

VG	Variation:	No L-PCoA + R-PCA P. (Q)					No R-PCoA + L-PCA P. (Q)				
		1	2	3	4	5	1	2	3	4	5
S	L-CCA	1.04	1.02	1.00	1.00	1.01	1.11	1.12	1.00	1.01	1.01
S	R-CCA	1.11	1.11	1.18	1.26	1.26	1.04	1.04	1.17	1.24	1.23
D	L-ECA	1.00	1.00	1.00	1.00	1.01	1.00	1.00	1.00	1.01	1.01
L	L-ICA P	1.07	1.05	0.97	1.00	1.00	1.19	1.26	0.89	1.00	1.00
R	R-ICA P	1.19	1.20	1.29	1.35	1.33	1.06	1.06	1.26	1.31	1.29
D	R-ECA	1.00	1.00	1.00	0.99	0.99	1.00	1.00	1.00	0.99	1.00
S	R Vert.	0.53	0.57	0.44	0.26	0.24	0.52	0.57	0.44	0.26	0.24
S	L Vert.	0.53	0.58	0.44	0.27	0.25	0.53	0.58	0.44	0.27	0.25
L	L-ICA D	1.07	1.16	0.00	1.57	1.75	0.91	0.87	-2.07	1.71	1.89
C	L-PCoA	-	-	-	-	-	-1042.80	4.91	-2.08	-0.24	-0.18
C	R-PCoA	43.81	50.02	-39.55	-5.78	-4.71	-	-	-	-	-
R	R-ICA D	0.92	0.88	1.06	1.22	1.21	1.07	1.07	1.25	1.29	1.26
S	Basilar	0.53	0.58	0.44	0.27	0.24	0.53	0.58	0.44	0.27	0.25
D	L-MCA	1.00	0.97	3.74	1.15	0.76	0.98	0.64	3.50	1.72	0.74
D	R-MCA	0.99	0.99	0.97	0.93	0.93	1.00	1.00	0.97	0.94	0.94
L	L-ACA P	1.18	1.16	0.00	1.58	1.48	0.79	0.87	-2.08	1.71	1.57
R	R-ACA P	0.82	0.65	1.14	1.31	1.28	1.18	1.24	1.50	1.40	1.35
L	L-PCA P	1.04	1.27	0.77	0.36	0.32	-	-	-	-	-
R	R-PCA P	-	-	-	-	-	1.06	1.05	1.04	1.01	1.01
D	L-ACA D	0.99	0.99	0.96	0.83	0.82	0.99	0.99	0.94	0.82	0.81
D	R-ACA D	0.99	0.99	0.97	0.89	0.89	0.99	0.99	0.96	0.89	0.89
C	ACoA	-3.39	1.65	1.39	1.41	1.36	5.80	0.52	2.30	1.52	1.44
D	L-PCA D	1.04	1.03	1.07	1.17	1.20	0.90	0.92	0.81	0.54	0.49
D	R-PCA D	0.91	0.91	0.89	0.84	0.83	1.04	1.03	1.06	1.16	1.19

Figure 5.11: Colour map of normalized results of flow for the configurations of the CoW without PCoA and the collateral PCA. Left side column indicates the vessel group of each vessel illustrated in Figure 4.1 (S = supply vessel, L or R = left or right sided CoW vessel, C = communicating vessel, D = distributing vessel). The ECAs are assumed to be in VGD (Distributing Vessel). The treatment path (L-ICAs and L-MCA) are highlighted as well as the L-ACA distal. Colour map key: Red < 1, White = 1, Blue > 1.

and L-PCA distal respectively. This increase also occurs in the opposing configuration (No R-PCoA and L-PCA).

When it comes to flow, these variations result in a restricted channel of flow from the basilar artery as the flow exiting from the PCA that has its proximal predecessor experiences all the flow. The collateral PCoA where most of the flow would occur in the missing PCA variants isn't present in these variations. The comparison in results from these variants show more volatile differences from the baseline in comparison to the PCA missing alone and PCoA missing alone. The flow in both variants for the basilar drops to 53%, 58%, 44% 27% and 24/25% in phases 1 through 5, significantly reduced from the missing PCA variants alone. With these variants, there is a significant use of the communicating vessels due to the nature of the re-distribution of flow which can be seen in the results isolated in Table 5.1. With the assumed positive direction of flow for the ACoA flowing from left cranial side to right for the simulations, it is clear that for all three of the presented simulations in Table 5.1 the use of the ACoA is present with slight increase in amplitude in the missing collateral variants than the baseline towards the left side of the CoW. In the baseline simulation, the treatment utilises the L-PCoA pathway in phases 4 and 5 with flows of 1.82 and 2.14 ml/s respectively into the junction that includes the ICA's. with the L-PCoA missing alongside the R-PCA, there is a demand on the R-PCoA to issue flow towards the distal R-PCA throughout the phases, dropping from 0.87 to 0.67 ml/s throughout the treatment process. Alternatively, the opposite variation sees the L-PCoA comply to a different flow requirement, similarly to the R-PCoA in the counterpart variant, it is required to supply flow towards the distal PCA. In the baseline, the treatment impacts the L-PCoA heavily forcing up to 2.14 ml/s of flow into the ICA junction whereas in this case, it attempts to supply the distal L-PCA between 0.89 and 0.38 ml/s throughout treatment.

When observing the impact of the missing collateral variants on the area of inci-

Simulation	Vessel	Flow (ml/s) for Phase:				
		1	2	3	4	5
Baseline	ACoA	-0.05	0.42	-0.81	-4.01	-4.71
	L-PCoA	0.00	-0.18	0.37	1.82	2.14
	R-PCoA	-0.02	-0.02	0.02	0.12	0.14
No L-PCoA & R-PCA Pr.	ACoA	0.16	0.70	-1.12	-5.66	-6.42
	R-PCoA	-0.84	-0.87	-0.84	-0.69	-0.67
No R-PCoA & L-PCA Pr.	ACoA	-0.28	0.22	-1.86	-6.08	-6.77
	L-PCoA	-0.84	-0.89	-0.76	-0.44	-0.38

Table 5.1: Flow values for the communicating vessels for Configurations of Missing PCoA with collateral PCA proximal compared with Baseline results.

dence, the L-MCA sees a pressure reduction in the final two phases of approximately 22% to 26% from the baseline results. This produces a slightly reduced flow into the L-MCA post-retrieval of the occlusion in comparison to the baseline, but still results in at least 0.8 ml/s of flow in both variants.

### 5.2.2 Configurations and the Treatment Path

With the treatment (balloon and aspiration) being present in the proximal region of the proximal L-ICA, the effects of the clot and aspiration directly affect the path from the ICA to the MCA where the ischaemic occlusion exists. With the MCA occluded in three out of five phases, flow is almost stationary within the L-MCA, thus the flow path then interferes with the L-ACA proximal. Observation of the different configurations for these three focus vessels (L-ICA proximal, distal and L-ACA proximal) is presented in the graphs shown in Figure 5.12.

The flow results in the L-ICA proximal show mostly consistent results apart from the configuration that excludes the L-ACA proximal, where the flow is approximately half as low in the first two phases in comparison to the rest of the configurations and the

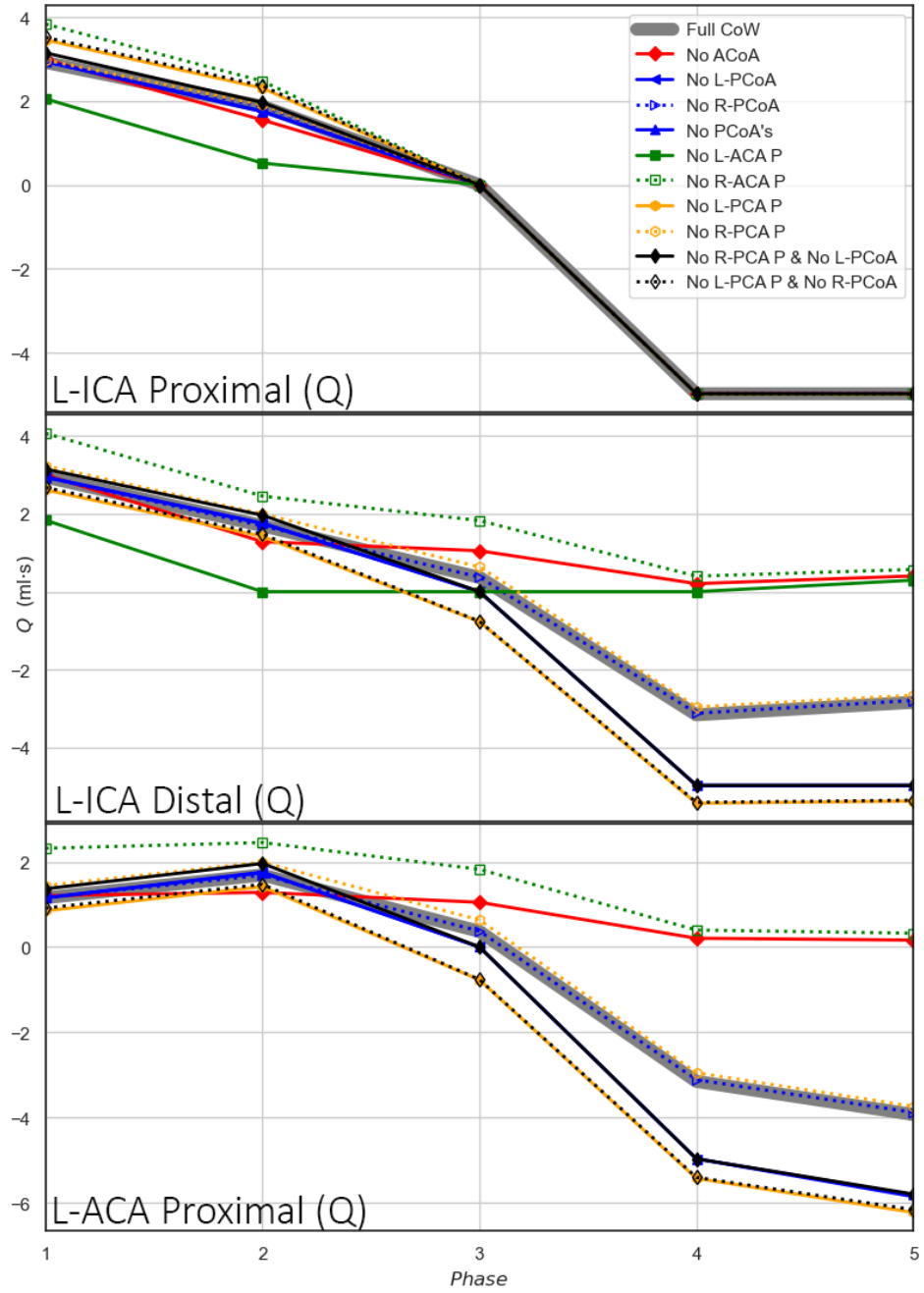


Figure 5.12: Averaged flow values for all the variations for vessels that are directly affected by the treatment and occlusive region excluding the L-MCA.

baseline. With the balloon and the aspiration applied in phases 2 and 3 respectively in the proximal region of the L-ICA proximal, all the results agree in the final three phases resulting in no flow in phase 3 and approximately -5 ml/s in phase 4 and 5.

Observing the results past the junction of the L-PCoA into the distal L-ICA, the configurations tell a different story entirely. In fact the line patterns of the averaged flow plots for the proximal L-ACA and the distal L-ICA are almost identical for phase 2 onward but with a different scale and missing the No L-ACA plot for the L-ACA graph for its obvious absence. Comparing the configurations to the complete CoW set-up, the results demonstrate that there is retrograde flow in the L-ACA proximal and L-ICA distal in all the configurations apart from three during phase 4 and 5, whilst it being relatively close to 0 ml/s or significantly reduced from phase 2 during phase 3 (-1 to 1 ml/s). The three outliers are the configurations with missing R-ACA proximal, L-ACA proximal and the ACoA. With these configurations in place, they cut off access to the respective distal ACA's or the opposing side in terms of the ACoA, which in terms for the missing ACoA and R-ACA configurations, a supply is still required from the L-ICA distal to be dealt through the distal ACA vessels according to the results, hence the lack of retrograde flow in these scenarios. With the L-ACA missing entirely, the results of flow for the L-ICA distal are almost stationary until the occlusion in the L-MCA is retrieved, allowing a small amount of flow to pass through.

Table 5.2 represents the flow results of all the configurations in phases 1 and 5, the only phases where the occlusion is not present in the L-MCA. Observations of flow results for phase 1 show small deviation with flow typically being  $1.79 \pm 0.05$  ml/s. The largest increase is experienced in the configuration of a missing L-ACA proximal and the lowest being the configuration with the opposing side to have the missing ACA proximal (R-ACA proximal). These configurations ultimately see the most drop in flow during phase 5 with a flow drop to under 0.3 ml/s. The characteristics of the CoW with-

Configuration	Phase 1 (ml/s)	Phase 5 (ml/s)
Full CoW	1.79	1.01
No ACoA	1.79	0.24
No L-PCoA	1.79	0.89
No R-PCoA	1.79	1.01
No PCoA's	1.79	0.85
No L-ACA Pr.	1.84	0.30
No R-ACA Pr.	1.75	0.25
No L-PCA Pr.	1.77	0.86
No R-PCA Pr	1.79	1.09
No R-PCA + L-PCoA	1.78	0.83
No L-PCA + R-PCoA	1.77	0.82

Table 5.2: Blood flow rates in the L-MCA during phase 1 and phase 5. Results for phases 2-4 are omitted as they very close to 0 ml/s.

out either of the proximal ACA's demonstrates a crucial change in the haemodynamics of the CoW and its impact on the treatment path.

Figure 5.13 shows the averaged pressure values for the configurations in the key vessels surrounding the treatment and its path for the five phases (L-ICAs and L-ACA proximal). The general trend of the pressure changes for each configurations follows the same behaviour. The most significant pressure drops are observed in the configurations that don't possess an ACoA and either ACA proximal. Alternatively the least pressure drops over the phases appear in the lack of existence in the right side PCoA or PCA proximal which match up fairly well with the baseline values.

### 5.3 Discussion

After analysing the simulations of all the configurations for the CoW, there were many haemodynamic characteristics that were observed in relation to the baseline model and other behaviours specific to certain vessels.

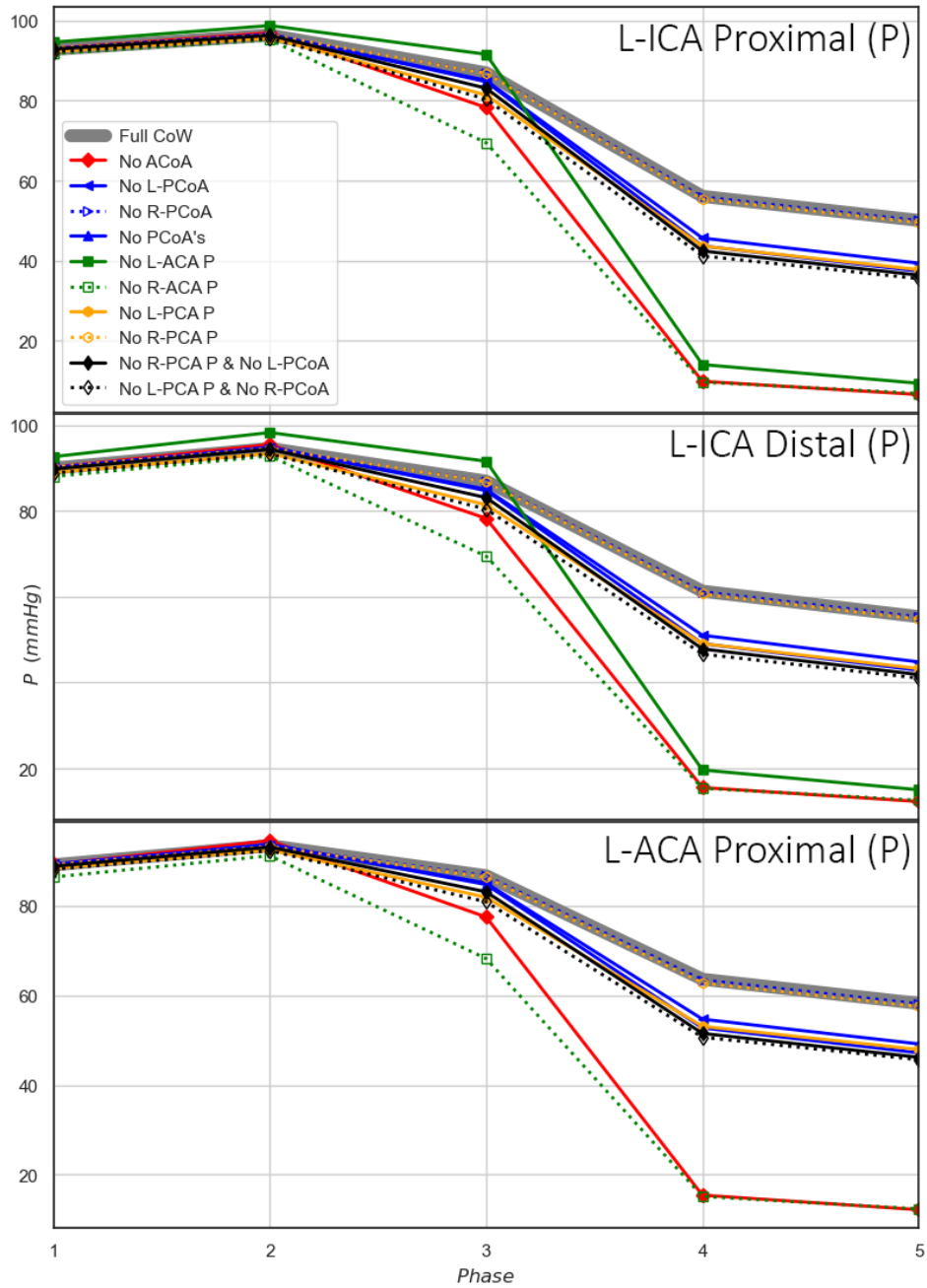


Figure 5.13: Averaged pressure values for all the variations for vessels that are directly affected by the treatment and occlusive region excluding the L-MCA.

The communicating vessels as described in Chapter 4 have an important role when it comes to the treatment application to the system. They provide crucial flow access to the other side of the CoW which can be favourable in maintaining consistent outflow to the distributing vessels when the treatment is present (clot, balloon or aspiration). Similarly, the same is observed with the various configurations. The general effects of the treatment phases on all the configurations also follow the same trends; retrograde flow is present in some but not all vessels that surround the area of the treatment, whereas the application of the treatment results in a pressure increase with the administration of the occlusion in the L-MCA which then relieves as phases 3 to 5 proceed. However, some configurations may work in favour or against the clinician and the procedure.

Retrograde flow in the configurations with a missing vessel have a common factor in the L-ICA proximal of experiencing retrograde flow during phases 4 and 5 although the L-ICA distal as mentioned, has three configurations (missing ACoA or missing either ACA proximal) where retrograde flow is not present. As the distributing vessels of the system are crucial providers of blood to the brain (VGD), the CoW's aim is to make sure there is a redistribution to provide flow to these areas. The extreme examples of this is with the anatomy with any of the three anterior CoW vessels missing (left or right ACA proximal or ACoA). Figure 5.14 demonstrates the missing L-ACA proximal flow behaviour in comparison to the complete CoW. With the ACA proximal missing on the left side, the flow to the L-ACA distal is required to be supplied from the right side of the CoW and given access through the ACoA. Alternatively, the full CoW would permit flow through the L-ACA proximal from the L-ICA's. When the treatment is applied, and the occlusion in the L-MCA is removed, the results demonstrate no retrograde flow but instead a positive flow in the L-MCA (although very small) in both cases; the full CoW and the missing vessel case. Similarly, both distal L-ACA's also had positive flow to distribute to the anterior part of the brain. The key factor to allow this is the presence

of the communicating vessels. Throughout the configurations, success of collateral and redistribution of flow within the CoW pre-treatment and during treatment to maintain flow output always relies on the use of the available communicating vessels.

From a clinical perspective, when applying the treatment, the target is to achieve retrograde flow if possible to reduce the likelihood of distal embolization. The simu-

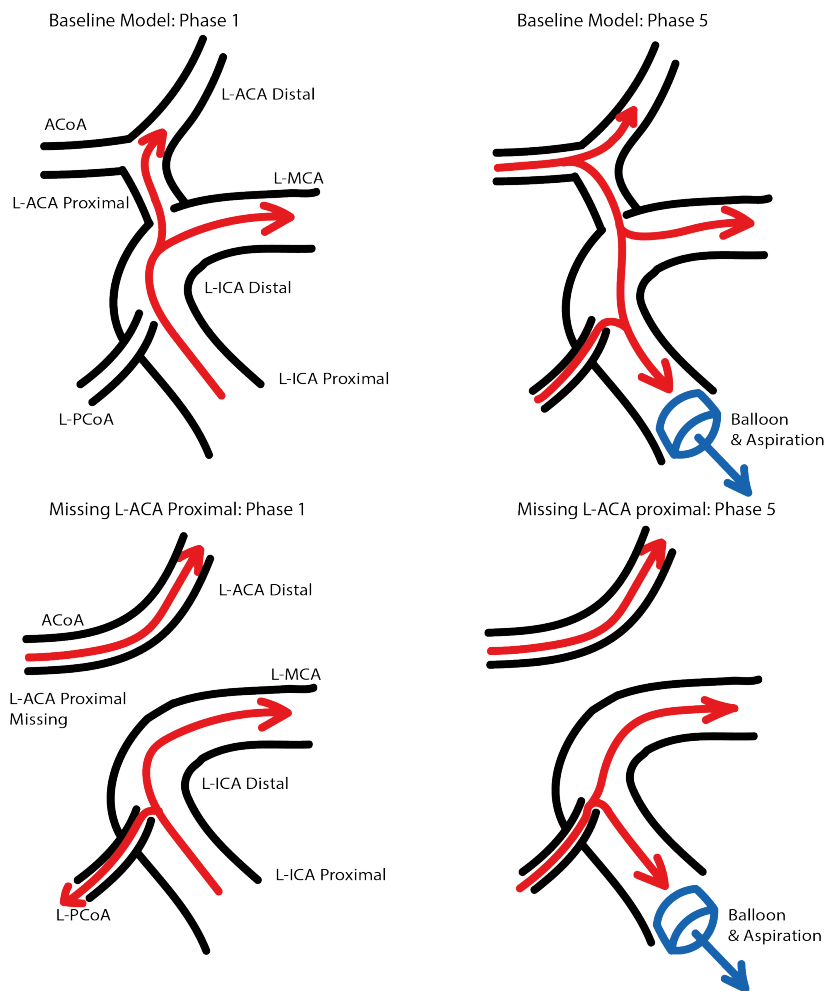


Figure 5.14: Flow path and circulation illustration of the simulations: baseline model phase 1 and 5 alongside missing L-ACA proximal phase 1 and 5.

lation results does not demonstrate a single configuration including the baseline that exhibits reverse flow in the vessel of incidence (L-MCA), but in certain cases, its reduced to a very small magnitude (missing ACoA, or missing either ACA proximal). These cases result in a more favourable outcome, although in all configurations there was a clear reduction in flow during the post-retrieval phase. Table 5.3 presents all the configurations and their effects on aspiration in the vessels that are on the treatment path. Although there is forward flow in the L-MCA post retrieval which is a risk factor of distal embolization downstream the MCA tree, as the clot is retrieved, distal embolization can still threaten other regions of the cerebrovascular network. The configurations that have either the ACoA or ACA proximal absent cause the L-PCoA to drive flow towards the left side of the CoW to then supply the MCA and ACA distal. During the retrieval of the clot, when passing through the distal L-ICA, flow is passing forward against the clot according to the results, potentially fragmenting the clot.

Configuration	Phase 4/5				Phase 5
	L-ICA Prox.	L-PCoA	L-ACA prox.	L-ACA Dist.	L-MCA
Baseline	R	R	R	F	F
No ACoA	R	R*	F	F	F
No L-PCoA	R	-	R	F	F
No R-PCoA	R	R	R	F	F
No PCoA's	R	-	R	F	F
No L-ACA	R	R*	F	F	F
No R-ACA	R	R*	F	F	F
No L-PCA	R	R	R	F	F
No R-PCA	R	R	R	F	F
No L-PCoA + R-PCA	R		R	F	F
No R-PCoA + L-PCA	R	R	R	F	F

Table 5.3: Network configurations and the treatment pathway during aspiration phases (Phase 4 and Phase 5). R = Retrograde flow, F = Forward Flow, R\* = Retrograde flow but flow supplied by this vessel assists with redistributing flow away from aspiration too.

The assumptions considered in this model simplified the simulation to demonstrate the capabilities of the 1D model. On this front, the model was able to provide useful quantitative data in every single vessel in the CoW and leading up from the heart. Considering the assumptions, it is clear that there are limitations to the study. With the phases set up to be at key and important moments of the treatment, the transient effects of the treatment are ignored, similarly to the baseline model, although the variation of networks opens new avenues for pre-incident outcomes. Although the simulations all assume occlusion in the L-MCA, the study is limited to assuming the possibility of an occlusion happening is in the same areas, whereas the different anatomy would mean altered thromboembolus trajectories and pathways in the CoW. This consideration also follows into the treatment phases as well with regards to fragments of the occlusion as haemodynamic forces drive embolus dynamics across the arterial network, embolus trajectories may not exactly follow the flow routing across the CoW communicating arteries owing to their finite inertia and their collisions with vessel walls [145].

With the baseline results used to compare against the ten chosen configurations of the CoW, there is clarity in understanding the quantitative behaviour of flow and pressure within the vessels in the configurations. Subject to the set-up with minimal variation from the baseline model for comparison purposes, it is clear that the haemodynamic behaviour is strongly dependant on the CoW's anatomy, especially the communicating vessels.

## **5.4 Conclusions**

In this chapter, ten CoW networks were configured and simulated to help understand their hamodynamic effects during the treatment. Results showed that all the configurations still presented no retrograde flow in the L-MCA but lower magnitudes to that

of the baseline simulation post-retrieval, however some configurations demonstrated more favourable outcomes with larger reverse flow in the treatment path. Variations that were missing distal parts of the CoW (missing ACoA or proximal ACAs) demonstrated the lowest outflow to the L-MCA and the distal L-ACA due to the L-PCoA recirculating flow towards the distal L-ICA. This meant that flow was not reversed in the distal L-ICA which presented these variations to have two out of the three treatment path vessels not reversing flow compared to the one out of three in the rest of the configurations.

## Chapter 6

# Aged Network Variations

### Summary

Certain risk factors as discussed in Chapter 2 demonstrate changes to the cerebrovascular systems mechanical mechanisms altering the haemodynamics. People of older age experience mechanical changes to their arterial structure as well as alteration in haemodynamic properties [38]. The network described in the baseline model in Chapter 4 demonstrates an anatomy of a younger individual. With age comes stiffening and dilation of vessels caused by changes to the arterial wall thickness, elastic modulus and lumen area. Within this chapter, simulation on an older individual was considered, using data from the literature to update appropriate model parameters. Simulation of this configuration was performed to compare characteristic differences between the older case and the baseline simulation to understand the effects on age and the treatment process and general haemodynamics.

## 6.1 Methodology

The parameters used for the model in the previous chapters were based on a typical young healthy adult considered from [61]. The justification for the physiological data used to create this network is based on several publications which include representative vascular properties. Properties of non-cerebral vessels up to the vertebral and carotid arteries were obtained from [129] whereas for the cerebral vessels (carotid and vertebral arteries on-wards), the data is compiled from [18] for vessel lengths and [146] for the arterial stiffness with  $E$  at 0.8 MPa for vertebral and carotid arteries (0.4 MPa for CCA) and 1.6 MPa for the remainder of the intracranial vessels. From [61], it was assumed that for intracranial vessels, values of wall thickness ( $h_0$ ) were 25% of the radius at reference conditions. The haemodynamic parameters and properties assumed were  $\mu$  of 0.004 Pa·s,  $\rho$  of 1060 Kg/m<sup>3</sup>, a cardiac cycle period of  $T$  of 1 second (60 bpm) and the inlet wave presented in Figure 3.2. Excluding changes of  $\rho$  and  $T$  with age, discussed so far are all the parameters and properties that can deviate within the aging population regarding the haemodynamics and mechanical anatomy that are parameters within the 1D model. To perform an analysis on an aged variation of the CoW, aging the current properties and parameters within the current network was required.

With stroke statistics suggesting higher occurrence in ages over 65, the current network was translated to represent an anatomy for a patient between the age of 65 and 70 years of age based on what data can be found in the literature [147]. Regarding the vascular mechanics, it is understood in the literature that wall thickness, characteristic lumen radius and wall elastic modulus all increase with age. For the radius, [57] shows that with age the aorta increases to approximately 18mm at 70 years of age, an increase of approximately 50% from the baseline value for the aorta radius of 12mm. Studies of normal aging also show fair agreement with applying the same radius increase to cerebrovascular vessels such as the CCA's (2.5mm to 3.75mm) and ICA's (2mm

to 3mm) [148]. From this, it was assumed that from the baseline anatomy, the 70 year old anatomy will have a 50% increase to radius values. For consistency, it is assumed that the wall thickness of cerebrovascular vessels is 25% of the vessel radius for the aged anatomy. For non cerebrovascular vessels two options were in contention. An estimation of the wall thickness is presented in Equation 6.1 from a study [149] estimates the approximate wall thickness of said vessel:

$$h_0(x) = R_0(x) \left( 0.2802e^{-5.053R_0(x)} + 0.1324e^{-0.1114R_0(x)} \right) \quad (6.1)$$

Where  $x$  is the position along the longitudinal axis. Alternatively, extrapolating the values from the baseline values for radius and thickness was the alternate route calculated through the following formula:

$$h_{0A} = \frac{h_{0B}}{R_{0B}} \cdot R_{0A} \quad (6.2)$$

Where subscript  $A$  and  $B$  stand for aged and baseline respectively (e.g.  $R_{0A}$  is the aged radius). Table 6.1 demonstrates the resultants of both methods of calculating wall thickness and resultant radii. For the cerebrovascular vessels, literature demonstrates CCA wall thicknesses of approximately 0.7 to above 1mm in thickness for ages upwards of 65, aligning with the method used to calculate the aged wall thickness for the CCA in Table 6.1 [73]. For non-cerebrovascular vessels, Equations 6.1 and 6.2 were in contention. A study of the aorta demonstrates that the average aortic thickness for patients aged 65 to 74 was approximately 2.26mm [150]. With consideration between the results of both methods used to predict the aortic thickness, the percentile difference were significantly different with the ascending aorta, subclavian and the brachial arteries for Equation 6.1 predicting lower results in comparison to Equation 6.2 by at least 17%. Although, when considering the aortic arch, the result of Equation 6.2 at 2.45mm was

closer to the averaged 2.26mm from the literature ([150]) in comparison to the 1.95mm predicted by Equation 6.1. Under review, the wall thickness estimates used was taken from extrapolation (Equation 6.2).

Regarding the elastic modulus, there is a consensus that with age the elastic modulus of arteries increase [151], although there are studies to show that age isn't a largely supporting factor of elastic modulus increase [146]. For certain vessels such as the aorta, there is clear contrast demonstrating extreme increases of the elastic modulus with age, with an increase from 400 kPa to 1.2 MPa (20 years of age to 70) a total approximate increase of 0.8 MPa [58]. With regards to smaller and cerebrovascular vessels, some studies demonstrate incremental elastic modulus at 100 mmHg to be approximately 2.5 MPa for the ICA and over 3 MPa for the ACA for a group of 7 patients aged between 58 and 88 [152]. With the current model exercising three different values for  $E$ , 0.4 MPa for extracranial vessels, 0.8 MPa for extra-intracranial vessels and 1.6 MPa for intracranial CoW vessels, an increment of 0.8 MPa was applied to all vessels as this would comply with the literature for the aorta, slightly lower for the ICA, and larger difference for the ACA, although this would maintain consistency with regards maintaining three values of  $E$  in the aged model, and minimising the number of parameter changes in the study.

From the discussed parameters,  $R_0$ ,  $h_0$  and  $E$ , the new generated aged network is presented in Table 6.2.

As previously mentioned, viscosity was set at 0.004 Pa·s in the previous studies. With aging, it is expected that the viscosity of the blood will increase in most cases. With the vessels in the network large enough to assume Newtonian flow, viscosity levels are approximately between 0.002 and 0.0045 Pa·s for most ages up to 80, but literature demonstrates that it is still common for people aged 70 to 100 to have viscosity levels ranging upwards of 0.004 beyond 0.006 Pa·s [153]. The viscosity is expected to affect pressure drop through vessels observed in the Hagen–Poiseuille equation (Equation 2.2)

Vessel	$R_0$ (mm)		$h_0$ (mm)				% Diff.
	$R_{0B}$	$R_{0A}$	$h_{0B}$	$h_{0A}$	$h_0(x)$		
Ascending Aorta	12	18.00	1.63		2.45	1.95	25.34%
Aortic Arch Proximal	11.2	16.80	1.26		1.89	1.85	2.40%
Brachiocephalic	6.2	9.30	0.8		1.20	1.13	5.83%
Aortic Arch Distal	10.7	16.05	1.15		1.73	1.78	-3.01%
L-CCA	2.5	3.75	0.63	0.94			
R-CCA	2.5	3.75	0.63	0.94			
R Subclavian	4.23	6.35	0.67		1.01	0.85	17.57%
Thoracicaorta	9.99	14.99	1.1		1.65	1.68	-1.85%
L Subclavian	4.23	6.35	0.67		1.01	0.85	17.57%
L-ECA	1.5	2.25	0.38	0.56			
L-ICA Proximal	2	3.00	0.5	0.75			
R-ICA Proximal	2	3.00	0.5	0.75			
R-ECA	1.5	2.25	0.38	0.56			
R Vertebral	1.36	2.04	0.34	0.51			
R Brachial	4.03	6.05	0.67		1.01	0.83	21.36%
L Brachial	4.03	6.05	0.67		1.01	0.83	21.36%
L Vertebral	1.36	2.04	0.34	0.51			
L-ICA Distal	2	3.00	0.5	0.75			
L-PCoA	0.73	1.10	0.18	0.27			
R-PCoA	0.73	1.10	0.18	0.27			
R-ICA Distal	2	3.00	0.5	0.75			
Basilar	1.62	2.43	0.4	0.61			
L-MCA	1.43	2.15	0.36	0.54			
R-MCA	1.43	2.15	0.36	0.54			
L-ACA Proximal	1.17	1.76	0.29	0.44			
R-ACA Proximal	1.17	1.76	0.29	0.44			
L-PCA Proximal	1.07	1.61	0.27	0.40			
R-PCA Proximal	1.07	1.61	0.27	0.40			
L-ACA Distal	1.2	1.80	0.3	0.45			
R-ACA Distal	1.2	1.80	0.3	0.45			
ACoA	0.74	1.11	0.19	0.28			
L-PCA Distal	1.05	1.58	0.26	0.39			
R-PCA Distal	1.05	1.58	0.26	0.39			

Table 6.1: This table presents all the vessels in the network and the new respective radii for the aged network ( $R_0$ ) and the wall thickness ( $h_0$ ). Subscript  $A$  and  $B$  is aged and baseline respectively. The table presents the two calculated outcomes for wall thicknesses ( $h_0(x)$  and  $h_{0A}$  for Equation 6.1 and 6.2 respectively) and their percentage difference.105

Vessel	ID	$L$ (mm)	$R_0$ (mm)		$E$ (MPa)		$h_0$ (mm)	
			Base	Aged	Base	Aged	Base	Aged
Ascending Aorta	1	40	12	18.00	0.4	1.2	1.63	2.45
Aortic Arch Proximal	2	20	11.2	16.80	0.4	1.2	1.26	1.89
Brachiocephalic	3	34	6.2	9.30	0.4	1.2	0.8	1.20
Aortic Arch Distal	4	39	10.7	16.05	0.4	1.2	1.15	1.73
L-CCA	5	208	2.5	3.75	0.4	1.2	0.63	0.94
R-CCA	6	177	2.5	3.75	0.4	1.2	0.63	0.94
R Subclavian	7	34	4.23	6.35	0.4	1.2	0.67	1.01
Thoracicaorta	8	156	9.99	14.99	0.4	1.2	1.1	1.65
L Subclavian	9	34	4.23	6.35	0.4	1.2	0.67	1.01
L-ECA	10	177	1.5	2.25	0.8	1.6	0.38	0.56
L-ICA Proximal	11	177	2	3.00	0.8	1.6	0.5	0.75
R-ICA Proximal	12	177	2	3.00	0.8	1.6	0.5	0.75
R-ECA	13	177	1.5	2.25	0.8	1.6	0.38	0.56
R Vertebral	14	148	1.36	2.04	0.8	1.6	0.34	0.51
R Brachial	15	422	4.03	6.05	0.4	1.2	0.67	1.01
L Brachial	16	422	4.03	6.05	0.4	1.2	0.67	1.01
L Vertebral	17	148	1.36	2.04	0.8	1.6	0.34	0.51
L-ICA Distal	18	5	2	3.00	1.6	2.4	0.5	0.75
L-PCoA	19	15	0.73	1.10	1.6	2.4	0.18	0.27
R-PCoA	20	15	0.73	1.10	1.6	2.4	0.18	0.27
R-ICA Distal	21	5	2	3.00	1.6	2.4	0.5	0.75
Basilar	22	29	1.62	2.43	1.6	2.4	0.4	0.61
L-MCA	23	119	1.43	2.15	1.6	2.4	0.36	0.54
R-MCA	24	119	1.43	2.15	1.6	2.4	0.36	0.54
L-ACA Proximal	25	12	1.17	1.76	1.6	2.4	0.29	0.44
R-ACA Proximal	26	12	1.17	1.76	1.6	2.4	0.29	0.44
L-PCA Proximal	27	5	1.07	1.61	1.6	2.4	0.27	0.40
R-PCA Proximal	28	5	1.07	1.61	1.6	2.4	0.27	0.40
L-ACA Distal	29	103	1.2	1.80	1.6	2.4	0.3	0.45
R-ACA Distal	30	103	1.2	1.80	1.6	2.4	0.3	0.45
ACoA	31	3	0.74	1.11	1.6	2.4	0.19	0.28
L-PCA Distal	32	86	1.05	1.58	1.6	2.4	0.26	0.39
R-PCA Distal	33	86	1.05	1.58	1.6	2.4	0.26	0.39

Table 6.2: Parameters of the baseline network and the new created aged network developed through literature studies and described assumptions.

and provided that  $R$  and  $L$  are characteristic (known values), applying an increase to  $\mu$  would result in an increase in  $\Delta P$  to compute the equivalent  $Q$ .

The aged model was assumed to be a normal aged network where atherosclerosis was not present. With this, the following simulations were produced for all five treatment phases:

- Aged network involving only vascular properties ( $R_0$ ,  $h_0$  and  $E$ );
- An isolated study observing two simulations applying incremental values of the viscosity ( $\mu$  at 0.0045 Pa·s (+12.5%) and 0.005 Pa·s (+25%).

In previous chapters, the results calculated by the model were presented in the form of  $Q$  and  $P$ , whereas for the simulation of altered vascular properties, other parameters such as  $c$  (pulse wave velocity) and  $\Delta R$  were also presented to evaluate the wall mechanics of the aged model. Chapter 4 was used as the comparative datum for normalizing the results. For this chapter, normalization observations will follow the same process demonstrated in Chapter 5 presented in Equation 5.1.

## 6.2 Results

### 6.2.1 Simulation of Network with Aged Radius, Wall Thickness and Elastic Modulus

In this simulation, the vascular properties  $R_0$ ,  $h_0$  and  $E$  were aged as presented in Table 6.2. Figure 6.1 presents the normalized results for pressure, flow, radius change and wave speed with vessels on the treatment path outlined.

The pressure results demonstrated that distal arteries in the network experience slightly higher average pressures over the cardiac cycle in comparison to the baseline simulation. Phases 4 and 5 also resulted in higher average pressure over the cardiac cycle

VG	Variation:	Pressure					Flow					$\Delta R$					Wave Speed				
		P1	P2	P3	P4	P5	P1	P2	P3	P4	P5	P1	P2	P3	P4	P5	P1	P2	P3	P4	P5
S	L-CCA	0.99	0.99	0.99	0.98	0.97	1.14	1.14	1.10	1.10	1.09	0.50	0.50	0.49	0.49	0.49	1.68	1.67	1.67	1.68	1.68
S	R-CCA	0.99	0.99	0.99	0.99	0.99	1.14	1.13	1.16	1.14	1.19	0.50	0.50	0.50	0.50	0.50	1.68	1.67	1.67	1.68	1.68
D	L-ECA	1.06	1.05	1.04	1.04	1.03	1.12	1.12	1.11	1.10	1.09	0.81	0.80	0.80	0.79	0.79	1.39	1.39	1.39	1.39	1.39
L	L-ICA P	1.03	1.02	1.10	1.51	1.63	1.15	1.16	1.46	1.00	1.00	0.77	0.76	0.82	1.14	1.22	1.40	1.40	1.40	1.41	1.41
R	R-ICA P	1.02	1.02	1.03	1.07	1.07	1.16	1.14	1.18	1.15	1.20	0.77	0.77	0.78	0.80	0.80	1.40	1.40	1.40	1.40	1.40
D	R-ECA	1.05	1.05	1.06	1.07	1.06	1.12	1.12	1.12	1.13	1.13	0.80	0.81	0.81	0.82	0.81	1.39	1.39	1.39	1.39	1.39
S	R Vert.	1.00	1.01	1.01	1.03	1.02	1.21	1.20	1.23	1.19	1.24	0.75	0.75	0.76	0.77	0.77	1.40	1.40	1.40	1.40	1.40
S	L Vert.	1.00	1.01	1.01	1.03	1.02	1.21	1.20	1.23	1.19	1.24	0.75	0.75	0.76	0.77	0.77	1.40	1.40	1.40	1.40	1.40
L	L-ICA D	1.05	1.03	1.10	1.40	1.49	1.16	1.17	1.30	0.95	0.86	1.05	1.03	1.10	1.40	1.49	1.22	1.22	1.22	1.22	1.22
C	L-PCoA	1.05	1.04	1.08	1.24	1.27	2.53	1.07	1.30	1.09	1.18	1.36	1.34	1.39	1.62	1.68	1.22	1.22	1.22	1.22	1.22
C	R-PCoA	1.05	1.05	1.07	1.13	1.14	59.30	-0.12	2.79	1.54	1.63	1.36	1.35	1.37	1.48	1.50	1.22	1.22	1.22	1.22	1.22
R	R-ICA D	1.05	1.04	1.07	1.14	1.15	1.17	1.15	1.19	1.15	1.21	1.05	1.04	1.07	1.14	1.15	1.22	1.22	1.22	1.22	1.22
S	Basilar	1.04	1.04	1.05	1.11	1.11	1.21	1.20	1.23	1.19	1.24	1.02	1.02	1.03	1.09	1.09	1.23	1.23	1.23	1.23	1.23
D	L-MCA	1.10	1.03	1.10	1.40	1.55	1.15	-3.99	-2.70	-4.64	1.63	1.27	1.18	1.27	1.64	1.94	1.22	1.22	1.22	1.22	1.19
D	R-MCA	1.10	1.09	1.11	1.19	1.20	1.15	1.14	1.17	1.25	1.26	1.27	1.26	1.28	1.39	1.40	1.22	1.22	1.22	1.22	1.22
L	L-ACA P	1.06	1.04	1.10	1.36	1.43	1.18	1.17	1.30	0.95	1.08	1.24	1.22	1.29	1.62	1.71	1.23	1.23	1.23	1.23	1.23
R	R-ACA P	1.06	1.05	1.08	1.18	1.20	1.19	1.17	1.21	1.13	1.20	1.24	1.23	1.26	1.40	1.43	1.23	1.23	1.23	1.23	1.23
L	L-PCA P	1.05	1.04	1.06	1.13	1.13	1.22	1.20	1.23	1.16	1.22	1.28	1.27	1.29	1.39	1.40	1.21	1.21	1.21	1.21	1.21
R	R-PCA P	1.05	1.04	1.06	1.12	1.13	1.21	1.20	1.24	1.31	1.33	1.28	1.27	1.29	1.38	1.39	1.21	1.21	1.21	1.21	1.21
D	L-ACA D	1.12	1.10	1.16	1.40	1.45	1.19	1.17	1.23	1.48	1.54	1.12	1.10	1.16	1.40	1.46	1.22	1.22	1.22	1.22	1.22
D	R-ACA D	1.12	1.11	1.15	1.29	1.31	1.19	1.17	1.22	1.37	1.39	1.12	1.11	1.15	1.29	1.31	1.22	1.22	1.22	1.22	1.22
C	ACoA	1.07	1.05	1.10	1.27	1.30	1.37	1.19	1.21	1.07	1.17	1.08	1.07	1.12	1.29	1.33	1.21	1.21	1.21	1.21	1.21
D	L-PCA D	1.11	1.10	1.13	1.20	1.21	1.18	1.18	1.20	1.28	1.29	1.34	1.33	1.36	1.47	1.49	1.22	1.22	1.22	1.22	1.22
D	R-PCA D	1.11	1.11	1.13	1.19	1.20	1.18	1.18	1.20	1.27	1.28	1.34	1.33	1.36	1.45	1.47	1.22	1.22	1.22	1.22	1.22

Figure 6.1: Normalized results for the aged vessel simulation for pressure, flow, change in radius and wave speed for all five clinical phases. Left side column indicates the vessel group of each vessel illustrated in Figure 4.1. The ECAs are assumed to be in VGD (Distributing Vessel). Colour map key: Red < 1, White = 1 (no change in comparison to the baseline simulation), Blue > 1. Main treatment pathway vessels and distal link (L-ICA's, L-MCA and L-ACA proximal) are outlined.

in the treatment path vessels and the vessels interacting with the treatment (L-ACA proximal and L-PCoA). The system saw an overall increase in pressure in comparison to the baseline simulation by 6%, 5%, 7%, 19% and 21% for phases 1 to 5 respectively. The flow in the network saw an overall increase throughout all vessels (excluding L-MCA) and phases of upward of 7%, apart from Phases 4 and 5 for the L-ICA proximal, L-ICA distal and L-ACA proximal.

The lumen area was on average 2.2 times larger than the baseline for all phases, although the average change in radius was lower than the baseline for the supplying vessels of the CoW, the ECAs and the proximal ICAs (apart from phases 4 and 5 for the L-ICA proximal). For the remainder of the vessels, the radial changes averaged over the cardiac cycle were on average larger than the baseline simulation. The wave speed was larger than the baseline throughout the network for all phases. Variation in the results over the phases for each vessel were visible only when viewing the normalized values at an accuracy higher than 3 significant figures.

Observing the treatment path vessels, flow reversal remains relatively close to 5 ml/s in both the aged and baseline simulation for phases 4 and 5. In the distal L-ICA, flow reversal is lower in the aged simulation by approximately 5% and 14% for both Phase 4 and 5 respectively, whereas in the proximal L-ACA, there is an increase in Phase 5 in flow reversal by approximately 8%. The L-MCA (the location of the clot), experiences a large increase in forward flow in the retrieval phase of approximately 63% (0.7 ml/s more).

### **6.2.2 Simulation of Network with Aged Viscosity**

In this simulation, the viscosity was adjusted to be 12.5% and 25% higher than the baseline to present two variations of aged blood in the non-modified network (baseline). Figure 6.2 presents the normalized results for pressure and flow for both simulations

VG	Phase:	$\mu = 0.0045 \text{ Pa}\cdot\text{s} \text{ (P)}$					$\mu = 0.0045 \text{ Pa}\cdot\text{s} \text{ (Q)}$					$\mu = 0.005 \text{ Pa}\cdot\text{s} \text{ (P)}$					$\mu = 0.005 \text{ Pa}\cdot\text{s} \text{ (Q)}$				
		P1	P2	P3	P4	P5	P1	P2	P3	P4	P5	P1	P2	P3	P4	P5	P1	P2	P3	P4	P5
S	L-CCA	1.00	1.00	1.00	1.00	1.01	0.98	0.98	0.99	0.99	0.99	1.00	1.00	1.00	1.00	1.01	0.96	0.96	0.97	0.97	0.97
S	R-CCA	1.00	1.00	1.00	1.00	1.00	0.98	0.98	0.98	0.98	0.98	1.00	1.00	1.00	1.00	1.00	0.96	0.96	0.96	0.96	0.95
D	L-ECA	0.99	0.99	0.99	0.99	1.00	0.98	0.98	0.98	0.98	0.99	0.98	0.98	0.99	0.99	0.97	0.97	0.97	0.97	0.97	
L	L-ICA P	1.00	1.00	0.99	0.92	0.92	0.98	0.98	1.01	1.00	1.00	0.99	1.00	0.98	0.85	0.83	0.96	0.96	1.05	1.00	1.00
R	R-ICA P	1.00	1.00	1.00	0.99	0.99	0.98	0.98	0.97	0.98	0.97	0.99	0.99	0.99	0.98	0.98	0.96	0.96	0.95	0.96	0.95
D	R-ECA	0.99	0.99	0.99	0.99	0.99	0.98	0.98	0.98	0.98	0.98	0.98	0.98	0.98	0.98	0.97	0.97	0.97	0.96	0.96	
S	R Vert.	1.00	1.00	1.00	0.99	1.00	0.98	0.98	0.97	0.98	0.97	1.00	1.00	1.00	0.99	0.99	0.96	0.96	0.95	0.96	0.95
S	L Vert.	1.00	1.00	1.00	0.99	1.00	0.98	0.98	0.97	0.98	0.97	1.00	1.00	1.00	0.99	0.99	0.95	0.96	0.95	0.96	0.95
L	L-ICA D	0.99	1.00	0.99	0.94	0.94	0.98	0.98	0.97	1.01	1.01	0.99	0.99	0.98	0.88	0.87	0.96	0.96	0.95	1.01	1.03
C	L-PCoA	0.99	0.99	0.99	0.96	0.97	1.02	0.97	0.97	0.99	0.98	0.99	0.99	0.98	0.93	0.93	1.04	0.95	0.95	0.98	0.96
C	R-PCoA	0.99	0.99	0.99	0.98	0.98	3.11	0.92	1.01	0.99	0.98	0.99	0.99	0.98	0.96	0.96	5.09	0.84	1.02	0.98	0.96
R	R-ICA D	0.99	0.99	0.99	0.98	0.98	0.98	0.98	0.97	0.98	0.97	0.99	0.99	0.98	0.96	0.96	0.96	0.96	0.95	0.96	0.95
S	Basilar	0.99	1.00	0.99	0.98	0.99	0.98	0.98	0.97	0.98	0.97	0.99	0.99	0.99	0.97	0.97	0.96	0.96	0.95	0.96	0.95
D	L-MCA	0.99	1.00	0.99	0.94	0.93	0.98	0.63	1.17	0.44	0.92	0.97	0.99	0.98	0.88	0.86	0.96	0.49	1.24	0.81	0.85
D	R-MCA	0.99	0.99	0.98	0.97	0.98	0.98	0.98	0.97	0.97	0.97	0.97	0.98	0.97	0.95	0.95	0.96	0.96	0.96	0.93	0.93
L	L-ACA P	0.99	0.99	0.99	0.95	0.95	0.98	0.98	0.97	1.00	0.99	0.98	0.99	0.97	0.90	0.89	0.95	0.96	0.95	1.01	0.98
R	R-ACA P	0.99	0.99	0.99	0.97	0.98	0.98	0.98	0.97	0.98	0.98	0.98	0.99	0.98	0.95	0.95	0.95	0.95	0.94	0.97	0.95
L	L-PCA P	0.99	0.99	0.99	0.98	0.98	0.98	0.98	0.97	0.98	0.98	0.99	0.99	0.98	0.96	0.96	0.95	0.95	0.95	0.96	0.95
R	R-PCA P	0.99	0.99	0.99	0.98	0.98	0.98	0.98	0.97	0.97	0.97	0.99	0.99	0.98	0.96	0.97	0.95	0.96	0.95	0.94	0.93
D	L-ACA D	0.98	0.99	0.98	0.94	0.94	0.98	0.98	0.97	0.94	0.94	0.97	0.97	0.96	0.89	0.89	0.95	0.96	0.94	0.88	0.87
D	R-ACA D	0.98	0.99	0.98	0.96	0.96	0.98	0.98	0.97	0.95	0.95	0.97	0.97	0.96	0.92	0.92	0.95	0.95	0.95	0.91	0.90
C	ACoA	0.99	0.99	0.99	0.96	0.96	0.98	0.98	0.97	0.99	0.98	0.98	0.99	0.98	0.92	0.92	0.95	0.96	0.94	0.98	0.96
D	L-PCA D	0.99	0.99	0.98	0.97	0.97	0.98	0.98	0.97	0.96	0.97	0.97	0.97	0.97	0.95	0.95	0.95	0.95	0.95	0.93	0.93
D	R-PCA D	0.99	0.99	0.98	0.97	0.98	0.98	0.98	0.97	0.96	0.97	0.97	0.97	0.97	0.95	0.95	0.95	0.95	0.95	0.93	0.93

Figure 6.2: Normalized results of pressure and flow for the two aged viscosity simulations ( $\mu$  is 0.0045 and 0.005 Pa·s) for all five clinical phases. Left side column indicates the vessel group of each vessel illustrated in Figure 4.1. The ECAs are assumed to be in VGD (Distributing Vessel). Colour map key: Red < 1, White = 1 (no change in comparison to the baseline simulation), Blue > 1. Main treatment pathway vessels and distal link (L-ICA's, L-MCA and L-ACA proximal) are outlined.

with vessels on the treatment path outlined.

From the results, the increased viscosity reduces in pressure and flow within all

non-treatment vessels apart from two anomalies: results in the R-PCoA and the L-MCA where these results are amplified due to near zero values being divided by even smaller values. During aspiration phases (Phases 4 and 5), the results suggest that the higher viscosity cause reduced pressures in these phases in comparison to the baseline model which effect the treatment path and the ACAs the most (up to 8% drop). With regards to the flow results, the increased viscosity resulted in lower outflow in the distal distributing vessels in comparison to the baseline model for all phases, but increasingly in the aspiration phases. A reduction of 13% in the L-ACA distal being the most for the distributing vessels during Phase 5, where other distributing vessels (R-MCA, R-ACA distal and distal PCAs) saw a drop of 7 to 10% in the last two phases for flow in comparison to the baseline.

With the clot removed and aspiration still active in the post-retrieval phase (Phase 5), the baseline simulation presented a forward flow of 1.1 ml/s in the L-MCA, a reduction by 38%, whereas with the increased viscosity, there was an 8% and 15% drop from the baseline results (for  $\mu = 0.0045$  and  $0.005$  Pa·s respectively), resulting in 1.01 ml/s and 0.93 ml/s for  $\mu = 0.0045$  and  $0.005$  Pa·s respectively. This is associated with a flow drop of 43% and 48% from Phase 5 of these simulations in comparison to Phase 1 of the baseline simulation.

Figure 6.3 presents the normalized values of pressure drop calculated by the difference in the arithmetic averaged pressure over the cardiac cycle at the first node of the vessel and the last node of the vessel for the two aged viscosity simulations ( $\mu$  is  $0.0045$  and  $0.005$  Pa·s) for all five clinical phases.

Referring back to Hagen-Poiseuille equation (Equation 2.2), as previously mentioned, an increase to the viscosity would suggest that a change in pressure drop would be required to maintain the same amount of flow. With a 12.5% increase to viscosity, the averaged pressure drop ( $\Delta P$ ) calculated from the results presented a 10-15% increase in

		$\mu = 0.0045 \text{ Pa}\cdot\text{s} (\Delta P)$					$\mu = 0.005 \text{ Pa}\cdot\text{s} (\Delta P)$				
VG	Phase:	P1	P2	P3	P4	P5	P1	P2	P3	P4	P5
S	L-CCA	1.10	1.10	1.11	1.11	1.11	1.20	1.20	1.22	1.22	1.22
S	R-CCA	1.10	1.10	1.10	1.10	1.10	1.20	1.20	1.20	1.20	1.19
D	L-ECA	1.11	1.11	1.11	1.11	1.11	1.21	1.21	1.22	1.22	1.22
L	L-ICA P	1.10	1.10	0.97	1.13	1.13	1.20	1.20	0.91	1.27	1.27
R	R-ICA P	1.10	1.10	1.10	1.10	1.10	1.20	1.20	1.19	1.20	1.19
D	R-ECA	1.11	1.11	1.11	1.11	1.11	1.21	1.21	1.21	1.21	1.21
S	R Vert.	1.10	1.10	1.10	1.10	1.10	1.20	1.20	1.19	1.20	1.19
S	L Vert.	1.10	1.10	1.10	1.10	1.10	1.19	1.20	1.19	1.20	1.19
L	L-ICA D	1.10	1.10	1.10	1.14	1.15	1.20	1.20	1.19	1.27	1.30
C	L-PCoA	1.15	1.10	1.10	1.12	1.11	1.31	1.19	1.19	1.23	1.21
C	R-PCoA	-3.66	1.03	1.14	1.12	1.10	-8.93	1.04	1.28	1.23	1.20
R	R-ICA D	1.10	1.10	1.10	1.10	1.10	1.20	1.20	1.19	1.20	1.19
S	Basilar	1.10	1.10	1.10	1.10	1.10	1.20	1.20	1.19	1.20	1.19
D	L-MCA	1.10	1.14	0.67	5.87	1.04	1.20	1.30	0.47	-5.59	1.06
D	R-MCA	1.10	1.10	1.10	1.09	1.09	1.20	1.20	1.20	1.17	1.17
L	L-ACA P	1.10	1.10	1.10	1.13	1.12	1.19	1.20	1.19	1.27	1.23
R	R-ACA P	1.10	1.10	1.09	1.11	1.10	1.19	1.19	1.18	1.21	1.19
L	L-PCA P	1.10	1.10	1.10	1.11	1.10	1.20	1.20	1.19	1.21	1.19
R	R-PCA P	1.10	1.10	1.10	1.09	1.09	1.20	1.20	1.19	1.18	1.17
D	L-ACA D	1.10	1.10	1.09	1.06	1.06	1.19	1.20	1.18	1.10	1.10
D	R-ACA D	1.10	1.10	1.10	1.07	1.08	1.19	1.20	1.19	1.14	1.14
C	ACoA	1.10	1.10	1.09	1.12	1.11	1.19	1.20	1.18	1.23	1.21
D	L-PCA D	1.10	1.10	1.10	1.08	1.09	1.20	1.20	1.19	1.16	1.16
D	R-PCA D	1.10	1.10	1.10	1.09	1.09	1.20	1.20	1.19	1.17	1.17

Figure 6.3: Normalized results for pressure drop calculated by the difference in the arithmetic averaged pressure over the cardiac cycle at the first node of the vessel and the last node of the vessel for the two aged viscosity simulations ( $\mu$  is 0.0045 and 0.005 Pa·s) for all five clinical phases. Left side column indicates the vessel group of each vessel illustrated in Figure 4.1. The ECAs are assumed to be in VGD (Distributing Vessel). Colour map key: Red < 1, White = 1 (no change in comparison to the baseline simulation), Blue > 1. Main treatment pathway vessels and distal link (L-ICA's, L-MCA and L-ACA proximal) are outlined.

clinical Phase 1, ignoring anomalies with small sensitive numbers when normalizing (R-PCoA). The other phases saw similar behaviours with 7-15% increases in non-treatment path vessels, and a lower increase of 4-15% in treatment path vessels. When viscosity was increased by 25% ( $\mu = 0.005$ ), a 19-31% increase was observed in Phase 1. Ignoring the anomalies from normalization of sensitive numbers (L-MCA during Phase 2-4 and R-PCoA), the results for Phases 2-5 present an increase of 14-27% in non-treatment path vessels. Similarly to the simulation where viscosity was 0.0045, the treatment path vessels experienced a larger range of pressure drop increase, 6-30%. Again, ignoring the anomalies from normalization of sensitive numbers (L-MCA during Phase 2-4 and R-PCoA), the L-ICA proximal, where the balloon is placed is the only vessel to experience a reduction in pressure drop in comparison to the baseline throughout all phases. This takes place during Phase 3 where the balloon is positioned within the vessel (L-ICA proximal). Results present a 3% and 9% reduction in the simulations ( $\mu$  is 0.0045 and 0.005 Pa·s respectively).

### **6.3 Discussion**

The aim of this study was to simulate the network under aged conditions through two different models, vascular aging through vessel properties and dimensions, and blood rheology.

Results of the study where vascular parameters were changed showed the aged model presented higher pressures and flows overall in comparison to the baseline model. Between the baseline and the aged model, the pressure for the aged simulations presented higher pressure per phase over the entire network in comparison (Table 6.3), suggesting the altered vascular parameters in older people induce a higher pressure requirement. However, the radial changes in the aged simulation presents two clear

ranges of results for intracranial and extra-intracranial vessels. Extra-intracranial vessels (CCAs, ECAs, proximal ICAs, vertebrals) all show a reduction in radial wall movements in comparison to the baseline model. Intracranial vessels however present an increase in radial movement in comparison to the baseline mode (as well as phases 4 and 5 for L-ICA proximal due to aspiration). With respect to the MT procedure, the increased lumen radius combined with larger radial movements within intracranial vessels provide higher flows, which dictated lower retrograde flows during aspiration phases in the L-ICA distal and an increase in forward flow by 63% in the L-MCA for post-retrieval.

Results of the study where viscosity was altered showed that with the larger pressure drops over each vessel generated from increased viscous forces provided a minute reduction to flow globally in comparison to the baseline model. This subsequently aided in the MT treatment as retrograde flow was still not present in the L-MCA, but was reduced by 8 and 15% for when  $\mu$  was 0.0045 and 0.005 Pa-s respectively.

	Phase 1	Phase 2	Phase 3	Phase 4	Phase 5
Baseline	89.9	92.9	89.9	76.6	73.4
Aged	94.7	97.1	96.3	89.3	86.6
Normalized	1.06	1.05	1.07	1.19	1.21

Table 6.3: Values for baseline and aged pressure is presented in mmHg. Results of averaged pressure values averaged over all cerebrovascular vessels for for baseline simulation and aged simulation (where  $R_0$ ,  $h_0$  and  $E$  are the effected variables as described from the Methodology). Aged value is normalized through its respective phase value from baseline.

It is evident from these results that these aged models suggest no major haemodynamic changes that directly effect the clinical procedure such as flow direction changes, instead the models show global trends such as amplifications/reductions to flow or pressures to vessel groups due to the alterations made to parameters. However, the representation within this model is still limited. The simulations presented are a possibility of many vascular and/or rheological combinations.

The aged study's parameterization was translated from the baseline network presented in Chapter 3 and maintained some consistent characteristics when producing the aged network such as wall thickness at 25% of the radii for cerebrovascular vessels, and maintaining three values of Young's modulus for vessels. A full comprehensive model would benefit from patient specific data for each vessel rather than assuming equivalent properties between vessel groups, in example suggesting a wall thickness equal to 25% of the vessel radius to all cerebrovascular vessels where some vessels like the CCAs wall thickness are known to increase two to three fold up to ages of 90 years [154]. Alongside this, vascular functions such as auto-regulation were not considered in this study, as literature shows that ageing affects vasodilation response in aging vessels [155].

In the study, assumption of normal ageing was considered, whereas diseased vessel walls is another likely parameter that was excluded in this study as atherosclerosis in vessel walls would provide a 3D problem as axis-symmetry would not be present (Figure 6.4). Under the circumstances that assuming diseased walls was implemented into the model, diseased walls would have to be applied to certain vessels as atherosclerosis presence is not uniform. Diseased vessels such as CCA's tend to have smaller lumen diameters in comparison to non-diseased vessels, which presents alternate parameters to normal aging where the CCAs present larger diameters [148]. Under the current capabilities of the 1D model, individual vessel geometry parameterization is possible whereas implementing diseased wall parameters is not which poses a question for future work. The distal network is parameterized through the Windkessel outlets. These outlets were not modified within this study, although peripheral arterioles up to capillary beds are also understood to change mechanical structure and effect peripheral resistance and impedance with age [57, 156].

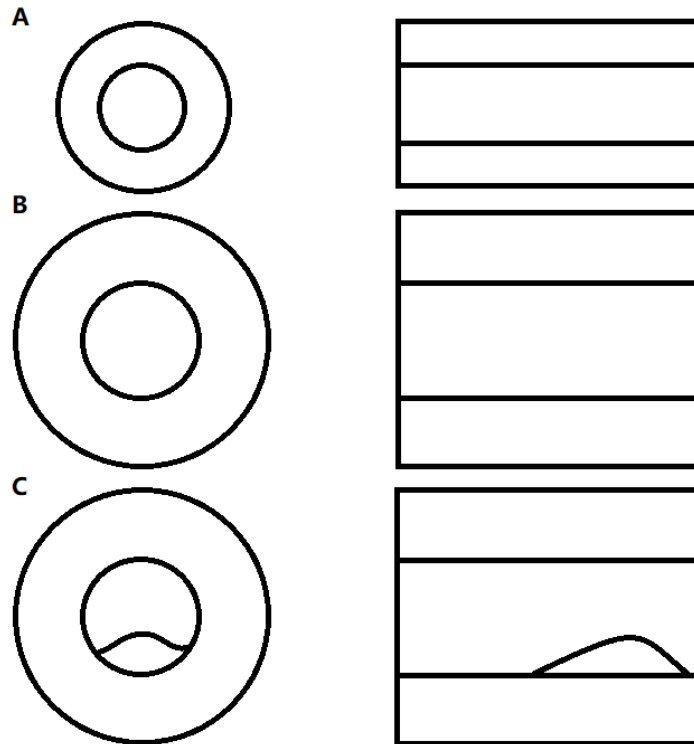


Figure 6.4: Illustration presenting A) typical young vessel; B) typical aged vessel; C) aged and diseased (atherosclerosis) vessel. Left side shows radial cross-section, right shows longitudinal cross-section.

## 6.4 Conclusions

Through guidance of the literature, the baseline model of a healthy young adult was transformed into a normally aged network through modifying the mechanical properties of the vessels ( $R_0$ ,  $h_0$  and  $E$ ) and the blood rheology through the viscosity. These models were simulated and assessed for their haemodynamic variances from the baseline model during MT treatment. Results showed global changes to pressures and flows, but provided no significant changes to clinical procedure such as retrograde flow in the L-MCA, although higher viscosity's showed reduced flow post-retrieval. Limitations of this study are prominent due to the numerous possibilities of variations present in ag-

ing networks and the study would benefit from more patient specific data of aged and diseased networks.



## **Chapter 7**

# **The Impact of a Catheter on the Haemodynamics**

### **Summary**

In the previous Chapters, the studies explored parameter variation of anatomical and physiological aspects and their impact on the treatment. The treatment modelling in these chapters was limited to including occlusions for the inflated balloon and the occluded vessel as well as aspiration in their respective phases. Although these aspects were considered as important conditions to help simulate a basic concept of BGC MT treatment, the presence of the catheter was not included. In this Chapter, a simplified description of the catheter presence is explored to help indicate the effects on a reduced network before considering the overall influence on hemodynamic results in the CoW. This chapter presents this in two studies: a simplified analytical model to help indicate how influential the catheter presence is and using a parallel study of a 3D CFD model in attempt to validate the results of the analytical solution.

## 7.1 Analytical Investigation

### 7.1.1 Methodology

For BGC MT treatment, within the five phases described in the previous methodologies of studies in this thesis, there is typically up to two different sized catheters present, the BGC and the micro-catheter, the latter being smaller in diameter than the former. The device is delivered into the arterial network through arteries accessible in the limbs, guided towards the desired location in the cerebrovascular network. The micro-catheter is then positioned near the area of injury through the help of the guide wire. The SR

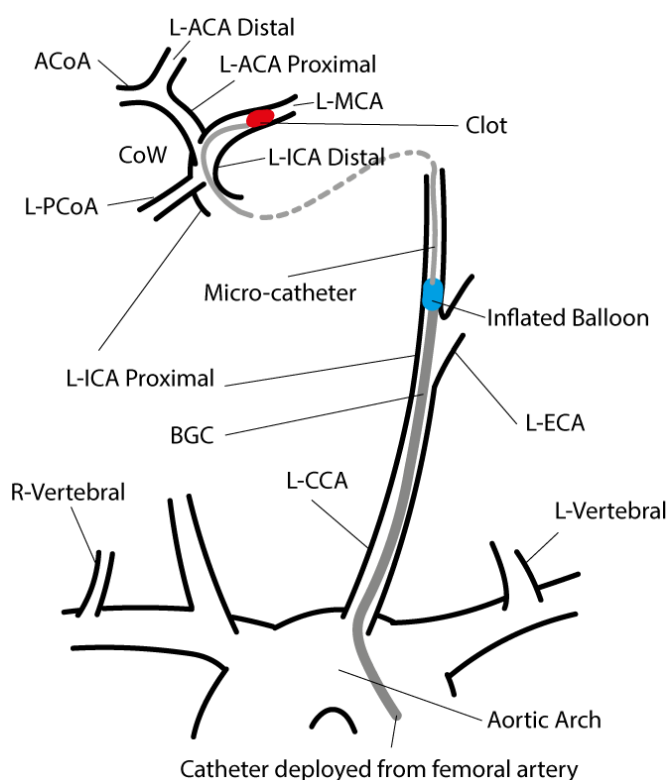


Figure 7.1: Illustration of typical MT deployment path of BGC and micro-catheter (SR device) through the femoral artery up to the aortic arch to access the carotid arteries.

device is then guided through the micro-catheter to interact with the clot. Figure 7.1 presents the set-up.

The focal region of catheter presence is between the balloon and the injury, which is the micro-catheter. With the balloon halting flow towards the CoW, vessels that occupy the BGC aren't expected to have much influence on the overall haemodynamic changes in the CoW as it resides in larger non-cerebrovascular vessels apart from the L-CCA where flow is tending to 0 ml/s under inflation.

Under the same circumstances described in Chapter 4 in regards to balloon placement, if the BGC is placed in the proximal region of the L-ICA in Phase 3, at this point a catheter is present in the L-CCA, descending part of the aortic arch and subsequently the thoracicaorta assuming typical intervention through the femoral artery. The placement of the SR device via the micro-catheter would also be present for Phase 3 as balloon inflation is typically performed after interaction with the clot. Table 7.1 conveys the described set-up.

	Baseline $R$ (mm)	Chapter 6 $R$ (mm)	Catheter present
Descending Aorta	10.7	16.05	BGC
Thoracicaorta	9.99	14.99	BGC
L-CCA	2.5	3.75	BGC
L-ICA Proximal	2	3	Micro
L-ICA Distal	2	3	Micro

Table 7.1: Present catheters for their respective housing vessels during MT treatment described in Chapter 4 with their radii both baseline and aged (Chapter 6). Catheter radii: BGC 1.35mm, SR pusher wire 0.23mm, micro-catheter 0.45mm.

With a catheter occupying the lumen, a reduction of flow area is now present. Subsequently, a larger total surface area would be in contact with the blood from the catheter increasing viscous losses. To begin to understand the haemodynamic effects, an observation of a single vessel with and without catheter was undertaken. Consider-

ing two separate observations of axisymmetric vessels of indefinite length, steady flow inlet of 4.96 and 2.92 ml/s (average flow over cardiac cycle in Phase 1 entering L-CCA and L-ICA respectively from Chapter 4), with a radius equivalent to the L-ICA and the other the L-CCA as used previously (Table 7.1), an analytical calculation was performed. The percentage loss of flow area with the catheter presence is the interest point of this evaluation and therefore the flow values of 4.96 and 2.92 ml/s for the L-CCA and L-ICA respectively are still used to assess the aged radii as well as the non-aged radii. Example devices; the FlowGate2 BGC paired with the Trevo XP SR guided by the Velocity micro-catheter was used to obtain authentic dimensions for the catheters. The BGC has a diameter of 2.7mm, whilst the SR has a pusher wire diameter of 0.46mm which is passable through the delivery micro-catheter of inner diameter 0.635mm and outer diameter option of 0.983mm or 0.867mm (assume 0.9mm). [157–159]. Using Hagen-Poiseuille equation (Equation 2.2), assuming  $\mu$  of 0.0032 Pa·s, it is possible to calculate the pressure drop ( $\Delta P$ ) over the length of a vessel, which in this case we consider per unit length ( $\Delta P/L$ ). Alongside this, respective average velocity and flow area can be

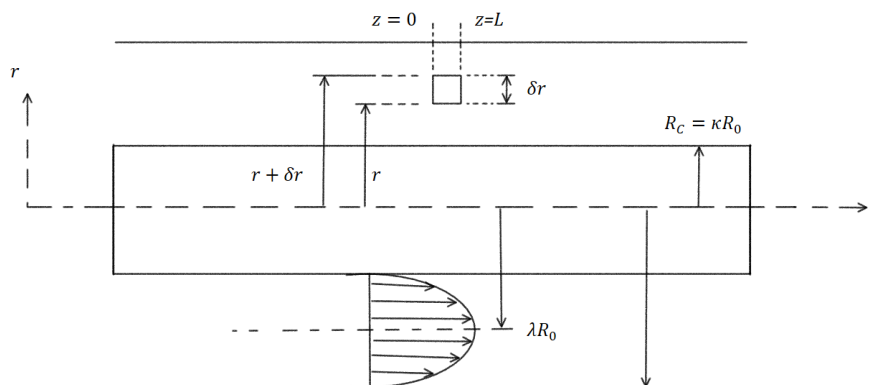


Figure 7.2: Cross section of the axisymmetric and concentric catheterized vessel. Representation of the infinitesimal in a cylindrical-coordinate system  $(z, r, \theta)$  where radius is  $R_0$ , catheter radius is  $R_C$  and the peak velocity position is at  $\lambda R_0$ .

calculated from the values presented previously. With the catheter present, flow area and average velocity can be calculated as dimensions for all parameters are present, although standard Hagen-Poiseuille formula is invalid for annular-like flow meaning an alternate route is required to calculate pressure drop.

Consider the Figure 7.2. Presented is a two-dimensional view of a vessel along the  $z$ -axis of radius  $R_0$  housing an axisymmetric catheter of radius  $R_C$ .  $\kappa$  is the coefficient of proportionality of catheter radius to lumen radius such that:

$$R_C = \kappa \cdot R_0, \quad 0 < \kappa < 1 \quad (7.1)$$

Assuming an infinitesimal element that exists between  $R_C$  and  $R_0$  of height  $\delta r$  positioned a distance  $r$  away from the  $z$ -axis with length proximity within 0 and  $L$  of  $z$ , following the conservation of momentum for the infinitesimal presents the following:

$$(P_0 - P_L) (2\pi r \delta r) - \tau_{zr} (2\pi r L) = 0 \quad (7.2)$$

Where  $P_0$  and  $P_L$  is the pressure at position 0 and  $L$  on the  $z$ -axis. With use of the cylindrical representation of  $\tau_{zr}$ , as well as assuming no changes to radial velocity with respect to the longitudinal direction ( $\partial v_r / \partial z$ ):

$$\tau_{zr} = -\mu \left( \frac{\partial v_r}{\partial z} + \frac{\partial v_z}{\partial r} \right), \quad \frac{\partial v_r}{\partial z} = 0 \quad (7.3)$$

$\tau_{zr}$  can be presented as:

$$\tau_{zr} = -\mu \left( \frac{\partial v_z}{\partial r} \right) \quad (7.4)$$

Substituting into Equation 7.4 into 7.2, rearranging and partial integrating both sides gives the velocity profile function:

$$v_z = -\frac{(P_0 - P_L)}{4\mu L}r^2 + B \ln(r) + C \quad (7.5)$$

Under no-slip wall conditions, then  $r$  is equal to  $R_0$  and  $R_C$  ( $\kappa R_0$ ) when  $v_z$  is 0 m/s. The other boundary conditions are as follows; when  $r$  is equal to  $\lambda R_0$ ,  $v_z$  is at the peak velocity such that  $\tau_{zr}$  is zero. From a combination of these conditions, Equation 7.5 can be simplified to:

$$v_z = \frac{\Delta P R_0^2}{4\mu L} \left( 1 - \frac{r^2}{R_0^2} + \frac{(\kappa^2 - 1)}{\ln(\kappa)} \ln\left(\frac{r}{R_0}\right) \right) \quad (7.6)$$

Where  $\Delta P$  is equivalent to  $P_0 - P_L$ . Due to the assumed axisymmetric shape, the blood flow ( $Q$ ), can be calculated through:

$$Q = \int_{\kappa R_0}^{R_0} 2\pi r v_z \delta r \quad (7.7)$$

Such that when substituting Equation 7.6 into Equation 7.7, the simplified solution can be presented as:

$$Q = \frac{\pi \Delta P R_0^4}{8\mu L} \left[ (1 - \kappa^4) + \frac{(\kappa^2 - 1)^2}{\ln(\kappa)} \right] \quad (7.8)$$

This presents the solution which gives the Hagen-Poiseuille equation when  $\kappa$  is 0 as it eliminates the additional term (which will be referred to as the catheter coefficient  $K$ ).  $K$  is present only if  $0 < \kappa < 1$ .

Equation 7.8 is able to estimate the unit pressure loss for the catheterised vessels for the single vessel set-up by calculating the corresponding  $\kappa$  values for the following scenarios:

- BGC in L-CCA;
- BGC in aged L-CCA;

- BGC in L-ICA;
- BGC in aged L-ICA;
- Micro-catheter in L-CCA;
- Micro-catheter in aged L-CCA;
- Micro-catheter in L-ICA;
- Micro-catheter in aged L-ICA.

### **7.1.2 Results**

The results of these analytical calculations are presented in Figure 7.3. Observing the analytical results, flow area is reduced with the catheter as expected with the largest area reduction being the catheters placed in the L-ICA with reduction of 45% with the BGC and only 5% for the micro-catheter. Observing the aged vessel anatomy response to catheter presence was important as this is the most likely of the two anatomies to experience the intervention, it was crucial to identify if the catheter presence provided a significant response to the results. Results demonstrate that the larger the size difference of lumen to catheter for each vessel (as flow parameters were different), the smaller the effect on the results. However, results of the micro-catheter are more important to the overall indication to understanding the difference of effects when having a catheter included as it is present upstream from the balloon inflation point, interacting with the CoW and aspiration regions directly. Comparison of having no catheter present to a micro-catheter demonstrates an increase in all four vessel simulations for velocity and pressure, the largest change being an increase of 78% and 73% for velocity, and 154% and 102% for pressure drop per unit length, in the L-ICA and L-ICA aged respectively. With the micro-catheter present in the L-CCA's, velocity changes were minute, approximately 3% and 1.5% for non-aged and aged L-CCA respectively. On the

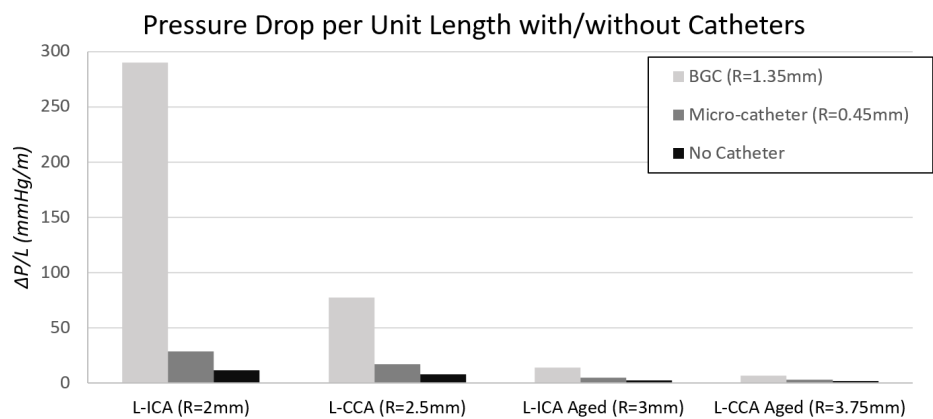
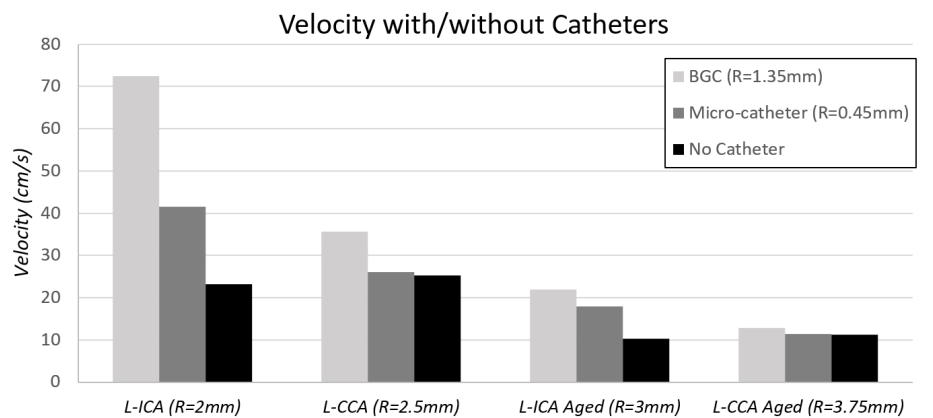
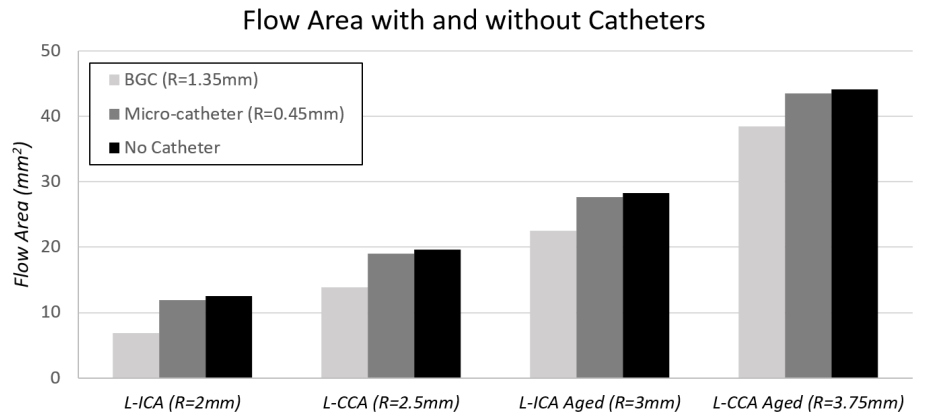


Figure 7.3: Bar charts of flow area changes, velocity changes and unit pressure loss when a catheter (BGC or micro-catheter) is present in the vessel (L-ICA and L-CCA).

contrary, pressure changes with the micro-catheter present was still significant in the L-CCA's with pressure drops increase from no catheter by 120% and 85% for non-aged and aged respectively.

### **7.1.3 Discussion**

From this simplified observation, it is clear in most cases that the catheter presence influences changes within the flow volume. The study did however consider rigid walls, and steady flow as significant simplifications. Although, using the simplified analytical solution to indicate the significance of the catheter presence through analysing area, velocity and pressure changes could be performed easily under these idealisations which presented an initial estimation of the impact.

The more considerable area of interest is upstream of the inflated balloon which is only occupied by the micro-catheter. With results clearly demonstrating that higher flow areas taken by the micro-catheter the more significant the change, but also larger percentage increases in velocity and pressure drops in ICA vessels are down to the different inlet flow value, which in this study was pre-set via the baseline study results. Building on this, flow distribution from bifurcating vessels that are catheterized such as the CCA passing into the ECA and ICA can perform differently to when they are not catheterized and this is not presented in this study.

Overall, this analytical solution indicates that catheter presence effects the basic haemodynamic results to a degree based on inflow conditions which leads to question how catheterized vessels interact with other catheterized and non-catheterized vessels.

## 7.2 3D Comparison and Validation

### 7.2.1 Methodology

In proceedings of the analytical solution, a parallel study [160] was performed using 3D CFD to model a simple straight cylindrical vessel, representing a typical CCA or ICA. The parameters of the model:

- Vessel diameter was 4.875mm;
- $\mu$  was 0.0032 Pa·s;
- Inlet flow was set as 3.6 ml/s;
- $\rho$  was 1054 kg/m<sup>3</sup>;
- Characteristic length was 0.178 m;
- The various catheter sizes in terms of  $\kappa$  were 0.1, 0.55, 0.75.

The model requires the flow to be fully developed in order to obtain comparable results to the analytical solution. To check that the length of 0.178 m was larger than the hydrodynamic length (length along the vessel/pipe to fully develop flow profile), Equation 7.9 was used to estimate the hydrodynamic length:

$$L_h \approx 0.06 \cdot Re \cdot D = 0.09m (< 0.178m) \quad (7.9)$$

Where  $L_h$  is hydrodynamic length and  $D$  is diameter.

Flow domains were created for the vessel and a concentric catheter for  $\kappa$  values of 0.1, 0.55 and 0.75. Using ANSYS Fluent solver the mesh was discretised using the Finite Volume Method (FVM) following a mesh refinement study. The mesh resolution was tested on a straight vessel without the catheter initially and improved incrementally via

increasing mesh density/number until the results matched the Hagen-Poiseuille equation as closely as possible. The final mesh density led to an error of 0.73% from the Hagen-Poiseuille equation, where further increases led to no significant changes therefore ensuring minimised mesh discretisation error. The minimum mesh density that provided these results was 51.8 elements per mm<sup>3</sup>.

Due to the parabolic nature of the flow paired with the shearing element, the choice of mesh topology used was a structured hexahedral mesh employed with a cartesian system. Alternate mesh topologies such as tetrahedral meshes are associated with complex geometries resulting in a randomly arranged and unstructured mesh. As the flow has a predominant direction of flow, the hexahedral mesh is not as numerically diffusive compared to a tetrahedral mesh and the shear layers are captured more accurately.

The fundamental purpose of this study was to use the 3D CFD simulation to verify and validate the results presented by the analytical solution before implementing the catheter into the 1D model. To do this, pressure drop over a selected length of fully developed flow, maximum velocity in this region and flow resistance were calculated from the analytical solution and extracted from the 3D simulation for comparison. The catheterised analytical solution is presented in the forms likened to the Hagen-Poiseuille equation as presented in Equations 7.6 and 7.8 in terms of velocity and flow functions respectively. Additionally, rearrangement of the Hagen-Poiseuille equation with the subject being  $\Delta P/Q$  yields the resistance to flow term:

$$\mathcal{R} = \frac{\Delta P}{Q} = \frac{8\mu L}{\pi R_0^4} \quad (7.10)$$

The same can be done to Equation 7.8 to yield the analytical value for flow resistance:

$$\mathcal{R} = \frac{\Delta P}{Q} = \frac{8\mu L}{\pi R_0^4} \left[ (1 - \kappa^4) + \frac{(\kappa^2 - 1)^2}{\ln(\kappa)} \right]^{-1} \quad (7.11)$$

ECCENTRIC (mm)	$\kappa = 0.1$	$\kappa = 0.55$	$\kappa = 0.75$
0			
0.2			
0.4			
0.6			
0.8			
1.0			
1.2			
1.4			
1.6			

Figure 7.4: All catheterized cases: the three concentric cases of  $\kappa$  values 0.1, 0.55 and 0.75 and cases of  $\kappa = 0.1, 0.55$  and  $0.75$  being eccentric in presented increments diverging from the centre-line.

With the analytical solution presenting capabilities for concentric physiological placements of catheters, ANSYS was useful to perform an analysis on the same geometries, but with the catheters displaced from the center-line forming eccentric cases for further analyses and comparison to the concentric. Figure 7.4 Presents all the setups of the cross-sections simulated in this sub-chapter.

### 7.2.2 Results

The analytical calculations and the extracted values from the 3D simulations for the concentric cases for the three different  $\kappa$  values are presented in Table 7.2.

Parameter	$\kappa$	3D CFD	Analytical	% Diff.
$\Delta P$ (mmHg)	0.10	0.438	0.437	-0.13%
	0.55	2.68	2.69	0.58%
	0.75	13.6	13.7	0.60%
$\mathcal{R}$ (Pa·s·m <sup>3</sup> )	0.10	1.62E+07	1.62E+07	-0.13%
	0.55	9.92E+07	9.98E+07	0.58%
	0.75	5.03E+08	5.06E+08	0.60%
$V_{MAX}$ (m/s)	0.10	0.302	0.296	-2.06%
	0.55	0.416	0.418	0.50%
	0.75	0.658	0.661	0.47%

Table 7.2: Comparison of the results from the 3D CFD ANSYS Fluent simulations against the analytical solution presented in Chapter 7.1. The characteristic length taken for the analytical solution input and where results were measured from the 3D results was at the outlet and 4cm inward from the outlet to guarantee a region of fully developed flow.

The results clearly indicate strong agreement with the analytical solution for all three parameters calculated ( $\Delta P$ ,  $\mathcal{R}$  and  $V_{MAX}$ ), with percentage changes of less than 1% for all comparison apart from the maximum velocity value for  $\kappa = 0.1$ , which is also considerably low at just over a 2% drop from the 3D simulation.

Observing the relationship of the fluid resistance as  $\kappa \rightarrow 1$ , an exponential relation-

ship can be observed proportional to the catheter coefficient ( $K$ ). This is demonstrated in Figure 7.5.

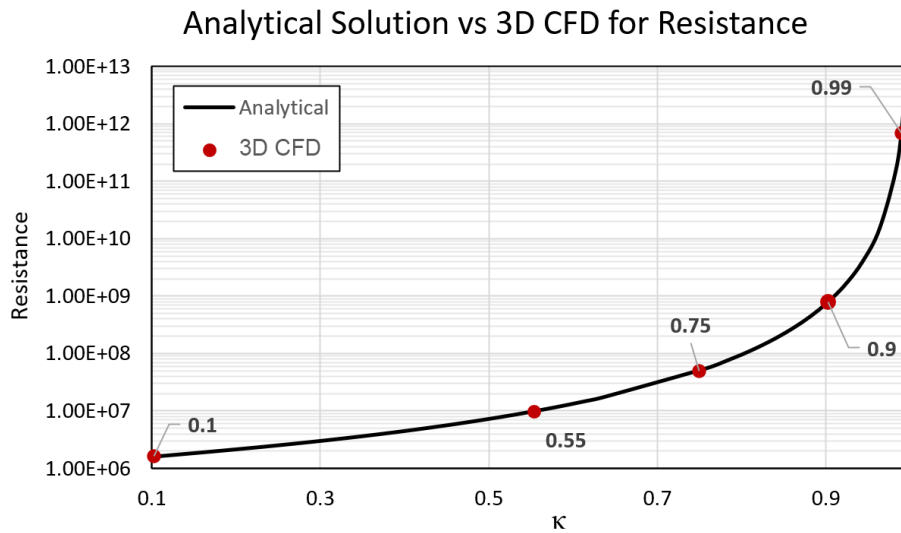


Figure 7.5: Resistance values from the 3D results simulated compared to the analytical solution ( $\kappa = 0.1, 0.55, 0.75$  and additionally  $0.9$  and  $0.99$  for larger data spread) against  $\kappa$ .

With regards to the eccentric cases, results for the resistance were measured for each eccentric case and plotted against the offset distance and presented as percentage difference. All cases of different  $\kappa$  values showed a reduction in resistance as the catheter was displaced further from the centre-line. Figure 7.6 presents these results.

### 7.2.3 Discussion

From the calculations provided for the simplified single vessel model as well as the comparison to the 3D CFD simulations, the analytical solution shows significant agreement for all three calculated parameters ( $\Delta P$ ,  $\mathcal{R}$  and  $V_{MAX}$ ). The results overall show almost perfect agreement which can be concluded as validated through 3D CFD in a state of rigid walls and steady flow. Although these limitations are significantly different to the

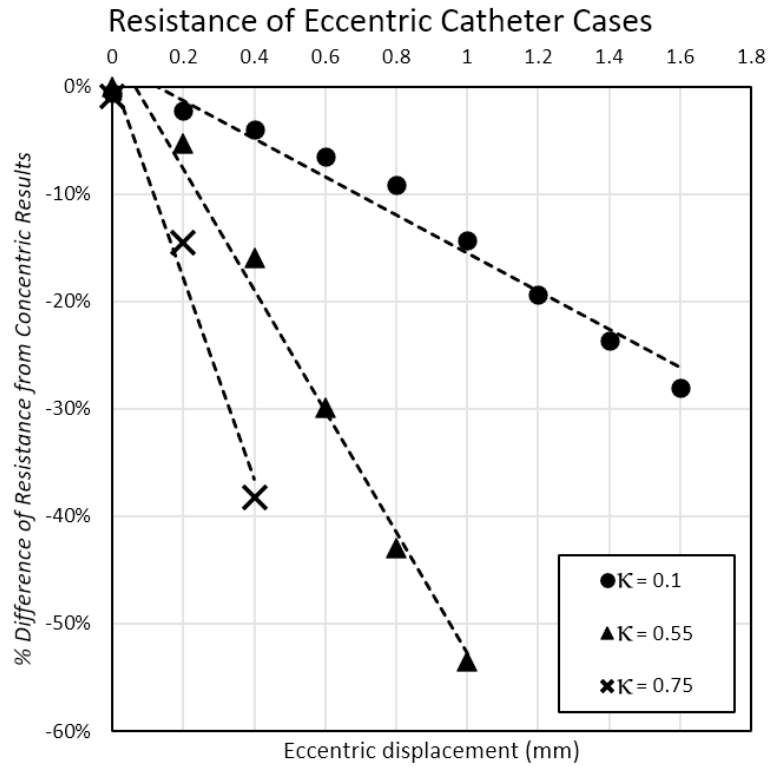


Figure 7.6: Percentage difference from the concentric analytical solution as the catheter deviates from the centre-line of the vessel for the three values of  $\kappa$ .

real situation, this provides a method to implement the analytical term to allow openBF to simulate the presence of the catheter.

In reality, the catheter is unlikely to be placed concentric at all times. The eccentric case helps represent this probability. The results demonstrate that the closer the catheter is to the vessel wall, it reduces the predominant areas of viscous losses and subsequently resistance. This is clearly presented in all three  $\kappa$  values as the smaller of the three experiences a resistance drop of approximately 28%, when  $\kappa$  is 0.55, due to the significant size difference, the resistance drop is up to 54% when closest to the wall and finally, when  $\kappa$  was 0.75, with the limited space there was to move from the centre,

there was a drop of up to 38% in resistance. This suggests that the largest effect the catheter has to the haemodynamics is when it is positioned centrally in the vessel. With the analytical value of resistance when no catheter is present being  $9233611 \text{ Pa}\cdot\text{s}\cdot\text{m}^{-3}$  for the same conditions for measuring pressure drop over a 0.04 m length, 54% resistance drop from the catheterised value of the most realistic  $\kappa$  value (0.55) would still yield  $45906055 \text{ Pa}\cdot\text{s}\cdot\text{m}^{-3}$  which is 4.97 times larger than the no catheter case. Therefore, even though there is a significant change in flow resistance as the catheter moves away from the centre-line, the analytical solution still provides a closer estimation of 46% of the analytical solution compared to 497% of the no catheter solution.

Overall, it is clear considering the scenarios clinically possible, the catheter presence has shown indication of considerable changes to velocity, pressure from the reduction in flow area and flow resistance. With limitations considered in this study such as rigid walls, steady flow, no interference from neighbouring vessels and no interaction alongside phases of aspiration and proximal occlusions the 1D model poses an opportunity to evaluate these interactions through implementing the analytical solution into openBF in future work.

### 7.3 Conclusions

In this chapter, the effect of a catheters presence in cerebral vessels was questioned and evaluated analytically. Results demonstrated that the catheters impact on the vessel was induced by the reduced flow area and increased wall surface area in contact with the blood causing increased resistances. The analytical solution was also validated under the same conditions (steady state, rigid walled, single vessel set-up) through 3D CFD simulation and results presented good agreement. Results also showed that the more likely positioning of the catheter (eccentric and close to the vessel wall) presented lower

resistances. This chapter poses a hypothesis that catheter presence should be considered and the analytical concentric cases suggest that haemodynamic changes are notable in a single vessel. Further work to continue the hypothesis is to evaluate the catheters presence with a pulsatile inlet, compliant walls and more realistic eccentric placement before implementing the a 1D solution of the catheter into openBF.



## Chapter 8

# Conclusion

Computational simulation of large network circulations such as the CoW was utilized for a more comprehensive understanding of haemodynamic behaviours during mechanical stroke treatment. To produce quick data for patient management onset of an acute stroke, a reduced order model was considered to hypothesise the development and validation of a model capable of simulating stroke events and its treatment which can be used to assist clinical decision. The aim of this project was to develop and assess an efficient computational tool to predict flow alterations caused by treatment of ischaemic stroke.

The methodology in Chapter 3 presented the use of simplified adaptations in openBF to simulate the presence of an occlusion (clot and balloon) and additional inlets to apply aspiration, coupled with a five-phased model of key intervals from the clinical procedure (use of BGC and SR). A network of a complete CoW was used alongside typical rheological properties to describe a baseline simulation (Chapter 4) which was used to initially assess the functionality of the five-phase methodology and the haemodynamic outcome with literature. The flow results presented characteristic similarities with the literature

where flow was never retrograde in the incident vessel (L-MCA) but was present in the other treatment pathway vessels (L-ICAs). This simulation was used as a benchmark for comparison data during later studies in Chapter 5 and 6.

In Chapter 5 and 6, modifications to the parameters were applied to assess various likely network alternatives in the population of the CoW as well as more typical range of vessel properties and blood rheology in older patients. Ten variations of absent vessels were presented in Chapter 5 where results of the 1D model were able to distinguish characteristics and importance of certain vessel groups and their impact on flow reversal, and subsequently inform how these variations affect the treatment procedure per phase by using the baseline model as a comparison. Chapter 6 presented two studies: the first demonstrating an aged network through vessel properties and the second presented a study on viscosity of older patients. The simulations present unfavourable haemodynamic outcome due to increased flow and pressure, complicating retrograde flow through aspiration and the treatment paths, although increased viscosity demonstrated increased pressure drop resulting in reduced flows.

In Chapter 4, 5 and 6, post-retrieval of the clot, no simulations presented retrograde flow in the L-MCA. The simulations presented more favourable results in the form of reduced flows rather than retrograde in some studies in the L-MCA. Networks that had missing anterior CoW vessels presented the most unfavourable clinical outcomes. These variations presented significant reduction in the L-MCA post-retrieval but also forced the distal L-ICA's flow to go against the aspiration. Regarding the distal L-ICA, most simulations presented retrograde flow.

Following the full network studies, Chapter 7 presented an analytical approach in understanding if and how much presence of the catheter would impact the haemodynamics within the vessels. A derived analytical expression defining annular flow was used to calculate differences in a single vessel case with and without a catheter. Re-

sults demonstrated the catheter had an influence on pressure and velocities due to the reduced flow areas. To further validate the analytical solution, a 3D CFD simulation of concentric and eccentric catheter in a single vessel was conducted to present  $< 1\%$  differences for pressure drop and flow resistance, and  $< 3\%$  difference for velocity. The eccentric cases presented reduction in flow resistance as the catheter became more offset, presenting the concentric case as the greatest increase in viscous resistance. Works to implement the catheter into openBF to investigate the catheter presence during MT treatment of ischaemic stroke is discussed as future work.

## 8.1 Key Findings

The main contributions of this work are outlined here.

Chapter 3 and 4 presents the methodology and the initial simulation of a MT treatment using a BGC in a comprehensive network including the CoW and the preliminary arteries. The simulation presents results aligning with literature and provides a foundation to develop a more comprehensive model through future work.

The variation studies in Chapters 5 and 6 present the models capability of modifying parameters of the geometry and vessel mechanical properties. Although the simulations in Chapters 4, 5 and 6 used a network comprising of 33 vessels, it is possible to increase this network to include larger ramifications of the cerebral artery branches. Along side this, due to the simplified nature of the occlusion and aspiration parameterization, alternative MT methods that utilise aspiration such as direct aspiration and bore catheters can be simulated with similar methodology to the one presented in Chapter 3.

Chapter 7 considers the influence of the catheter presence. The analytical solution presented shows good agreement with 3D CFD results for concentric cases. From the

extent of the study, the catheter presence impacts the flow area drastically and increases flow resistances due to the increase of surface area in the flow volume. This creates a strong case for vessels that include catheters that take up a larger percentage of the lumen area such as bore catheters or the BGC. Additionally, the concentric case was shown to produce the largest resistances to flow where eccentric cases presented less catheter surface to regions of higher velocities.

## 8.2 Limitations

The methodology proposed in this thesis certainly lacks features, these are presented below:

- The model lacks the representation of pressure losses through tortuosity in key vessels such as the ICA as well as influence of varying bifurcation angles. In reference to the methodology (Chapter 3), the bifurcation region between the L-ICA distal, the L-MCA and the L-ACA proximal demonstrates a key area in haemodynamics of the treatment. Inclusion of the bifurcation angle and tortuosity would provide better insight on flow direction pre- and post-retrieval of the occlusion in the L-MCA.
- Building upon the previous point, the catheter presence is easily idealised as concentric due to the analytical solution being of limited dimensionality. Understanding the nature of the catheter placement with regards to the tortuosity would provide a more comprehensive representation of the catheter presence in the network.
- The current methodology presents a static five-phase model. To understand the true haemodynamic natures would require a more transient study of the procedure. Although the five phases are positioned at key interval, they assume

clinical and physical success of the previous phase, which may not be the case.

- Following the previous point on a transient application of the methodology, inclusion of vascular and external mechanisms such as auto-regulation and external pressure (intra-cranial pressure, ICP). These mechanisms effect the radii, wall thickness and pressure on the vessel which are all characteristics shown to alter the haemodynamics in Chapter 6.
- Alongside aged vascular mechanics and rheology, aging can impose additional changes to the cardiac output. In this study, the heart was simulated as a flow inlet boundary condition and this was not changed throughout the simulation phases for baseline, various networks or aged models. This meant that ventricular haemodynamics were not considered and inclusion of a more comprehensive heart model would benefit the model when simulating the cardiac response through the treatment phases.

### 8.3 Future Works

Following from the limitations, for the current five-phased methodology the most significant of them to be proposed as future work is the implementation and simulation of arterial and external mechanisms (auto-regulation and ICP). Producing a transient methodology would require significant work and alteration, whereas for the present model, literature or clinician advised auto-regulation effects at the key phases and external pressure through the wall mechanics equation of openBF ( $P_{ext}$ ) would provide more details on their effects to the treatment. In addition to the current five-phased model, further comparison through *in-vivo* and *in-vitro* data to validate further the results at those five phases, and to identify any other key intervals of the procedure that should also be modelled.

The studies in this thesis were presented using a singular geometry which was modified to the parameterization of the simulations in Chapters 5 and 6. Validation of the model would benefit from more real case data of network geometry, age, clot location and its obstructive presence (is it fully obstructing the vessel flow) as well as the treatment method used and its outcome to be simulated with the model to further understand limitations of the results. Additionally to geometrical accuracy, the studies presented in this thesis were limited to small parameter changes. With very low simulation times per case, an uncertainty quantification study of key parameters through a Gaussian process emulator would generate a more comprehensive understanding of the parameters during the treatment. Future work in this area is already commencing at the University of Sheffield's INSIGNEO Institute for *in-silico* medicine.

With regards to the catheter presence, implementation of the analytical solution into openBF is currently in progress. The next stages in the methodology would be to simulate using steady state and pulsatile conditions on a single vessel and comparing the results to 3D CFD before adapting the changes to a full CoW model. With the CoW model, the simulation will be able to help assess the overall importance on the treatment outcome with the catheter presence included in a system more complicated than a single vessel.

# References

- [1] T. Truelsen, S. Begg, and C. Mathers, “The global burden of cerebrovascular,” in *Who Int*, 2006.
- [2] J. D. Easton, J. L. Saver, G. W. Albers, M. J. Alberts, S. Chaturvedi, E. Feldmann, T. S. Hatsukami, R. T. Higashida, S. C. Johnston, C. S. Kidwell, *et al.*, “Definition and evaluation of transient ischemic attack: a scientific statement for healthcare professionals from the American Heart Association/American Stroke Association Stroke Council; Council on Cardiovascular Surgery and Anesthesia; Council on Cardiovascular Radiology and Intervention; Council on Cardiovascular Nursing; and the Interdisciplinary Council on Peripheral Vascular Disease. The American Academy of Neurology affirms the value of this statement as an educational tool for neurologists,” *Stroke*, vol. 40, pp. 2276–2293, jun 2009.
- [3] A. S. Go, D. Mozaffarian, V. L. Roger, E. J. Benjamin, J. D. Berry, W. B. Borden, D. M. Bravata, S. Dai, E. S. Ford, C. S. Fox, S. Franco, H. J. Fullerton, C. Gillespie, S. M. Hailpern, J. A. Heit, V. J. Howard, M. D. Huffman, B. M. Kissela, S. J. Kittner, D. T. Lackland, J. H. Lichtman, L. D. Lisabeth, D. Magid, G. M. Marcus, A. Marelli, D. B. Matchar, D. K. McGuire, E. R. Mohler, C. S. Moy, M. E. Mussolino, G. Nichol, N. P. Paynter, P. J. Schreiner, P. D. Sorlie, J. Stein, T. N. Turan, S. S. Virani, N. D. Wong,

- D. Woo, and M. B. Turner, “Heart Disease and Stroke Statistics—2013 Update,” *Circulation*, vol. 127, jan 2013.
- [4] E. J. Benjamin, S. S. Virani, C. W. Callaway, A. M. Chamberlain, A. R. Chang, S. Cheng, S. E. Chiuve, M. Cushman, F. N. Delling, R. Deo, *et al.*, “Heart disease and stroke statistics—2018 update: a report from the american heart association,” *Circulation*, vol. 137, no. 12, pp. e67–e492, 2018.
- [5] J. Emberson, K. R. Lees, P. Lyden, L. Blackwell, G. Albers, E. Bluhmki, T. Brott, G. Cohen, S. Davis, G. Donnan, J. Grotta, G. Howard, M. Kaste, M. Koga, R. Von Kummer, M. Lansberg, R. I. Lindley, G. Murray, J. M. Olivot, M. Parsons, B. Tilley, D. Toni, K. Toyoda, N. Wahlgren, J. Wardlaw, W. Whiteley, G. J. Del Zoppo, C. Baigent, P. Sandercock, and W. Hacke, “Effect of treatment delay, age, and stroke severity on the effects of intravenous thrombolysis with alteplase for acute ischaemic stroke: a meta-analysis of individual patient data from randomised trials,” *The Lancet*, vol. 384, pp. 1929–1935, nov 2014.
- [6] A. Zangerle, S. Kiechl, M. Spiegel, M. Furtner, M. Knoflach, P. Werner, A. Mair, G. Wille, C. Schmidauer, K. Gautsch, T. Gotwald, S. Felber, W. Poewe, and J. Willeit, “Recanalization after thrombolysis in stroke patients,” *Neurology*, vol. 68, pp. 39–44, jan 2007.
- [7] O. O. Zaidat, A. C. Castonguay, I. Linfante, R. Gupta, C. O. Martin, W. E. Holloway, N. Mueller-Kronast, J. D. English, G. Dabus, T. W. Malisch, F. A. Marden, H. Bozorgchami, A. Xavier, A. T. Rai, M. T. Froehler, A. Badruddin, T. N. Nguyen, M. A. Taqi, M. G. Abraham, A. J. Yoo, V. Janardhan, H. Shaltoni, R. Novakovic, A. Abou-Chebl, P. R. Chen, G. W. Britz, C.-H. J. Sun, V. Bansal, R. Kaushal, A. Nanda, and R. G. Nogueira, “First Pass Effect,” *Stroke*, vol. 49, no. 3, pp. 660–666, 2018.

- [8] A. Lambrinos, A. K. Schaink, I. Dhalla, T. Krings, L. K. Casaubon, N. Sikich, C. Lum, A. Bharatha, V. M. Pereira, G. Stotts, G. Saposnik, L. Kelloway, X. Xie, and M. D. Hill, "Mechanical Thrombectomy in Acute Ischemic Stroke: A Systematic Review," *Canadian Journal of Neurological Sciences*, vol. 43, pp. 455–460, feb 2016.
- [9] J. S. Balami, B. A. Sutherland, L. D. Edmunds, I. Q. Grunwald, A. A. Neuhaus, G. Hadley, H. Karbalai, K. A. Metcalf, G. C. DeLuca, and A. M. Buchan, "A Systematic Review and Meta-Analysis of Randomized Controlled Trials of Endovascular Thrombectomy Compared with Best Medical Treatment for Acute Ischemic Stroke:," <https://doi.org/10.1111/ijvs.12618>, vol. 10, pp. 1168–1178, aug 2015.
- [10] P. Sardar, S. Chatterjee, J. Giri, A. Kundu, A. Tandar, P. Sen, R. Nairooz, J. Huston, J. J. Ryan, R. Bashir, S. A. Parikh, C. J. White, P. M. Meyers, D. Mukherjee, J. J. Majersik, and W. A. Gray, "Endovascular therapy for acute ischaemic stroke: a systematic review and meta-analysis of randomized trials," *European Heart Journal*, vol. 36, pp. 2373–2380, sep 2015.
- [11] J.-H. Rha and J. L. Saver, "The impact of recanalization on ischemic stroke outcome: A meta-analysis," *Stroke*, vol. 38, pp. 967–973, mar 2007.
- [12] T. E. Mayer, G. F. Hamann, and H. J. Brueckmann, "Treatment of Basilar Artery Embolism With a Mechanical Extraction Device," *Stroke*, vol. 33, pp. 2232–2235, sep 2002.
- [13] J.-Y. Chueh, A. L. Kühn, A. S. Puri, S. D. Wilson, A. K. Wakhloo, and M. J. Gounis, "Reduction in distal emboli with proximal flow control during mechanical thrombectomy: a quantitative in vitro study," *Stroke*, vol. 44, pp. 1396–1401, may 2013.
- [14] D. H. Lee, J. H. Sung, S. U. Kim, H. J. Yi, J. T. Hong, and S. W. Lee, "Effective use of balloon guide catheters in reducing incidence of mechanical thrombectomy

- related distal embolization,” *Acta neurochirurgica*, vol. 159, pp. 1671–1677, sep 2017.
- [15] M. Mokin, C. N. Ionita, S. V. S. Nagesh, S. Rudin, E. I. Levy, and A. H. Siddiqui, “Primary stentriever versus combined stentriever plus aspiration thrombectomy approaches: in vitro stroke model comparison,” *Journal of neurointerventional surgery*, vol. 7, no. 6, pp. 453–457, 2015.
- [16] T. Liebig, M. Holtmannspötter, R. Crossley, J. Lindkvist, P. Henn, L. Lönn, and A. G. Gallagher, “Metric-Based Virtual Reality Simulation: A Paradigm Shift in Training for Mechanical Thrombectomy in Acute Stroke,” *Stroke*, vol. 49, pp. e239–e242, jul 2018.
- [17] M. S. Alnæs, J. Isaksen, K.-A. Mardal, B. Romner, M. K. Morgan, and T. Ingebrigtsen, “Computation of hemodynamics in the circle of Willis,” *Stroke*, vol. 38, pp. 2500–2505, sep 2007.
- [18] S. Moore, T. David, J. G. Chase, J. Arnold, and J. Fink, “3D models of blood flow in the cerebral vasculature,” *Journal of Biomechanics*, vol. 39, pp. 1454–1463, jan 2006.
- [19] Y. Shi, D. Cheshire, F. Lally, and C. Roffe, “Suction force-suction distance relation during aspiration thrombectomy for ischaemic stroke: a computational fluid dynamics study,” *Physics in Medicine*, vol. 3, pp. 1–8, dec 2016.
- [20] N. Xiao, J. D. Humphrey, and C. A. Figueroa, “Multi-Scale Computational Model of Three-Dimensional Hemodynamics within a Deformable Full-Body Arterial Network,” *Journal of computational physics*, vol. 244, pp. 22–40, jul 2013.
- [21] S. J. Sherwin, L. Formaggia, J. Peiró, and V. Franke, “Computational modelling of 1D blood flow with variable mechanical properties and its application to the sim-

- ulation of wave propagation in the human arterial system,” *International Journal for Numerical Methods in Fluids*, vol. 43, pp. 673–700, oct 2003.
- [22] S. Sherwin, V. Franke, J. Peiró, and K. Parker, “One-dimensional modelling of a vascular network in space-time variables,” *Journal of Engineering Mathematics* 2003 47:3, vol. 47, pp. 217–250, dec 2003.
- [23] K. S. Matthys, J. Alastruey, J. Peiró, A. W. Khir, P. Segers, P. R. Verdonck, K. H. Parker, and S. J. Sherwin, “Pulse wave propagation in a model human arterial network: assessment of 1-D numerical simulations against in vitro measurements,” *Journal of biomechanics*, vol. 40, no. 15, pp. 3476–3486, 2007.
- [24] J. Alastruey, A. W. Khir, K. S. Matthys, P. Segers, S. J. Sherwin, P. R. Verdonck, K. H. Parker, and J. Peiró, “Pulse wave propagation in a model human arterial network: Assessment of 1-D visco-elastic simulations against in vitro measurements,” *Journal of biomechanics*, vol. 44, pp. 2250–2258, aug 2011.
- [25] N. Xiao, J. Alastruey, and C. Alberto Figueroa, “A systematic comparison between 1-D and 3-D hemodynamics in compliant arterial models,” *International journal for numerical methods in biomedical engineering*, vol. 30, pp. 204–231, feb 2014.
- [26] A. Melis, F. Moura, I. Larrabide, K. Janot, R. H. Clayton, A. P. Narata, and A. Marzo, “Improved biomechanical metrics of cerebral vasospasm identified via sensitivity analysis of a 1D cerebral circulation model,” *Journal of Biomechanics*, vol. 90, pp. 24–32, jun 2019.
- [27] T. I. Józsa, W. El-Bouri, R. Padmos, S. Payne, and A. Hoekstra, “A cerebral circulation model for in silico clinical trials of ischaemic stroke,” in *CompBioMed Conf., London, UK, 25–27 September 2019*, 2019.
- [28] R. R. Stevens, W. P. Donders, S. Quicken, F. N. Van De Vosse, W. H. Mess, T. Delhaas, and W. Huberts, “The role of one-dimensional model-generated inter-

subject variations in systemic properties on wall shear stress indices of intracranial aneurysms,” *IEEE Transactions on Biomedical Engineering*, vol. 67, no. 4, pp. 1030–1039, 2019.

- [29] A. Melis, *Gaussian process emulators for 1D vascular models*. PhD thesis, University of Sheffield, 2017.
- [30] A. Melis, “openBF: Julia software for 1D blood flow modelling,” 2018.
- [31] W. F. Boron and E. L. Boulpaep, *Medical Physiology 3rd Edition*, ch. 17. Organization of the Cardiovascular System. Philadelphia: Elsevier, 2017.
- [32] A. Tameem and H. Krovvidi, “Cerebral physiology,” *Continuing Education in Anaesthesia, Critical Care & Pain*, vol. 13, no. 4, pp. 113–118, 2013.
- [33] W. F. Boron and E. L. Boulpaep, *Medical Physiology 3rd Edition*, ch. 18. Blood. Philadelphia: Elsevier, 2017.
- [34] B. Alberts, A. Johnson, J. Lewis, M. Raff, K. Roberts, and P. Walter, *Molecular Biology of the Cell 5th Edition*, ch. 23. Specialized Tissues, Stem Cells and Tissue Renewal. New York: Garland Science, 2008.
- [35] Y.-c. Fung, *Biomechanics: mechanical properties of living tissues*. Springer Science & Business Media, 1993.
- [36] D. E. Brooks, J. W. Goodwin, and G. V. Seaman, “Interactions among erythrocytes under shear,” *Journal of applied physiology*, vol. 28, no. 2, pp. 172–177, 1970.
- [37] R. L. Whitmore, *Rheology of the Circulation*. Pergamon, 1968.
- [38] C. Vlachopoulos, M. O’Rourke, and W. W. Nichols, *McDonald’s blood flow in arteries: theoretical, experimental and clinical principles*. CRC press, 2011.
- [39] J. E. Hall and M. E. Hall, *Guyton and Hall textbook of medical physiology e-Book*. Elsevier Health Sciences, 2020.

- [40] Y.-c. Fung, *Biomechanics Circulation*. Springer Science & Business Media, 1997.
- [41] T. Kenner, “The measurement of blood density and its meaning,” tech. rep., 1989.
- [42] M. J. Cipolla, “The cerebral circulation,” *Integrated systems physiology: From molecule to function*, vol. 1, no. 1, pp. 1–59, 2009.
- [43] N. A. Lassen and M. S. Christensen, “PHYSIOLOGY OF CEREBRAL BLOOD FLOW,” tech. rep., 1976.
- [44] R. E. Klabunde, *Cardiovascular Physiology Concepts 2nd Edition*. Baltimore: Lippincott Williams & Wilkins, 2nd editio ed., 2012.
- [45] N. A. Lassen, “Cerebral blood flow and oxygen consumption in man,” Tech. Rep. 2, 1959.
- [46] W. M. Armstead, “Cerebral Blood Flow Autoregulation and Dysautoregulation,” *Anesthesiology Clinics*, vol. 34, no. 3, pp. 465–477, 2016.
- [47] M. F. O’Rourke, “Arterial aging: pathophysiological principles,” *Vascular medicine*, vol. 12, no. 4, pp. 329–341, 2007.
- [48] Å. R. Ahlgren, F. Hansen, B. Sonesson, and T. Länne, “Stiffness and diameter of the common carotid artery and abdominal aorta in women,” *Ultrasound in medicine & biology*, vol. 23, no. 7, pp. 983–988, 1997.
- [49] G. M. Fischer and J. G. Llaurado, “Collagen and elastin content in canine arteries selected from functionally different vascular beds,” *Circulation research*, vol. 19, no. 2, pp. 394–399, 1966.
- [50] J. E. Wagenseil and R. P. Mecham, “Elastin in large artery stiffness and hypertension,” *Journal of cardiovascular translational research*, vol. 5, no. 3, pp. 264–273, 2012.

- [51] R. P. Mecham, "Overview of extracellular matrix," *Current protocols in cell biology*, no. 1, pp. 10–1, 1998.
- [52] S. Glagov, "Hemodynamic risk factors: mechanical stress, mural architecture, medial nutrition and the vulnerability of arteries to atherosclerosis," *The pathogenesis of atherosclerosis*, pp. 164–199, 1972.
- [53] A. U. Ferrari, A. Radaelli, and M. Centola, "Physiology of Aging Invited Review: Aging and the cardiovascular system," *J Appl Physiol*, vol. 95, pp. 2591–2597, 2003.
- [54] R. Virmani, A. P. Avolio, W. J. Mergner, M. Robinowitz, E. E. Herderick, J. F. Cornhill, S. Y. Guo, T. H. Liu, D. Y. Ou, and M. O'Rourke, "Effect of aging on aortic morphology in populations with high and low prevalence of hypertension and atherosclerosis: Comparison between occidental and Chinese communities," *American Journal of Pathology*, vol. 139, no. 5, pp. 1119–1129, 1991.
- [55] P. M. Cogswell, S. K. Lants, L. T. Davis, and M. J. Donahue, "Vessel wall and lumen characteristics with age in healthy participants using 3T intracranial vessel wall magnetic resonance imaging," *Journal of Magnetic Resonance Imaging*, vol. 50, pp. 1452–1460, nov 2019.
- [56] E. Fonck, G. G. Feigl, J. Fasel, D. Sage, M. Unser, D. A. Rüfenacht, and N. Stergiopulos, "Research Letters Effect of Aging on Elastin Functionality in Human Cerebral Arteries," 2009.
- [57] W. W. Nichols, M. F. O'Rourke, A. P. Avolio, T. Yaginuma, J. P. Murgu, C. J. Pepine, and C. R. Conti, "Effects of age on ventricular-vascular coupling," *The American Journal of Cardiology*, vol. 55, pp. 1179–1184, apr 1985.
- [58] E. R. Gozna, A. E. Marble, A. Shaw, and J. G. Holland, "Age related changes in the mechanics of the aorta and pulmonary artery of man," *Journal of Applied Physiology*, vol. 36, no. 4, pp. 407–411, 1974.

- [59] D. E. Busby and A. C. Burton, "The effect of age on the elasticity of the major brain arteries.," *Canadian journal of physiology and pharmacology*, vol. 43, pp. 185–202, 1965.
- [60] D. L. Edward G. Lakatta, "Arterial and Cardiac Aging: Major Shareholders in Cardiovascular Disease Enterprises A Trilogy of Heart Disease Manifestations Emerges With Advancing Age Age-Associated Changes in Cardiac Structure and Function in Persons Without a Heart Disease Diagnosis," *Circulation*, vol. 107, no. 2, pp. 346–354, 2003.
- [61] J. Alastruey, K. H. Parker, J. Peiró, S. M. Byrd, and S. J. Sherwin, "Modelling the circle of Willis to assess the effects of anatomical variations and occlusions on cerebral flows," *Journal of Biomechanics*, vol. 40, no. 8, pp. 1794–1805, 2007.
- [62] L. B. Hindenes, A. K. Håberg, L. H. Johnsen, E. B. Mathiesen, D. Robben, and T. R. Vangberg, "Variations in the Circle of Willis in a large population sample using 3D TOF angiography: The Tromsø Study," *PLOS ONE*, vol. 15, p. e0241373, nov 2020.
- [63] D. L. Cooke, C. E. Stout, W. T. Kim, A. P. Kansagra, J. P. Yu, A. Gu, N. P. Jewell, S. W. Hetts, R. T. Higashida, C. F. Dowd, and V. Van Halbach, "Cerebral arterial fenestrations," 2014.
- [64] K. Kapoor, B. Singh, and L. I. J. Dewan, "Variations in the configuration of the circle of Willis," *Anatomical Science International*, vol. 83, pp. 96–106, jun 2008.
- [65] D. G. Nordon and R. Júnior, "Variations in the brain circulation-the circle of Willis," Tech. Rep. 4, jan 2012.
- [66] L. Badimon, T. Padró, and G. Vilahur, "Atherosclerosis, platelets and thrombosis in acute ischaemic heart disease," *European Heart Journal: Acute Cardiovascular Care*, vol. 1, pp. 60–74, apr 2012.

- [67] G. Lippi, M. Franchini, and G. Targher, “Arterial thrombus formation in cardiovascular disease,” sep 2011.
- [68] R. G. Hart, H. C. Diener, S. B. Coutts, J. D. Easton, C. B. Granger, M. J. O’Donnell, R. L. Sacco, and S. J. Connolly, “Embolic strokes of undetermined source: The case for a new clinical construct,” 2014.
- [69] B. B. Love and B. H. Bendixen, “Classification of subtype of acute ischemic stroke definitions for use in a multicenter clinical trial,” *Stroke*, vol. 24, no. 1, pp. 35–41, 1993.
- [70] R. Alexandru, E. O. Terecoasă, O. A. Băjenaru, and C. Tiu, “Etiologic classification of ischemic stroke: Where do we stand?,” aug 2017.
- [71] H. Ay, K. L. Furie, A. Singhal, W. S. Smith, A. G. Sorensen, and W. J. Koroshetz, “An evidence-based causative classification system for acute ischemic stroke,” *Annals of Neurology*, vol. 58, pp. 688–697, nov 2005.
- [72] E. M. Arsava, E. Ballabio, T. Benner, J. W. Cole, M. P. Delgado-Martinez, M. Dichgans, F. Fazekas, K. L. Furie, K. Illoh, K. Jood, S. Kittner, A. G. Lindgren, J. J. Majersik, M. J. MacLeod, W. J. Meurer, J. Montaner, A. A. Olugbodi, A. Pasdar, P. Redfors, R. Schmidt, P. Sharma, A. B. Singhal, A. G. Sorensen, C. Sudlow, V. Thijs, B. B. Worrall, J. Rosand, and H. Ay, “The causative classification of stroke system: An international reliability and optimization study,” *Neurology*, vol. 75, pp. 1277–1284, oct 2010.
- [73] G. Sirimarco, P. C. Lavallée, J. Labreuche, E. Meseguer, L. Cabrejo, C. Guidoux, I. F. Klein, J. M. Olivot, H. Abboud, V. Adraï, J. Kusmierrek, S. Ratani, P. J. Touboul, M. Mazighi, P. G. Steg, and P. Amarenco, “Overlap of diseases underlying ischemic stroke: The ASCOD phenotyping,” *Stroke*, vol. 44, pp. 2427–2433, sep 2013.

- [74] M. J. O'Donnell, S. L. Chin, S. Rangarajan, D. Xavier, L. Liu, H. Zhang, P. Rao-Melacini, X. Zhang, P. Pais, S. Agapay, P. Lopez-Jaramillo, A. Damasceno, P. Langhorne, M. J. McQueen, A. Rosengren, M. Dehghan, G. J. Hankey, A. L. Dans, A. Elsayed, A. Avezum, C. Mondo, H. C. Diener, D. Ryglewicz, A. Czlonkowska, N. Pogosova, C. Weimar, R. Iqbal, R. Diaz, K. Yusoff, A. Yusufali, A. Oguz, X. Wang, E. Penaherrera, F. Lanas, O. S. Ogah, A. Ogunniyi, H. K. Iversen, G. Malaga, Z. Rumboldt, S. Oveisgharan, F. Al Hussain, D. Magazi, Y. Nilanont, J. Ferguson, G. Pare, and S. Yusuf, "Global and regional effects of potentially modifiable risk factors associated with acute stroke in 32 countries (INTERSTROKE): a case-control study," *The Lancet*, vol. 388, pp. 761–775, aug 2016.
- [75] S. Lewington, R. Clarke, N. Qizilbash, R. Peto, and R. Collins, "Age-specific relevance of usual blood pressure to vascular mortality: A meta-analysis of individual data for one million adults in 61 prospective studies," *Lancet*, vol. 360, pp. 1903–1913, dec 2002.
- [76] B. Neal, S. MacMahon, N. Chapman, J. Cutler, R. Fagard, P. Whelton, S. Yusuf, L. Agodoa, C. Baigent, H. Black, J. P. Boissel, B. Brenner, M. Brown, C. Bulpitt, R. Byington, J. Chalmers, R. Collins, B. Dahlöf, B. Davis, R. Estacio, K. Fox, L. Hansson, R. Holman, L. Hunsicker, J. Kostis, K. Kuramoto, J. Kusek, R. Lees, E. Lewis, L. H. Lindholm, L. Liu, J. Lubsen, E. Malacco, G. Mancina, I. Martin, C. Pepine, M. Pfeffer, B. Pitt, P. Poole-Wilson, G. Remuzzi, A. Rodgers, P. Ruggenti, R. Schrier, P. Sever, P. Sleight, J. Staessen, K. Teo, R. Turner, L. Wing, A. Zanchetti, C. Algert, and M. Woodward, "Effects of ACE inhibitors, calcium antagonists, and other blood-pressure-lowering drugs: Results of prospectively designed overviews of randomised trials," *Lancet*, vol. 356, pp. 1955–1964, dec 2000.

- [77] J. A. Staessen, R. Fagard, L. Thijs, H. Celis, G. G. Arabidze, W. H. Birkenhäger, C. J. Bulpitt, P. W. de Leeuw, C. T. Dollery, A. E. Fletcher, F. Forette, G. Leonetti, C. Nachev, E. T. O'Brien, J. Rosenfeld, J. L. Rodicio, J. Tuomilehto, and A. Zanchetti, "Randomised double-blind comparison of placebo and active treatment for older patients with isolated systolic hypertension," *The Lancet*, vol. 350, pp. 757–764, sep 1997.
- [78] F. Gueyffier, C. Bulpitt, J. P. Boissel, E. Schron, T. Ekblom, R. Fagard, E. Casiglia, K. Kerlikowske, and J. Coope, "Antihypertensive drugs in very old people: A subgroup meta-analysis of randomised controlled trials," *Lancet*, vol. 353, pp. 793–796, mar 1999.
- [79] P. A. Wolf, R. B. D'agostino, W. B. Kannel, R. Bonita, and A. J. Belanger, "Cigarette Smoking as a Risk Factor for Stroke: The Framingham Study," *JAMA: The Journal of the American Medical Association*, vol. 259, pp. 1025–1029, feb 1988.
- [80] R. D. Abbott, Y. Yin, D. M. Reed, and K. Yano, "Risk of Stroke in Male Cigarette Smokers," *New England Journal of Medicine*, vol. 315, pp. 717–720, sep 1986.
- [81] G. A. Colditz, R. Bonita, M. J. Stampfer, W. C. Willett, B. Rosner, F. E. Speizer, and C. H. Hennekens, "Cigarette Smoking and Risk of Stroke in Middle-Aged Women," *New England Journal of Medicine*, vol. 318, pp. 937–941, apr 1988.
- [82] K. Reynolds, L. B. Lewis, J. D. L. Nolen, G. L. Kinney, B. Sathya, and J. He, "Alcohol Consumption and Risk of Stroke: A Meta-analysis," feb 2003.
- [83] T. Kurth, J. M. Gaziano, K. Berger, C. S. Kase, K. M. Rexrode, N. R. Cook, J. E. Buring, and J. A. E. Manson, "Body mass index and the risk of stroke in men," *Archives of Internal Medicine*, vol. 162, pp. 2557–2562, dec 2002.

- [84] T. Kurth, J. M. Gaziano, K. M. Rexrode, C. S. Kase, N. R. Cook, J. A. E. Manson, and J. E. Buring, "Prospective study of body mass index and risk of stroke in apparently healthy women," *Circulation*, vol. 111, pp. 1992–1998, apr 2005.
- [85] C. D. Lee, A. R. Folsom, and S. N. Blair, "Physical activity and stroke risk: A meta-analysis," *Stroke*, vol. 34, pp. 2475–2481, oct 2003.
- [86] K. J. Joshipura, A. Ascherio, J. A. E. Manson, M. J. Stampfer, E. B. Rimm, F. E. Speizer, C. H. Hennekens, D. Spiegelman, and W. C. Willett, "Fruit and vegetable intake in relation to risk of ischemic stroke," *Journal of the American Medical Association*, vol. 282, pp. 1233–1239, oct 1999.
- [87] K. He, Y. Song, M. L. Davi, K. Liu, L. Van Horn, A. R. Dyer, U. Goldbourt, and P. Greenland, "Fish consumption and incidence of stroke: A meta-analysis of cohort studies," *Stroke*, vol. 35, pp. 1538–1542, jul 2004.
- [88] P. B. Mellen, T. F. Walsh, and D. M. Herrington, "Whole grain intake and cardiovascular disease: A meta-analysis," *Nutrition, Metabolism and Cardiovascular Diseases*, vol. 18, pp. 283–290, may 2008.
- [89] M. Umesawa, H. Iso, C. Date, A. Yamamoto, H. Toyoshima, Y. Watanabe, S. Kikuchi, A. Koizumi, T. Kondo, Y. Inaba, N. Tanabe, and A. Tamakoshi, "Dietary intake of calcium in relation to mortality from cardiovascular disease: The JACC study," *Stroke*, vol. 37, pp. 20–26, jan 2006.
- [90] K. He, A. Merchant, E. B. Rimm, B. A. Rosner, M. J. Stampfer, W. C. Willett, and A. Ascherio, "Dietary fat intake and risk of stroke in male US healthcare professionals: 14 Year prospective cohort study," *British Medical Journal*, vol. 327, pp. 777–781, oct 2003.
- [91] B. V. Howard, L. Van Horn, J. Hsia, J. A. E. Manson, M. L. Stefanick, S. Wassertheil-Smoller, L. H. Kuller, A. Z. LaCroix, R. D. Langer, N. L. Lasser, C. E. Lewis, M. C.

Limacher, K. L. Margolis, W. J. Mysiw, J. K. Ockene, L. M. Parker, M. G. Perri, L. Phillips, R. L. Prentice, J. Robbins, J. E. Rossouw, G. E. Sarto, I. J. Schatz, L. G. Snetselaar, V. J. Stevens, L. F. Tinker, M. Trevisan, M. Z. Vitolins, G. L. Anderson, A. R. Assaf, T. Bassford, S. A. Beresford, H. R. Black, R. L. Brunner, R. G. Brzyski, B. Caan, R. T. Chlebowski, M. Gass, I. Granek, P. Greenland, J. Hays, D. Heber, G. Heiss, S. L. Hendrix, F. A. Hubbell, K. C. Johnson, and J. M. Kotchen, "Low-fat dietary pattern and risk of cardiovascular disease: The Women's Health Initiative randomized controlled dietary modification trial," *Journal of the American Medical Association*, vol. 295, pp. 655–666, feb 2006.

- [92] M. Hamer, G. J. Molloy, and E. Stamatakis, "Psychological Distress as a Risk Factor for Cardiovascular Events. Pathophysiological and Behavioral Mechanisms," *Journal of the American College of Cardiology*, vol. 52, no. 25, pp. 2156–2162, 2008.
- [93] A. K. Boehme, C. Esenwa, and M. S. V. Elkind, "Stroke Risk Factors, Genetics, and Prevention," *Circulation research*, vol. 120, p. 472, feb 2017.
- [94] P. Belani, J. Schefflein, S. Kihira, B. Rigney, B. N. Delman, K. Mahmoudi, J. Mocco, S. Majidi, J. Yeckley, A. Aggarwal, D. Lefton, and A. H. Doshi, "COVID-19 Is an independent risk factor for acute ischemic stroke," *American Journal of Neuroradiology*, vol. 41, pp. 1361–1364, aug 2020.
- [95] W. Hacke, M. Kaste, T. S. Olsen, J. M. Orgogozo, and J. Bogousslavsky, "European Stroke Initiative recommendations for stroke management," 2000.
- [96] W. Hacke, M. Kaste, J. Bogousslavsky, M. Brainin, A. Chamorro, K. Lees, D. Leys, H. Kwiecinski, D. Toni, T. S. Olsen, P. Langhorne, H. C. Diener, M. Hennerici, J. Ferro, J. Sivenius, N. G. Wahlgren, and P. Bath, "European Stroke Initiative Recommendations for Stroke Management - Update 2003," 2003.

- [97] P. A. Ringleb, M. G. Bousser, G. Ford, P. Bath, M. Brainin, V. Caso, Á. Cervera, A. Chamorro, C. Cordonnier, L. Csiba, A. Davalos, H. C. Diener, J. Ferro, W. Hacke, M. Hennerici, M. Kaste, P. Langhorne, K. Lees, D. Leys, J. Lodder, H. S. Markus, J. L. Mas, H. P. Mattle, K. Muir, B. Norrving, V. Obach, S. Paolucci, E. B. Ringelstein, P. D. Schellinger, J. Sivenius, V. Skvortsova, K. S. Sunnerhagen, L. Thomassen, D. Toni, R. Von Kummer, N. G. Wahlgren, M. F. Walker, and J. Wardlaw, “Guidelines for management of ischaemic stroke and transient ischaemic attack 2008,” may 2008.
- [98] S. R. Levine, “A Systems Approach to Immediate Evaluation and Management of Hyperacute Stroke,” *Stroke*, vol. 28, pp. 1530–1540, aug 1997.
- [99] J. E. Acker, A. M. Pancioli, T. J. Crocco, M. K. Eckstein, E. C. Jauch, H. Larrabee, N. M. Meltzer, W. C. Mergendahl, J. W. Munn, S. M. Prentiss, C. Sand, J. L. Saver, B. Eigel, B. R. Gilpin, M. Schoeberl, P. Solis, J. R. Bailey, K. B. Horton, and S. K. Stranne, “Implementation strategies for emergency medical services within stroke systems of care: A policy statement from the American Heart Association/American Stroke Association expert panel on emergency medical services systems and the stroke council,” nov 2007.
- [100] M. J. Alberts, R. E. Latchaw, W. R. Selman, T. Shephard, M. N. Hadley, L. M. Brass, W. Koroshetz, J. R. Marler, J. Booss, R. D. Zorowitz, J. B. Croft, E. Magnis, D. Mulligan, A. Jagoda, R. O’Connor, C. M. Cawley, J. J. Connors, J. A. Rose-DeRenzy, M. Emr, M. Warren, and M. D. Walker, “Recommendations for comprehensive stroke centers: A consensus statement from the brain attack coalition,” jul 2005.
- [101] A. O. Zurick, *CT and MRI Cardiovascular Hemodynamics*, pp. 183–204. Cham: Springer International Publishing, 2019.

- [102] M. J. Donahue, M. K. Strother, and J. Hendrikse, “Novel MRI Approaches for Assessing Cerebral Hemodynamics in Ischemic Cerebrovascular Disease,” 2012.
- [103] T. N. I. o. N. D. Group and S. rt PA Stroke Study, “Tissue Plasminogen Activator for Acute Ischemic Stroke,” *New England Journal of Medicine*, vol. 333, pp. 1581–1588, dec 1995.
- [104] T. He, M. Ulticenter, A. Cute, S. Troke, T. Rial -E Urope, S. Tudy, and G. Roup, “Thrombolytic Therapy with Streptokinase in Acute Ischemic Stroke,” *New England Journal of Medicine*, vol. 335, pp. 145–150, jul 1996.
- [105] D. Tirschwell, “Intra-arterial prourokinase for acute ischemic stroke.,” apr 2000.
- [106] C. M. Alvarez, D. J. McCarthy, S. Sur, B. M. Snelling, and R. M. Starke, “Comparing Mechanical Thrombectomy Techniques in the Treatment of Large Vessel Occlusion for Acute Ischemic Stroke,” *World Neurosurgery*, vol. 100, pp. 681–682, apr 2017.
- [107] A. Velasco, B. Buerke, C. P. Stracke, S. Berkemeyer, P. J. Mosimann, W. Schwindt, P. Alcázar, C. Cnyrim, T. Niederstadt, R. Chapot, and W. Heindel, “Comparison of a Balloon Guide Catheter and a Non-Balloon Guide Catheter for Mechanical Thrombectomy,” *Radiology*, vol. 280, pp. 169–176, jul 2016.
- [108] T. N. Nguyen, T. Malisch, A. C. Castonguay, R. Gupta, C. H. J. Sun, C. O. Martin, W. E. Holloway, N. Mueller-Kronast, J. D. English, I. Linfante, G. Dabus, F. A. Marden, H. Bozorgchami, A. Xavier, A. T. Rai, M. T. Froehler, A. Badruddin, M. Taqi, M. G. Abraham, V. Janardhan, H. Shaltoni, R. Novakovic, A. J. Yoo, A. Abou-Chebl, P. R. Chen, G. W. Britz, R. Kaushal, A. Nanda, M. A. Issa, H. Masoud, R. G. Nogueira, A. M. Norbash, and O. O. Zaidat, “Balloon guide catheter improves revascularization and clinical outcomes with the solitaire device : Analysis of the

north american solitaire acute stroke registry,” *Stroke*, vol. 45, pp. 141–145, jan 2014.

- [109] E. A. Mistry, A. M. Mistry, M. O. Nakawah, R. V. Chitale, R. F. James, J. J. Volpi, and M. R. Fusco, “Mechanical Thrombectomy Outcomes with and Without Intravenous Thrombolysis in Stroke Patients: A Meta-Analysis,” *Stroke*, vol. 48, pp. 2450–2456, sep 2017.
- [110] A. S. Turk, A. Spiotta, D. Frei, J. Mocco, B. Baxter, D. Fiorella, A. Siddiqui, M. Mokin, M. Dewan, H. Woo, R. Turner, H. Hawk, A. Miranpuri, and I. Chaudry, “Initial clinical experience with the ADAPT technique: A direct aspiration first pass technique for stroke thrombectomy,” *Journal of NeuroInterventional Surgery*, vol. 6, no. 3, pp. 231–237, 2014.
- [111] J. Madjidyar, L. Pineda Vidal, N. Larsen, and O. Jansen, “Influence of Thrombus Composition on Thrombectomy: ADAPT vs Balloon Guide Catheter and Stent Retriever in a Flow Model,” *RoFo Fortschritte auf dem Gebiet der Rontgenstrahlen und der Bildgebenden Verfahren*, vol. 192, pp. 257–263, mar 2020.
- [112] D.-H. Kang, B. M. Kim, J. H. Heo, H. S. Nam, Y. D. Kim, Y.-H. Hwang, Y.-W. Kim, Y.-S. Kim, D. J. Kim, H. S. Kwak, *et al.*, “Effect of balloon guide catheter utilization on contact aspiration thrombectomy,” *Journal of neurosurgery*, vol. 131, no. 5, pp. 1494–1500, 2018.
- [113] R. Arslanian, M. Marosfoi, C. Raskett, M. Gounis, A. Puri, and J. Chueh, “E-095 BGC protected ADAPT reduced risk of distal embolization: an in vitro study,” pp. A100.2–A101, BMJ, jul 2019.
- [114] J. Y. Chueh, A. S. Puri, A. K. Wakhloo, and M. J. Gounis, “Risk of distal embolization with stent retriever thrombectomy and ADAPT,” *Journal of NeuroInterventional Surgery*, vol. 8, pp. 197–202, feb 2016.

- [115] D. N. Ku, “Blood flow in arteries,” *Annual Review of Fluid Mechanics*, vol. 29, no. 1, pp. 399–434, 1997.
- [116] J. R. Womersley, “Method for the calculation of velocity, rate of flow and viscous drag in arteries when the pressure gradient is known,” *The Journal of Physiology*, vol. 127, pp. 553–563, mar 1955.
- [117] A. F. Stalder, A. Frydrychowicz, M. F. Russe, J. G. Korvink, J. Hennig, K. Li, and M. Markl, “Assessment of flow instabilities in the healthy aorta using flow-sensitive MRI,” *Journal of Magnetic Resonance Imaging*, vol. 33, pp. 839–846, apr 2011.
- [118] N. Westerhof, *Snapshots of hemodynamics : an aid for clinical research and graduate education*. New York: Springer, 2010.
- [119] H. Liu, D. Wang, X. Leng, D. Zheng, F. Chen, L. K. S. Wong, L. Shi, and T. W. H. Leung, “State-of-the-Art Computational Models of Circle of Willis with Physiological Applications: A Review,” 2020.
- [120] S. Z. Zhao, X. Y. Xu, A. D. Hughes, S. A. Thom, A. V. Stanton, B. Ariff, and Q. Long, “Blood flow and vessel mechanics in a physiologically realistic model of a human carotid arterial bifurcation,” *Journal of Biomechanics*, vol. 33, pp. 975–984, aug 2000.
- [121] M. Neidlin, T. A. Kaufmann, U. Steinseifer, and T. Schmitz-Rode, “Multiscale multiphysic approaches in vascular hemodynamics,” in *Biomedical Technology*, pp. 67–76, Springer, 2018.
- [122] K. T and M. M, “Flow visualization in isolated transparent natural blood vessels,” *Biorheology*, vol. 20, no. 2, pp. 119–127, 1983.

- [123] P. K and R. M, “Numerical flow studies in human carotid artery bifurcations: basic discussion of the geometric factor in atherogenesis,” *Journal of biomedical engineering*, vol. 12, no. 2, pp. 111–123, 1990.
- [124] T. G. Phan, H. Ma, M. Goyal, J. Hilton, M. Sinnott, V. Srikanth, and R. Beare, “Computer Modeling of Clot Retrieval—Circle of Willis,” *Frontiers in Neurology*, vol. 11, no. August, pp. 1–11, 2020.
- [125] G. Romero, C. Talayero, G. Pearce, and J. Wong, “Modeling of blood clot removal with aspiration thrombectomy devices,” *Journal of Mechanical Engineering and Sciences*, vol. 14, no. 1, pp. 6238–6250, 2020.
- [126] M. Neidlin, M. Büsen, C. Brockmann, M. Wiesmann, S. J. Sonntag, U. Steinseifer, and T. A. Kaufmann, “A numerical framework to investigate hemodynamics during endovascular mechanical recanalization in acute stroke,” *International journal for numerical methods in biomedical engineering*, vol. 32, no. 4, p. e02748, 2016.
- [127] G. Luraghi, S. Bridio, J. F. R. Matas, G. Dubini, N. Boodt, F. J. Gijssen, A. van der Lugt, B. Fereidoonzezhad, K. M. Moerman, P. McGarry, *et al.*, “The first virtual patient-specific thrombectomy procedure,” *Journal of Biomechanics*, vol. 126, p. 110622, 2021.
- [128] X. O. Nikoubashman, X. D. Wischer, X. H. M. Hennemann, X. M. Büsen, X. C. Brockmann, and X. M. Wiesmann, “Under Pressure: Comparison of Aspiration Techniques for Endovascular Mechanical Thrombectomy,”
- [129] N. Stergiopoulos, D. F. Young, and T. R. Rogge, “Computer simulation of arterial flow with applications to arterial and aortic stenoses,” *Journal of Biomechanics*, vol. 25, no. 12, pp. 1477–1488, 1992.

- [130] R. Fahrig, H. Nikolov, A. J. Fox, and D. W. Holdsworth, “A three-dimensional cerebrovascular flow phantom,” *Medical Physics*, vol. 26, no. 8, pp. 1589–1599, 1999.
- [131] E. F. Toro, *Riemann solvers and numerical methods for fluid dynamics: a practical introduction*. Springer Science & Business Media, 2013.
- [132] P. Reymond, F. Merenda, F. Perren, D. Rüfenacht, and N. Stergiopoulos, “Validation of a one-dimensional model of the systemic arterial tree,” *American Journal of Physiology - Heart and Circulatory Physiology*, vol. 297, pp. 208–222, jul 2009.
- [133] J. Peiró and A. Veneziani, *Reduced models of the cardiovascular system*, pp. 347–394. Milano: Springer Milan, 2009.
- [134] R. G. Nogueira, D. Ryan, L. Mullins, J. Thornton, and S. Fitzgerald, “Maximizing the catheter-to-vessel size optimizes distal flow control resulting in improved revascularization in vitro for aspiration thrombectomy New devices and techniques,” *J NeuroIntervent Surg*, vol. 0, pp. 1–6, 2021.
- [135] S. Fitzgerald, D. Ryan, J. Thornton, R. G. Nogueira, T. Cite, and a. J. NeuroIntervent Surg, “Preclinical evaluation of Millipede 088 intracranial aspiration catheter in cadaver and in vitro thrombectomy models New devices and techniques,” *J NeuroIntervent Surg*, vol. 13, pp. 447–452, 2021.
- [136] H. Okada, Y. Matsuda, A. Malisch, J. Chung, D. M. Heiferman, and D. K. Lopes, “Evaluation of the Intracranial Flow Alteration during Manual Syringe and Continuous Pump Aspiration,” *Journal of Stroke and Cerebrovascular Diseases*, vol. 28, pp. 2574–2579, sep 2019.
- [137] C. Qiu, Y. Zhang, C. Xue, S. Jiang, and W. Zhang, “MRA study on variation of the circle of Willis in healthy Chinese male adults,” *BioMed Research International*, vol. 2015, jan 2015.

- [138] B. Forgo, A. D. Tarnoki, D. L. Tarnoki, D. T. Kovacs, L. Szalontai, A. Persely, A. Hernyes, M. Szily, L. Littvay, E. Medda, A. Szabo, L. R. Kozak, G. Rudas, A. Sas, M. Sepsi, L. Kostyal, and C. Olah, “Are the variants of the circle of willis determined by genetic or environmental factors results of a twin study and review of the literature,” oct 2018.
- [139] M. S. Van Kammen, C. J. Moomaw, I. C. Van Der Schaaf, R. D. Brown, D. Woo, J. P. Broderick, J. S. Mackey, G. J. Rinkel, J. Huston, and Y. M. Ruigrok, “Heritability of circle of Willis variations in families with intracranial aneurysms,” *PLoS ONE*, vol. 13, jan 2018.
- [140] M. J. Krabbe-Hartkamp, J. Van Der Grond, F. E. De Leeuw, J. C. De Groot, A. Algra, B. Hillen, M. M. Breteler, and W. P. Mali, “Circle of Willis: Morphologic variation on three-dimensional time-of-flight MR angiograms,” *Radiology*, vol. 207, pp. 103–112, apr 1998.
- [141] H. E. Riggs and C. Rupp, “Variation in Form of Circle of Willis: The Relation of the Variations to Collateral Circulation: Anatomic Analysis,” *Archives of Neurology*, vol. 8, pp. 8–14, jan 1963.
- [142] A. Hoksbergen, D. Legemate, L. Csiba, G. Csáti, P. Síró, and B. Fülesdi, “Absent Collateral Function of the Circle of Willis as Risk Factor for Ischemic Stroke,” *Cerebrovascular Diseases*, vol. 16, no. 3, pp. 191–198, 2003.
- [143] T. van Seeters, J. Hendrikse, G. J. Biessels, B. K. Velthuis, W. P. Mali, L. J. Kappelle, and Y. van der Graaf, “Completeness of the circle of Willis and risk of ischemic stroke in patients without cerebrovascular disease,” *Neuroradiology*, vol. 57, pp. 1247–1251, dec 2015.
- [144] H. Lippert and R. Pabst, *Arterial Variations in Man: Classification and Frequency*. J.F. Bergmann-Verlag München, 1985.

- [145] D. Mukherjee, N. D. Jani, J. Narvid, and S. C. Shadden, “The Role of Circle of Willis Anatomy Variations in Cardio-embolic Stroke: A Patient-Specific Simulation Based Study,” *Annals of Biomedical Engineering*, vol. 46, 2017.
- [146] K. Hayashi, H. Handa, S. Nagasawa, A. Okumura, and K. Moritake, “Stiffness and elastic behavior of human intracranial and extracranial arteries,” *Journal of Biomechanics*, vol. 13, pp. 175–184, jan 1980.
- [147] B. M. Kissela, J. C. Khoury, K. Alwell, C. J. Moomaw, D. Woo, O. Adeoye, M. L. Flaherty, P. Khatri, S. Ferioli, F. De Los Rios La Rosa, J. P. Broderick, and D. O. Kleindorfer, “Age at stroke: Temporal trends in stroke incidence in a large, biracial population,” *Neurology*, vol. 79, pp. 1781–1787, oct 2012.
- [148] A. V. Kamenskiy, I. I. Pipinos, J. S. Carson, J. N. Mactaggart, and B. T. Baxter, “Age and disease-related geometric and structural remodeling of the carotid artery,” *Journal of Vascular Surgery*, vol. 62, pp. 1521–1528, dec 2015.
- [149] A. P. Avolio, “Multi-branched model of the human arterial system,” *Medical & Biological Engineering & Computing*, vol. 18, pp. 709–718, Nov. 1980.
- [150] A. E. Li, I. Kamel, F. Rando, M. Anderson, B. Kumbasar, J. A. C. Lima, and D. A. Bluemke, “Using MRI to Assess Aortic Wall Thickness in the Multiethnic Study of Atherosclerosis: Distribution by Race, Sex, and Age,” *American Journal of Roentgenology*, vol. 182, pp. 593–597, mar 2004.
- [151] B. Jani, “Ageing and vascular ageing,” *Postgrad Med J*, vol. 82, pp. 357–362, 2006.
- [152] A. G. Hudetz, G. Márk, A. G. Kovách, T. Kerényi, L. Fody, and E. Monos, “Biomechanical properties of normal and fibrosclerotic human cerebral arteries,” *Atherosclerosis*, vol. 39, no. 3, pp. 353–365, 1981.

- [153] R. S. Ajmani, E. J. Metter, R. Jaykumar, D. K. Ingram, E. L. Spangler, O. O. Abugo, and J. M. Rifkind, “Hemodynamic changes during aging associated with cerebral blood flow and impaired cognitive function,” tech. rep., 2000.
- [154] E. G. Lakatta and D. Levy, “Arterial and cardiac aging: major shareholders in cardiovascular disease enterprises: Part i: aging arteries: a “set up” for vascular disease,” *Circulation*, vol. 107, no. 1, pp. 139–146, 2003.
- [155] M. A. James, P. A. Watt, J. F. Potter, H. Thurston, and J. D. Swales, “Pulse pressure and resistance artery structure in the elderly,” *Hypertension*, vol. 26, no. 2, pp. 301–306, 1995.
- [156] K. Jin, X. Xu, B. Wang, C. Ren, J. Hu, D. A. Greenberg, T. Chen, and L. Xie, “Age-related Impairment of Vascular Structure and Functions,” 2017.
- [157] Stryker Neurovascular, “stryker neurovascular | flowgate<sup>2</sup> balloon guide catheter.” <https://www.strykerneurovascular.com/us/products/ais/flowgate-balloon-guide-catheter>, 2021.
- [158] Stryker Neurovascular, “stryker neurovascular | Trevo XP Stentriever™.” <https://www.strykerneurovascular.com/us/products/ais/trevo-xp-provue-retriever>, 2021.
- [159] Penumbra, “Penumbra | Velocity® Delivery Microcatheter.” <https://www.penumbrainc.com/neuro-device/velocity-delivery-microcatheter/>, 2021.
- [160] K. Hanlon, “Computational investigation of blood flow alterations during the treatment of stroke,” Master’s thesis, University of Sheffield, 2019.



# Dissemination

## Co-authored Conference Works

- Melis, A., Clayton, R.H., Narata, A.P., Mustafa, A., Marzo, A. (2019) Use of a Gaussian process emulator and 1D circulation model to characterize cardiovascular pathologies and guide clinical treatment. - CompBiomed Conference, London, UK.
- Benemerito, I., Jordam, B., Mustafa, A., Marzo, A. (2021) Quantification of the effects of ageing, hypertension and atherosclerosis on flow reversal during a mechanical thrombectomy procedure. – BioMedEng Conference, Sheffield, UK.

## Guest Presentation

- Computational Framework for Thrombectomy; 1D Modelling Approaches (openBF) (2019) Project INSIST Meeting, Politecnico di Milano, Milan, Italy.